

NAVAL POSTGRADUATE SCHOOL

Monterey, California

2

AD-A277 040



DTIC
ELECTE
MAR 23 1994
S F D

THESIS

CORRELATION OF FLUX COMPOSITION AND INCLUSION CHARACTERISTICS
WITH SUBMERGED ARC WELD METAL PROPERTIES IN HY-100 STEEL

by

Kent William Kettell

September 1993

Thesis Advisor:

Alan G. Fox

Approved for public release: Distribution unlimited.

94-09121



94 3 22 000

Unclassified

SECURITY CLASSIFICATION OF THIS PAGE

REPORT DOCUMENTATION PAGE				Form Approved OMB No 0704-0188	
1a. REPORT SECURITY CLASSIFICATION UNCLASSIFIED			1b. RESTRICTIVE MARKINGS		
2a. SECURITY CLASSIFICATION AUTHORITY			3. DISTRIBUTION/AVAILABILITY OF REPORT Approved for public release; distribution unlimited.		
2b. DECLASSIFICATION/DOWNGRADING SCHEDULE					
4. PERFORMING ORGANIZATION REPORT NUMBER(S)			5. MONITORING ORGANIZATION REPORT NUMBER(S)		
6a. NAME OF PERFORMING ORGANIZATION Naval Postgraduate School		6b. OFFICE SYMBOL (If applicable) ME	7a. NAME OF MONITORING ORGANIZATION Naval Postgraduate School		
6c. ADDRESS (City, State, and ZIP Code) Monterey, CA 93943-5000			7b. ADDRESS (City, State, and ZIP Code) Monterey, CA 93943-5000		
8a. NAME OF FUNDING/SPONSORING ORGANIZATION		8b. OFFICE SYMBOL (If applicable)	9. PROCUREMENT INSTRUMENT IDENTIFICATION NUMBER		
8c. ADDRESS (City, State, and ZIP Code)			10. SOURCE OF FUNDING NUMBERS		
			PROGRAM ELEMENT NO.	PROJECT NO.	TASK NO.
11. TITLE (Include Security Classification) CORRELATION OF FLUX COMPOSITION AND INCLUSION CHARACTERISTICS WITH SUBMERGED ARC WELD METAL PROPERTIES IN HY-100 STEEL					
12. PERSONAL AUTHOR(S) Kettell, Kent William					
13a. TYPE OF REPORT Master's Thesis		13b. TIME COVERED FROM Aug 92 TO Sep 93		14. DATE OF REPORT (Year,Month,Day) September 1993	
15. PAGE COUNT 107					
16. SUPPLEMENTARY NOTATION The views expressed in this thesis are those of the author and do not reflect the official policy or position of the Department of Defense or the U.S. Government.					
17. COSATI CODES			18. SUBJECT TERMS (Continue on reverse if necessary and identify by block number) HY-100 steel, submerged arc welding, SAW, fluxes, basicity index, non-metallic inclusions		
FIELD GROUP SUB-GROUP					
19. ABSTRACT (Continue on reverse if necessary and identify by block number) Submerged arc weldments of HY-100 steel prepared under standard conditions with five commercially available fluxes were analyzed to discern a basis for the variation in mechanical properties associated with different flux use. The variations in flux chemistry resulted in alloyed weldments with diverse weld metal mechanical properties as evident by Charpy impact, tensile, dynamic tear, and microhardness tests. The microstructures and macrostructures were examined using optical and electron microscopy in order to determine the basis for the variations in strength and toughness. Scanning electron microscope and energy dispersive x-ray experiments were performed to determine the size, type, distribution and volume fraction of the non-metallic inclusions in the weld metal. Inclusion characterization revealed that the role of the flux in alloying had a more significant effect on the strength and toughness than did the presence of specific inclusions.					
20. DISTRIBUTION/AVAILABILITY OF ABSTRACT <input checked="" type="checkbox"/> UNCLASSIFIED/UNLIMITED <input type="checkbox"/> SAME AS RPT. <input type="checkbox"/> DTIC USERS			21. ABSTRACT SECURITY CLASSIFICATION UNCLASSIFIED		
22a. NAME OF RESPONSIBLE INDIVIDUAL Alan G. Fox.			22b. TELEPHONE (Include Area Code) 408 656-2142		22c. OFFICE SYMBOL ME/FX

DD Form 1473, JUN 86

Previous editions are obsolete.

SECURITY CLASSIFICATION OF THIS PAGE

S/N 0102-LF-014-6603

Unclassified

Approved for public release: Distribution unlimited.

**CORRELATION OF FLUX COMPOSITION AND INCLUSION
CHARACTERISTICS WITH SUBMERGED ARC WELD METAL PROPERTIES
IN HY-100 STEEL**

by

Kent William Kettell

**Lieutenant , United States Navy
B.S., United States Naval Academy, 1985**

Submitted in partial fulfillment of the
requirements for the degrees of

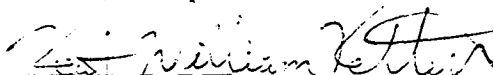
**MASTERS OF SCIENCE IN MECHANICAL ENGINEERING
and
MECHANICAL ENGINEER**

from the

NAVAL POSTGRADUATE SCHOOL

September 1993

Author:



Kent William Kettell

Approved by:

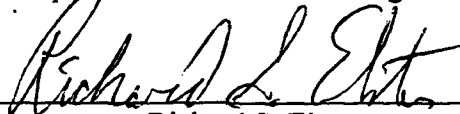


Alan G. Fox, Thesis Advisor



Matthew D. Kelleher, Chairman,

Department of Mechanical Engineering



Richard S. Elster,

Dean of Instruction

ABSTRACT

Submerged arc weldments of HY-100 steel prepared under standard conditions with five commercially available fluxes were analyzed to discern a basis for the variation in mechanical properties associated with different flux use. The variations in flux chemistry resulted in alloyed weldments with diverse weld metal mechanical properties as evident by Charpy impact, tensile, dynamic tear, and microhardness tests. The microstructures and macrostructures were examined using optical and electron microscopy in order to determine the basis for the variations in strength and toughness. Scanning electron microscope and energy dispersive x-ray experiments were performed to determine the size, type, distribution and volume fraction of the non-metallic inclusions in the weld metal. Inclusion characterization revealed that the role of the flux in alloying had a more significant effect on the strength and toughness than did the presence of specific inclusions.

Accession For	
NTIS	CRA&I
DTIC	TAB
Unannounced	
Justification	
By	
Distribution /	
Availability Codes	
Dist	Avail and/or Special
A-1	

TABLE OF CONTENTS

	Page
I. INTRODUCTION	1
II. BACKGROUND	2
A. HY-100 STEEL	2
B. SUBMERGED ARC WELDING PROCEDURE	3
1. Heat Input	4
a. Arc Voltage	4
b. Welding Current	5
c. Welding Speed	5
2. Weld Pool Solidification and Cooling Rate	5
3. Preheat/Interpass Temperature	7
4. Electrode Diameter	7
5. Number of Passes, Weld Sequence and Reheat Zones	7
6. Electrode Stick Height	8
7. Joint Geometry, Thickness and Restraint	8
C. WELDING CONSUMABLES	8
1. Wire Electrode	8
2. Fluxes	8
D. WELD METAL ALLOYING	11
1. General	11
a. Hardenability	11
b. Dilution	12
2. Carbon	13
3. Manganese	13
4. Nickel	14
5. Molybdenum	14
6. Copper	15
7. Chromium	15
8. Vanadium	15
9. Silicon	15
10. Aluminum	16
11. Titanium	16
12. Zirconium	16
13. Boron	17
14. Oxygen	17
15. Nitrogen	17
16. Hydrogen	17
17. Phosphorus	18
18. Sulfur	18
E. WELD METAL MICROSTRUCTURE	19
1. Non-Metallic Inclusions	19
a. Sources	19

b. Sizes	19
2. Acicular Ferrite	20
F. SCOPE OF THE PRESENT WORK	21
III. EXPERIMENTS AND TESTS	23
A. HY-100 STEELS	23
B. SUBMERGED ARC WELDING PROCEDURE	23
C. WELDING CONSUMABLES	24
1. Wire Electrode	24
2. Fluxes	24
D. WELD METAL ALLOYING	27
1. Chemical Determinations	27
2. Dilution	28
E. MECHANICAL TESTS	30
1. Tensile Test	31
2. Charpy Toughness Test	31
3. Dynamic Tear Test	32
4. Microhardness Test	32
F. SCANNING ELECTRON MICROSCOPY	32
1. Inclusion Analysis	33
2. Energy Dispersive X-Ray Analysis	33
G. OPTICAL MICROSCOPY	34
IV. EXPERIMENTAL RESULTS AND DISCUSSION	35
A. MECHANICAL TESTS	35
1. Tensile Test	35
2. Charpy Toughness Test	39
3. Dynamic Tear Test	42
4. Microhardness Test	43
B. SCANNING ELECTRON MICROSCOPY	44
1. Non-Metallic Inclusions	44
2. EDX Analysis of Inclusions	50
C. CHEMICAL COMPOSITION	60
D. METALLOGRAPHY	67
1. Weld Metal Reheat	67
2. Microscopy	67
V. CONCLUSIONS	69
APPENDIX A. FLUX CHEMISTRY DATA	70
APPENDIX B. CHARPY AND FATT CURVES	73
APPENDIX C. PHOTOGRAPHS AND MICROGRAPHS	78
LIST OF REFERENCES	93
INITIAL DISTRIBUTION LIST	96

LIST OF TABLES

Table	Page
2-1. REQUIRED HY-100 SAW ELECTRODE CHEMISTRY	2
2-2. REQUIRED MECHANICAL PROPERTIES	3
3-1. HY-100 BASE PLATE AND FILLER WIRE CHEMISTRY	23
3-2. WELDING EXPERIMENT CONTROL PARAMETERS	24
3-3. FLUXES AND DESIGNATIONS USED BY VARIOUS RESEARCHERS	25
3-4. FLUX CHEMISTRIES IN W% FOR THE FIVE TYPES OF FLUX USED	26
3-5. BASICITY INDEX FOR FLUXES USED	26
3-6. CHEMICAL COMPOSITION OF THE BASE, FILLER, AND WELDMENTS	28
3-7. CORRELATION TOOLS	29
4-1. TENSILE TEST DATA	36
4-2. CHARPY TOUGHNESS TEST DATA	39
4-3. FRACTURE APPEARANCE TEST DATA	40
4-4. TRANSITION TEMPERATURE DATA	40
4-5. DYNAMIC TEAR TEST DATA	42
4-6. DIAMOND PYRAMID HARDNESS VALUES	43
4-7A. INCLUSION QUANTITIES CATEGORIZED BY SIZES	45
4-7B. INCLUSION STATISTICS BASED ON 100 RANDOM FIELDS	45
4-8. INCLUSION STATISTICS BASED ON INCLUSIONS ≥ 0.25 MICRONS	48
4-9. INCLUSION CHEMISTRY	51
4-10. MEAN INCLUSION SOLIDIFICATION TEMPERATURES	52
4-11. F289 WELDMENT INCLUSION CHEMISTRY CORRELATION DATA	53
4-12. F292 WELDMENT INCLUSION CHEMISTRY CORRELATION DATA	54
4-13. F293 WELDMENT INCLUSION CHEMISTRY CORRELATION DATA	55
4-14. F295 WELDMENT INCLUSION CHEMISTRY CORRELATION DATA	56
4-15. F296 WELDMENT INCLUSION CHEMISTRY CORRELATION DATA	57
4-16. INCLUSION CHEMISTRY CORRELATION DATA FOR ALL WELDMENTS	58
4-17. TITANIUM RELATED INCLUSION DATA FOR ALL WELDMENTS	59
4-18. RESULTS OF REHEAT ANALYSIS	67
A-1. RESULT OF XRF ANALYSIS ON THE FLUXES	70
A-2. RESULT OF OES ANALYSIS ON THE FLUXES	71
A-3. RESULT OF ICP ANALYSIS ON THE FLUXES	72

LIST OF FIGURES

Figure	Page
2-1. Schematic of Continuous Cooling Transformation Curve.	6
3-1. Non-diffusible hydrogen versus Basicity.	30
3-2. Weld metal sulfur versus Basicity.	31
4-1. Yield Strength vs. Weld metal residual hydrogen.	36
4-2. Yield Strength vs. Basicity (w/CaF ₂) by the Easterling relationship.	37
4-3. Yield Strength vs. Basicity Index (w/CaF ₂) by the Eagar relationship.	37
4-4. UTS vs. Basicity (w/CaF ₂) by the Easterling relationship.	38
4-5. UTS vs. Basicity Index (w/CaF ₂) by the Eagar relationship.	38
4-6. Basicity versus 50% Fracture Appearance Transition Temperature.	40
4-7. Basicity versus Ductile to Brittle Transition Temperature.	41
4-8. Dynamic Tear Test Energy vs. Basicity.	42
4-9. Diamond Pyramid Hardness vs. Basicity.	44
4-10. SEM micrograph of non-metallic inclusions using BSE imaging under 4000x magnification.	45
4-11a. Non-metallic inclusions categorized by size and quantity.	46
4-11b. Non-metallic inclusions categorized by size and quantity.	46
4-12. Diamond Pyramid Hardness versus the quantity of inclusions per 100 random fields of view.	47
4-13. Buoyancy effect shown by fewer inclusions as their size increases.	48
4-14. Effect of flux basicity on quantity of inclusions.	49
4-15. Effect of inclusion volume % on DBTT.	49
4-16. Phase relations at liquidus temperatures in the MnO-Al ₂ O ₃ -SiO ₂ system.	52
4-17. Ternary diagram for inclusions in F289 weld metal.	53
4-18. Ternary diagram for inclusions in F292 weld metal.	54
4-19. Ternary diagram for inclusions in F293 weld metal.	55
4-20. Ternary diagram for inclusions in F295 weld metal.	56
4-21. Ternary diagram for inclusions in F296 weld metal.	57
4-22. Ternary diagram for inclusions in all the weldments studied.	58
4-23. Ternary diagram for inclusions in all weld metals.	59
4-24. Correlation of Mn/Si ratio in weld metal with the average solidification temperature of the 100 inclusions analyzed for each sample.	61
4-25. Correlation of Al/O ratio in weld metal with the average solidification temperature of the 100 inclusions analyzed for each sample.	61
4-26. SEM micrograph of F293 weldment inclusion with faceted TiN particle etched with Sodium-picrate under 43100x magnification with BSE.	64
4-27. Correlation of weld metal titanium versus titanium in the inclusions.	65
4-28. Correlation of weld metal oxygen versus titanium in the inclusions.	66
4-29. Correlation of weld metal Al/O ratio versus titanium in the inclusions.	66
B-1. Sample F289 toughness curves.	73
B-2. Sample F292 toughness curves.	74
B-3. Sample F293 toughness curves.	75

B-4.	Sample F295 toughness curves.....	76
B-5.	Sample F296 toughness curves.....	77
C-1.	Photograph of sample F289 weldment etched with 5% Nital.	78
C-2.	Macrograph of F289 weld metal etched with 5% Nital.	78
C-3.	Photograph of sample F292 weldment etched with 5% Nital.	79
C-4.	Macrograph of F292 weld metal etched with 5% Nital.	79
C-5.	Photograph of sample F293 weldment etched with 5% Nital.	80
C-6.	Macrograph of F293 weld metal etched with 5% Nital.	80
C-7.	Photograph of sample F295 weldment etched with 5% Nital.	81
C-8.	Macrograph of F295 weld metal etched with 5% Nital.	81
C-9.	Photograph of sample F296 weldment etched with 5% Nital.	82
C-10.	Macrograph of F296 weld metal etched with 5% Nital.	82
C-11.	SEM of F289 weldment columnar region microstructure etched with 5% Nital under 4000x magnification.....	83
C-12.	SEM of F289 weldment grain refined region microstructure etched with 5% Nital under 4000x magnification.	83
C-13.	SEM of F292 weldment columnar region microstructure etched with 5% Nital under 4000x magnification.....	84
C-14.	SEM of F292 weldment grain refined region microstructure etched with 5% Nital under 4000x magnification.	84
C-15.	SEM of F293 weldment columnar region microstructure etched with 5% Nital under 4000x magnification.....	85
C-16.	SEM of F293 weldment grain refined region microstructure etched with 5% Nital under 4000x magnification.	85
C-17.	SEM of F295 weldment columnar region microstructure etched with 5% Nital under 4000x magnification.....	86
C-18.	SEM of F295 weldment grain refined region microstructure etched with 5% Nital under 4000x magnification.	86
C-19.	SEM of F296 weldment columnar region microstructure etched with 5% Nital under 4000x magnification.....	87
C-20.	SEM of F296 weldment grain refined region microstructure etched with 5% Nital under 4000x magnification.	87
C-21.	Optical micrograph of F289 weldment microstructure etched with 5% Nital under 1000x magnification.	88
C-22.	Optical micrograph of F292 weldment microstructure etched with 5% Nital under 1000x magnification.	88
C-23.	Optical micrograph of F293 weldment microstructure etched with 5% Nital under 1000x magnification.	89
C-24.	Optical micrograph of F295 weldment microstructure etched with 5% Nital under 1000x magnification.	89
C-25.	Optical micrograph of F296 weldment microstructure etched with 5% Nital under 1000x magnification.	90
C-26.	SEM micrograph of F296 weldment dendritic microstructure in region of macrosegregation etched with 5% Nital under 265x magnification.....	90

C-27.	SEM micrograph of F296 weldment microstructure in region of solidification cracking one micron polish under 20x magnification.	91
C-28.	SEM micrograph of F296 weldment microstructure in region of solidification crack etched with 5% Nital under 1000x magnification.	91
C-29.	SEM micrograph of F296 weldment microstructure in region of solidification crack etched with 5% Nital under 1670x magnification.	92

I. INTRODUCTION

The evolving requirement to build naval combatants with steels of higher strength to weight ratio has led to the development of high strength steels like HY-100. The U.S. Navy desires the steel to have the required mechanical properties of strength and toughness in the base plate and a chemistry to permit welding which meets specific strength and toughness standards without causing cracks at any location in or near the weld. Ideally, one would like to have consumables capable of welding the HY-100 base plate in such a manner as to minimize energy expenditure during preheat and postheat and optimize the mechanical properties.

The solidification behavior of HY-100 steel is extremely complex because of the many factors that affect the austenite to ferrite and cementite transformation. This complexity arises because the large number of interacting variables makes it difficult to determine distinct relationships and the validity of trends. Since welding in a laboratory is better controlled than in an industrial environment, there exists a need to establish improved structure-property correlations in complex weld metal microstructures using variables that are easily controllable. It is important to understand the sensitivity of the fusion zone microstructure to variations in chemical composition independent of cooling rate. Although some improvements have been made in submerged arc weld, SAW, fluxes designed for HY steels, most changes have come by trial and error. Thus an investigation is necessary to determine the effects of the chemical composition of the flux and microstructure of the weld metal on the strength and toughness of HY-100 steel weldments.

II. BACKGROUND

A. HY-100 STEEL

HY-100 steel is a quenched and tempered martensitic steel with strength and toughness optimized primarily through heat treatment and the addition of nickel, chromium, molybdenum and vanadium alloying elements as delineated in MIL-S-16216. It is austenitized at a temperature between 1550-1650 °F and quenched in water, followed by tempering near 1150 °F to precipitate carbides and stress relieve the martensitic microstructure. When welded, HY-80 steel has essentially a bainitic microstructure no matter what the cooling rate, and HY-130 steel is usually martensitic no matter what the cooling rate. The difficulty in welding HY-100 steel lies in the fact that HY-100 steel can vary between the martensitic microstructure and bainitic microstructure through slight variations in chemical composition and cooling rate. For this study special care was used to ensure that cooling rate did not vary, so that the effect of changes in chemical composition could be analyzed. Table 2-1 gives further details on the required electrode chemistry from MIL-E-23765.

TABLE 2-1. REQUIRED HY-100 SAW ELECTRODE CHEMISTRY.

Element Sample↓	C w%	Mn w%	Si w%	P w%	S w%	Ni w%	Mo w%	Cr w%	V w%	Al w%	Ti w%	Zr w%	Cu w%	O w%	N w%	B w%	H ml/100gm
Min.	-	0.90	-	-	-	1.0	0.30	-	-	-	-	-	-	-	-	-	-
Max.	0.09	2.35	0.60	0.012	0.008	3.0	1.00	0.80	0.03	0.10	0.10	0.10	-	-	-	-	5.5

Various military specifications exist for ensuring that the steel weld will be able to perform the functions for which it is required. Table 2-2 details some of those specifications [Ref. 1:p. 9] for SAW weldments produced with a neutral granular flux. The "*" denotes that no two specimens of the five tested shall have values below the minimum average specified and that only one may have a value 10 ft-lb below the minimum average

specified. The "+" denotes that one specimen of the two tested can have a value 50.0 ft-lb below the minimum average specified. The "*" denotes that one specimen of the two tested can have a value 25.0 ft-lb below the minimum average specified.

TABLE 2-2. REQUIRED MECHANICAL PROPERTIES.

PROPERTY	LIMIT
Yield Strength	min. 102 ksi max. 122 ksi
Percent Elongation	14 percent
Charpy Impact Toughness @ -60 °F	min. avg. 45 ft-lb*
Charpy Impact Toughness @ 0 °F	min. avg. 60 ft-lb*
Dynamic Tear Toughness @ -20 °F	min. avg. 400 ft-lb ⁺
Dynamic Tear Toughness @ 30 °F	min. avg. 575 ft-lb*

B. SUBMERGED ARC WELDING PROCEDURE

In submerged arc welding the consumable electrode joins the molten filler wire and the base metal in a dynamic pool of liquid metal while submerged under a layer of granulated flux. The flux is poured from a hopper onto the work piece ahead of the mechanized electrode and removed by vacuum as the electrode moves along. The flux, which is primarily composed of oxides, melts and rises to the surface of the solidifying weld pool where it forms a slag covering to protect the weld pool from the atmosphere. The molten flux is also designed to clean the liquid weld pool by forming oxides which then rise to the surface as slag. Due to problems with hydrogen related cracking in HY steel weldments, it has become necessary to bake the flux before use to remove any moisture. This mechanized or automated fabrication process is capable of high deposition rates that may lead to poor welds if the process is not well balanced. Many issues affect the success of the welding procedure, and therefore some of the most important factors will be addressed in the following paragraphs.

1. Heat Input

A lower heat input in the root pass results in less dilution of the higher carbon base plate, thereby minimizing the likelihood of hydrogen induced cracking, HIC, in the root pass. In higher level weld passes the maximum heat input is also limited to reduce the susceptibility to HIC. Some researchers have addressed the subject of heat input without addressing the aspect of whether the voltage or the current was the predominant variable of the energy transferred into the dynamic weld pool. It is important to understand the effects of high voltage versus high current and the relationship of weld pool circulation tearing off dendrite tips providing for a finer grained and more homogenous microstructure. The heat input, HI, is determined by the simple relationship shown below.

$$HI = \frac{\text{welding current} \times \text{arc voltage} \times 60 \text{ sec / min}}{\text{welding speed}}$$

As HI increases, the cooling rate decreases, but current, voltage and welding speed can not be arbitrarily changed without altering the efficiency of the electrode. The magnitude of HI effects solidification, austenitization, quenching, tempering, and hydrogen diffusion because the position of continuous cooling transformation, CCT, curve is determined by alloy content, solidification microstructure, and prior austenite microstructure.

a. Arc Voltage

The arc voltage is initially adjusted to accommodate the distance between the electrode and the weld metal and the type of flux that is being used. When a constant voltage power supply is used, changes in the arc gap distance or flux composition alter the resistance. If the arc resistance increases, then the arc current decreases, resulting in slower melting of the electrode which allows the arc gap to rapidly return to its proper length. It is for this reason that a constant voltage power supply is desirable.

b. *Welding Current*

A higher direct current results in stronger weld pool circulation, tearing off dendrite tips more rapidly in the mushy zone. This can promote a more equiaxed microstructure. Wilson noted that current affected the loss of manganese in the weld metal when welded with a flux that had no manganese [Ref. 2:p. 52]. With a higher current less manganese is lost from the weld metal; this is preferred since manganese is purposefully added to prevent solidification cracking.

c. *Welding Speed*

For the sake of cost reduction, every process is driven toward a reduction of fabrication time. As welding speed is increased, the current must be raised to maintain a constant heat input, but there is a realistic limit for current as arc instability results when current is raised to a certain level.

2. *Weld Pool Solidification and Cooling Rate*

Weld pool solidification begins at the fusion boundary where partially melted grains of the surrounding metal serve as nucleation sites for columnar growth. To prevent solidification cracking, the tolerances of sulfur and phosphorus are maintained below 0.01% and 0.012% respectively with manganese present in the flux to scavenge these. The mere presence of the flux cover on the weld helps to minimize radiant heat loss, resulting in a very efficient use of energy.

Since transformation kinetics and weld metal chemistries are complex, the welding engineer needs to obtain the correct CCT diagram for the alloy system in question. Once the CCT diagram is estimated, accurate knowledge of the cooling rate, CR, in the weld fusion zone is required. Fortunately cooling rate is predictable as a function of heat input as shown here $CR = \frac{A(T-T_0)^2}{HI}$ where A is a constant, T is the instantaneous temperature, and T_0 is the base plate temperature.

It is important to understand the effect of cooling rate on solidification microstructure with regions of grain boundary ferrite, acicular ferrite, bainite and martensite; however, the CCT diagram must be pertinent to the particular chemistry of the weld metal, especially when the weld metal composition varies with flux composition. Figure 2-1 is a schematic of a typical CCT curve for high yield strength steels [Ref. 3]. A slower cooling rate will enhance the microstructure since martensite is avoided and will allow some tempering with a better environment for hydrogen diffusion. Since martensite formation increases as cooling rate increases, it is desirable to limit heat input and thereby minimize strength in preference to toughness. A steel alloyed for a 110 ksi yield strength is capable of achieving much higher strengths when the cooling rate is excessive. The higher strength martensitic steel has a degraded toughness and provides one more factor necessary for hydrogen embrittlement.

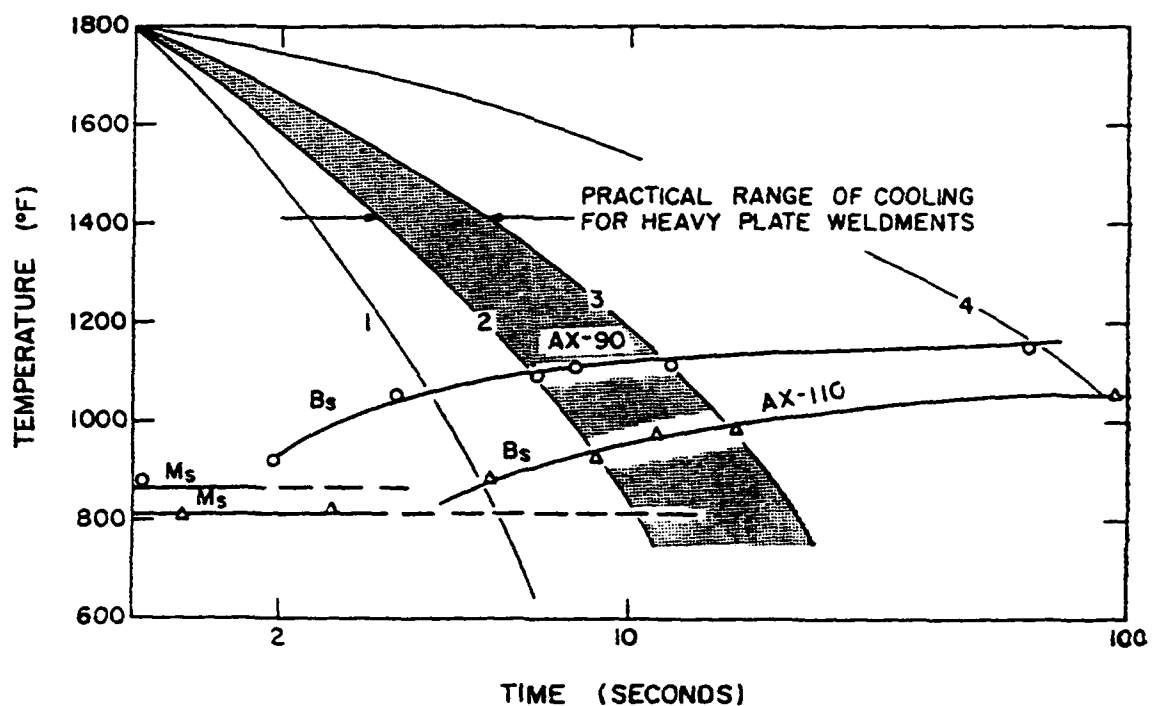


Figure 2-1. Schematic of Continuous Cooling Transformation Curve.

3. Preheat/Interpass Temperature

A higher base plate preheat/interpass temperature, T_0 , results in a lower cooling rate that, as stated previously, minimizes the formation of martensite and reduces the shrinkage that occurs in the weld metal during and after cooling. This in turn reduces the residual stresses that may enhance hydrogen induced cracking, HIC. The potential for HIC can also be minimized through the higher T_0 since the more time at higher temperatures is available for the diffusion of hydrogen.

4. Electrode Diameter

While welding with a larger diameter electrode allows a higher deposition rate, a larger weld pool is more prone to cracking problems. The electrode diameter determines maximum current for a given voltage since the ability to support high currents obviously diminishes as the diameter is lowered. Smaller diameter electrodes produce smaller deposits that inherently involve smaller magnitudes of thermal stresses, but too small a deposit requires more weld passes with an increase in cost.

5. Number of Passes, Weld Sequence and Reheat Zones

With more passes, a greater proportion of the weld metal is subjected to the heating and cooling cycles; this seems to have a positive effect as automatic bead tempering anneals the multi-run weldment. It is important that multipass welds are made over a stable microstructure using a placement sequence that minimizes shrinkage. There has been much research involving the reheated volume surrounding the fusion zone. For the purpose of this study, the reheat zone was divided into two regions around the remelted fusion zone, a coarse grain region and a fine grain region working outward from the fusion line. The grain coarsening occurs as a result of reaustenitization. The grain refining occurs as a result of phase transformation due to thermal cycling low in the austenite range and some amount of tempering.

6. Electrode Stick Height

The electrode stick height and electrode arc gap are intended to describe the same distance from the electrode tip to the molten weld pool. When the arc gap is small, there is less interaction between the filler wire plasma, the flux and the atmosphere. This is preferred when trying to control the weld metal chemistry.

7. Joint Geometry, Thickness and Restraint

Joint geometry and thickness affect the number of passes required to join the pieces. As the thickness of the joined sections increases, the potential heat sink is greater, increasing the cooling rate. Thus, the preheat temperature must be raised to a higher temperature for each successive pass. One can also reduce the time between passes to maintain a constant cooling rate. This is a good reason for using a robotic welder which can sense the weld pool temperature and adjust the heat input to achieve the desired cooling rate. As base plate thickness increases, the stresses caused by restraint rise, increasing the likelihood of HIC.

C. WELDING CONSUMABLES

1. Wire Electrode

The combined electrode and filler wire used in welding the samples was a L-TEC 120, HT 120022 with the required chemistry as shown above in Table 2-1. The actual chemistry is shown later in Table 3-1. This spooled wire had a mean diameter of 3/32 inches.

2. Fluxes

The purpose of the agglomerated flux is to melt and provide a shielding for the filler wire during metal transfer and weld pool solidification. The shielding protects the weld from atmospheric oxygen and nitrogen gases. The slag which forms on the surface prevents further contamination of the weld by atmospheric gases. Arc stabilization

provided by group 1A ions ensures that a more consistent power is applied to the weld. Jackson noted that oxides of Na and K have improved arc stability because of their relatively low work functions [Ref. 4]. With a more stable arc, a higher power can be applied allowing a higher deposition rate. A more stable heat and mass transfer also provides for a more homogeneous weld as a result of a more efficient melting and solidification process. Since the binders in the flux are anhydrous, the flux was dehydrated before use by heating to drive off moisture, minimizing the introduction of hydrogen and oxygen.

Deoxidization of the weld pool is achieved with deoxidants and impurity scavengers in the flux that preferentially form with oxygen and rise to the weld pool surface as slag. However, since the flux is primarily composed of oxides that may or may not decompose in the welding arc, oxygen may still be introduced into the weld pool. Detachability of the slag is also important because surface slag inclusions act as stress concentrations that can initiate fatigue cracks.

Alloying takes place in the weld pool as a result of elements intended for deoxidation and slag detachment. This alloying may serve to purposefully alter the mechanical properties of the weldment. Ideally the flux should be neutral in that it would not alloy or de-alloy the weld metal. Since the base plate and filler wire are not of the same composition, the use of a neutral flux would not provide the opportunity for weld metal enhancement. Since mechanical properties of the weld metal are dependent on flux composition, the extent of the alloying will be of utmost importance. Further knowledge of flux composition, when correlated with the factors that affect the weld metal properties, can be used to engineer an optimum flux for SAW application with HY-100 steel.

High oxygen in the weld pool can result in high concentrations of O_2 and CO , leading to porosity. An optimum flux chemistry will prevent porosity but leave a sufficient quantity of inclusions in the matrix to provide strengthening and toughening. It is

therefore desirable to control inclusions with a basic flux to reduce oxygen in the weld pool. Fluxes of higher basicity are expected to reduce weld metal oxygen leading to a lower volume percentage of inclusions. High basicity fluxes, however, are not chemically neutral, and they do alter the weld metal chemistry through slag-metal interactions. One means of categorizing fluxes is with a basicity index, BI, which is merely a ratio of the basic oxides to the non-basic oxides.

$$BI = \frac{\sum (\% \text{ basic oxides})}{\sum (\% \text{ non - basic oxides})}$$

Eagar has developed the following basicity index through empirical formulation to fit his observations [Ref. 5:p. 78s]. Calculations were made with and without the CaF_2 term which had been added by the author.

$$BI = \frac{\text{CaO (+CaF}_2\text{)} + \text{MgO} + \text{Na}_2\text{O} + \text{K}_2\text{O} + \text{Li}_2\text{O} + .5(\text{MnO} + \text{FeO})}{\text{SiO}_2 + .5(\text{Al}_2\text{O}_3 + \text{TiO}_2 + \text{ZrO}_2)}$$

Easterling has also developed an empirical relationship for the basicity, B , [Ref. 6:p. 6]. The author has added the CaF_2 term since it was found to make the equation reflect reality for the data and observations made during the course of this study. Note that there is quite a difference in how the elements are thought to behave as acids or bases in the equation below.

$$B = \frac{\text{CaO (+ CaF}_2\text{)} + 1.4\text{MgO} + 0.90\text{Na}_2\text{O} + 0.60\text{K}_2\text{O} + 0.45\text{ZrO}_2}{\text{SiO}_2 + 0.59\text{Al}_2\text{O}_3}$$

One compound that is not included in either original basicity relationship is CaF_2 which is believed to aid in decreasing the viscosity of the molten flux, allowing the non-metallic inclusions a less restrictive ascent to the weld pool surface. This reduces overall weld metal oxygen through fewer inclusions than there would have been if there were no CaF_2 and through a more rapid formation of the slag cover to minimize diffusion of gases from the atmosphere.

D. WELD METAL ALLOYING

1. General

To achieve an optimum balance of weld metal strength and toughness, the metallurgist must understand the positive and negative effects of adding certain elements to the welding consumables. Even if the exact recipes were known, a slight variation of the base plate alloy or filler wire would alter the expected results through dilution. It is important to fully understand all the factors that affect the entire system from the arc plasma to the weld pool and molten slag. When given time to react under equilibrium conditions, chemical driving forces, such as time and temperature, can provide an equilibrium composition. Equilibrium implies that all reactions have gone to completion; in a weld pool this is not the case. Hence, the impact of solo elements must be considered before the concert of all the elements can be assembled.

a. Hardenability

Hardenability is the ease with which martensite is formed. When hardenability levels are higher, the lower transformation products of bainite and martensite are more predominant. The critical cooling rate, CCR, is the lowest cooling rate that produces martensite. Steels which form martensite at lower CCR's have higher hardenability. The martensite start temperature which is controlled by chemistry drives the hardenability, but hardenability is also affected by grain size. Since bainite is preferred over martensite in HY-100 steel, the bainite start temperature is important for calculating the preheat and interpass temperatures. Pickering has provided the following empirical relationships for the bainite start and finish temperatures in high strength steels [Ref. 7:p. 120].

$$B_s (\circ C) = 830 - 270(\%C) - 90(\%Mn) - 37(\%Ni) - 70(\%Cr) - 83(\%Mo)$$

$$B_f (\circ C) = B_s - 120$$

The carbon equivalent number, CE, is used to relate the influence of alloying elements to both the ease with which martensite will form and the ability to resist hydrogen induced cracking. This CE can then be used to infer a relative delayed cracking susceptibility, currently referred to as hydrogen induced cracking, HIC, since a greater percentage of martensite will have a strong influence on the formation of cracks. Because of base plate dilution, filler wire addition and flux induced alloying, the CE associated with either the base metal or the filler wire will not give an accurate measure of the HIC susceptibility in the weld metal. In other words, a high CE will signify caution for welding with certain alloys, but a low CE should still be approached cautiously until the specific metal and consumables have been proven through rigorous testing to meet standards of strength and toughness. Because the weldment sample used in the dynamic tear test encompasses more weld passes and the HAZ, it is better suited for comparing base metal CE to overall toughness. A weld metal CE was calculated to compare the compositional effect of the weld metal after dilution. Again, the CE does not take into account the variations in the welding parameters or the diversity of elements in the flux. This diversity in both alloys and welding parameters has resulted in a myriad of CE equations; the following is ITO-Bessyo cold cracking parameter is the required correlation tool for analysis of the filler wire [Ref. 1:p. 17].

$$CE = \%C + \frac{\%Si}{30} + \frac{(\%Mn + \%Cr + \%Cu)}{20} + \frac{\%Ni}{60} + \frac{\%Mo}{15} + \frac{\%V}{10} + 5(\%B)$$

b. Dilution

Dilution of the base plate into the weldment is important since it is not just the filler wire-flux interaction that determines the final chemistry of the weld. In multi-pass welds a concentration gradient is set up by the dilution that occurs with each successive pass. Because of this, it is necessary to follow a consistent pattern in weld bead placement to ensure that effects of alloy variations can be attributed to flux chemistry. Since certain elements, which are present in low concentrations in the filler,

can make their way into the weld metal from the base plate, the following simple ratio can be used to compare relative amounts of dilution between samples.

$$\text{Dilution} = \frac{\{\% \text{Element}(\text{weld metal}) - \% \text{Element}(\text{filler})\}}{\{\% \text{Element}(\text{base plate}) - \% \text{Element}(\text{filler})\}}$$

Caution must be observed, however, in using this tool that so seriously neglects the role of flux composition in weld metal alloying and depends on chemical analyses which may not have been performed under the same conditions. The element selected for comparison should be one that does not readily form an oxide and ascend to the slag.

2. Carbon

Carbon, C, plays several roles in the alloying of steel. It is the element with the strongest effect on producing martensite, hence it is a dominant hardenability agent. As a solid solution strengthener, carbon has long been desired as the primary element for *securing high strength in steels*. Grain size refinement can also be achieved through an increase in carbon. Since carbides may provide crack nucleation sites, there must be some limit to the percentage present in the weld.

3. Manganese

Manganese, Mn, lowers the austenite to ferrite transformation temperature, and as an austenite stabilizer increases the hardenability of the steel thereby refining the lath size of the weld metal microstructure. As a solid solution strengthener, Mn allows for a reduction in the carbon that is necessary for high strength. An Mn range of 1.0-1.5% was shown to be optimum by Abson, who saw that CVN toughness increases through microstructural refinement by an increase in the amount of acicular ferrite formed at the expense of grain boundary ferrite [Ref. 8:p. 145]. Other researchers also showed Mn to control the growth of ferrite at the austenite grain boundaries [Refs. 9,10].

Manganese serves also in deoxidizing and desulfurizing the weld metal. A decrease in oxygen present in the weld metal has been achieved through a higher Mn/Si ratio [Ref. 11:p 1802]. Wilson showed that when the flux contained very little Mn, its loss in the weld metal was significant; therefore it is important that the flux contain MnO [Ref. 8:p. 70]. In the desulfurization process MnS is precipitated instead of FeS, lessening the tendency for hot crack formation along the grain boundaries in the presence of FeS which has a lower melting point. The welding engineer desires an Mn/S ratio greater than 50 to ensure no likelihood of solidification cracking. The amount of Mn necessary for reaction with sulfur is reported by Bell to be 30 times the atom percentage of the sulfur [Ref. 12].

4. Nickel

Nickel, Ni, is a potent toughening agent, such that an increase in Ni provides for a tougher alloy through a reduction of the ductile to brittle transition temperature, DBTT, and an increase in the CVN upper shelf impact energy [Ref. 13:pp. 63-82]. Ni also lowers the austenite to ferrite transformation temperature, and as an austenite stabilizer increases the hardenability of the steel thereby further refining the lath size of the weld metal microstructure. Ni has been shown to provide grain size strengthening by controlling the growth of ferrite at the grain boundaries [Refs. 9,10]. Ni prevents hot shortness associated with the welding of steels containing copper [Ref. 14:p. 260] and reduces solidification cracking in the presence of sulfur and phosphorus.

5. Molybdenum

Molybdenum, Mo, is a ferrite stabilizer but significantly increases the hardenability of the steel thereby further refining the lath size of the weld metal microstructure. As a solid solution strengthener, Mo allows for a reduction in the carbon that is necessary for high strength. It also prevents temper embrittlement during annealing. During cooling an increase in Mo has been found to increase the presence of acicular ferrite and thus increase toughness [Ref. 8:p. 166].

6. Copper

Copper, Cu, also lowers the austenite to ferrite transformation temperature, and as an austenite stabilizer increases the hardenability of the steel thereby further refining the lath size of the weld metal microstructure. It is considered to promote the formation of acicular ferrite. As a weak solid solution strengthener, Cu allows for some reduction in the carbon which is necessary for high strength. It is usually desired to minimize the percentage of Cu to prevent hot shortness during welding, but the presence of nickel helps prevent this.

7. Chromium

Chromium, Cr, is a ferrite stabilizer, and it also increases the hardenability of the steel thereby further refining the lath size of the weld metal microstructure. As a solid solution strengthener, Cr allows for a reduction in the carbon that is necessary for high strength. Cr is a strong carbide former and corrosion inhibitor when present in sufficient quantity.

8. Vanadium

Vanadium is a strong carbide and nitride former which is thought to have a secondary hardening effect in the reheated zones and to promote acicular ferrite formation.

9. Silicon

As a reactive solid solution strengthener, Silicon, Si, allows for a reduction in the carbon that is necessary for high strength. Silicon also lowers the austenite to ferrite transformation temperature, and as an austenite stabilizer increases the hardenability. Although known to improve mechanical properties for isothermal hardening, Si also causes a loss of ductility. Silicon serves also in deoxidizing the weld metal; yet at high levels above 0.5%, it has been attributed to a lowering of weld metal toughness [Ref. 8:p. 159]. Shackleton reports that silicon increases the fluidity of the weld pool; this is positive

since it allows the oxides scavenged in the molten pool to escape more easily to the surface [Ref. 14:p. 287].

10. Aluminum

Aluminum, Al, is a very strong deoxidizer and nitride former. The AlN type inclusions pin grain boundaries, inhibit ferrite grain growth and promote a refined grain structure. AlN formation also serves to remove N from solid solution, thereby lowering lattice resistance to dislocation motion and lowering DBTT [Ref. 15:p. 376]. Aluminum is also believed to have a role in determining the size and quantity of non-metallic inclusions present in the weld metal [Ref. 16:p. 249].

11. Titanium

Titanium, Ti, is another deoxidizing agent. TiO_2 , TiN or TiC may serve as nucleation sites for intragranular acicular ferrite. Mori noted that acid soluble Ti differed from the total Ti for total Ti concentrations above about 0.01 weight percent, and assumed the acid insoluble Ti to be TiN. He also presented evidence in favor of a Ti-B interaction. For Al concentrations less than 0.04 weight percent, increasing the weld metal titanium concentration caused the amount of acicular ferrite to increase and with a simultaneous decrease in the amount of grain boundary ferrite [Ref. 17:p. 1180]. Note that this is an indirect effect of Ti on the amount of acicular ferrite. Brownlee, Matlock and Edwards note [Ref. 16:p. 249] that instead of the intragranular regions transforming to acicular ferrite, the transformation proceeds to ferrite with aligned carbide due to the small number of intragranular precipitates; thus Ti serves as a precipitation hardener.

12. Zirconium

Zirconium, Zr, is a strong carbide and nitride former which in small amount is beneficial for lowering the austenite transformation temperature and promoting the formation of acicular ferrite.

13. Boron

The Ti-B interaction model presented by Mori suggests that boron is not desirable unless sufficient Ti is available to scavenge the nitrogen and prevent boron nitride formation [Ref. 17].

14. Oxygen

Oxygen, O, is an impurity that is detrimental because of its propensity toward microvoid coalescence leading to porosity and its role in the formation of non-metallic inclusions. The free energy of FeO at weld pool temperatures near 2000 °C is higher than the free energy of Al_2O_3 , TiO_2 , or SiO_2 , thus these others will form preferentially [Ref. 18:p. 4].

15. Nitrogen

Nitrogen, N, is an impurity that lowers toughness of the weld metal through the formation of non-metallic inclusions. Removal of Nitrogen by Al additions and the formation of small AlN inclusions lowers the lattice resistance to dislocation motion and lowers the DBTT. Other nitride formers, besides Al, are Ti, Si, and Zr, all of which are preferred over the brittle Fe_4N intermetallic.

16. Hydrogen

It is desired to lower H to improve ductility by minimizing hydrogen embrittlement. The hydrogen problem in HY-100 steel has drawn attention to itself as local areas of welds exceeded the 130 ksi susceptibility level. Weld pool stirring allows the mixing of ionized hydrogen gas that diffused from the surface, from the welding wire, or hydrocarbon contaminants. During solidification to austenite the cooling rate is high enough to allow retention of hydrogen, thus obtaining a supersaturated austenite phase. As cooling progresses, diffusion continues, but the ferrite and martensite phases that follow have even lower solubility limits for hydrogen. This situation sets up a condition of internal strain induced by the supersaturated level of hydrogen. In the past it was thought

that compositional differences in welding consumables did not play an important factor on the amount of non-diffusible hydrogen, but differences have been observed. The Ship Structure Committee has recommended against the recycling of any recovered flux since it may have picked up dirt or oil which can not be removed by oven dehumidification. This report also addressed the conditions necessary for HIC and a potential solution through hydride formers. The stated conditions necessary for HIC are a critical concentration of diffusible H in a weldment with hard microstructure under residual stress at temperatures between -100°C and 200°C [Ref. 19]. It is recommended that fluxes contain specific amounts of hydride formers such as Ca, Mg, Ti, Zr, Hf, Ce, La, Pr, Sr, and Y which may not participate in the embrittlement [Ref. 20:pp. 167-169]. It is certain that research into the stability of these individual hydrides in the welding environment needs to be accomplished before the case on hydrogen induced cracking can be closed.

17. Phosphorus

Phosphorus, P, is an impurity that contributes to hot cracking and poor ductility, but the magnitude of these effects is not so well known. Nevertheless, the requirement is that it be maintained less than 0.01% in the high strength steel and weld metal.

18. Sulfur

Sulfur, S, is an impurity that contributes to hot cracking and poor ductility. The hot cracking can be eliminated by Mn addition to preferentially form MnS over FeS which has a much lower melting point. Nucleation of voids can begin at the surface of MnS inclusions, thus as S increases toughness decreases as is common in the lowering of the CVN upper shelf energy and DBTT. For this reason, high strength steels and weld metals require sulfur to be maintained less than 0.008% and less than 0.005 % if possible to minimize rejection of sulfur from solution and hence FeS formation at the grain boundaries.

E. WELD METAL MICROSTRUCTURE

The size, shape and distribution of non-metallic inclusions are important since they affect the austenite-ferrite transformation temperature and are known to promote the formation of acicular ferrite in alloys with certain transformation kinetics. Ricks, Howell and Barrite note that the energy barrier for nucleation of acicular ferrite with inclusions is a function of inclusion size. The energy barrier decreases as inclusion size increases up to 1.0 micron and then becomes independent of inclusion size [Ref. 21:pp. 463-468]. Pickering noted that spherical inclusions provide for improved toughness and increased transverse and through-thickness ductility [Ref. 7:p. 82].

1. Non-Metallic Inclusions

a. Sources

Indigenous inclusions are typically oxides from deoxidation reactions or precipitation reactions. These inclusions that remain in the weld metal are those that for some reason did not escape to the surface as slag. Reasons for this are still under investigation but include a complex mixture of weld pool buoyancy, viscosity, and circulation. The equilibrium formation of the inclusions is limited by the cooling rate and the concentrations of elements present which will be likely to precipitate at their natural stoichiometric composition. Because of the rapid cooling rate, some inclusions may not achieve a stoichiometric ratio of elements based on their solidification temperature and the temperature for which the delta-iron phase is complete. Exogenous inclusions are detrimental although typically sporadic in occurrence and irregular in shape and are the result of entrapped slag or trash.

b. Sizes

Small inclusions, less than 1.0 micron, are effective at pinning grain boundaries in high temperature austenite; thus they restrict grain growth allowing more grain boundary area for nucleation of grain boundary ferrite [Ref. 22:p. 767]. Since the

austenite microstructure and acicular ferrite nucleation are interrelated through the presence of inclusions, it seems that a high volume fraction of inclusions of mean diameter less than 1.0 micron would be preferable. The conflict lies in the transformation kinetics because the slower cooling rate provides more time for the non-metallic inclusions to nucleate, grow and rise to the slag. The larger inclusions have a higher buoyancy; hence it is reasonable, through Stokes Law, that the welds with larger inclusions would have fewer inclusions because the larger inclusions can achieve a higher escape velocity. The shape of the inclusions is dependent on the chemical composition and whether there had been sufficient time for the inclusion to reach an equilibrium composition.

2. Acicular Ferrite

Acicular ferrite is a finely grained microstructure consisting mainly of intragranularly nucleated Widmanstätten ferrite with ferrite grains of about 1 to 2 microns in width. Acicular ferrite is preferred since an entirely acicular ferrite microstructure eliminates the grain boundary ferrite or bainite fracture paths. For this reason it is necessary to optimize the time-temperature window for acicular ferrite nucleation by controlling the cooling rate based on the predicted chemistry of the weld metal.

According to Ricks, Howell, and Barritte there are three ways that inclusions promote intragranular nucleation of acicular ferrite [Ref. 21:p. 736]. Inclusions reduce the energy barrier to nucleation since they act as an inert substrate. Nucleated acicular ferrite orients itself with respect to the inclusion and the austenite, causing low energy interfaces to form between the austenite and the inclusion. Inclusions also affect the local chemistry of the austenite increasing the transformation driving energy. Abson recommends an optimum weld metal oxygen content of 0.030%. For oxygen levels that are much less than 0.025% the microstructure is mainly bainitic with little or no acicular ferrite. When the oxygen content is too low, there are not enough nucleants, hence the cooling weld is less

likely to form acicular ferrite. He also notes that inclusion size and type are more important than volume fraction [Ref. 23].

Kiessling states that intragranular nucleation of acicular ferrite at inclusions is preferentially associated with Al-Mn silicates which contain a small amount of Ti [Ref. 24:p. 105]. To optimize nucleation of acicular ferrite with large austenite grains, a high density of intragranular inclusions and sufficient weld metal cooling time was recommended. Grong and Matlock state that weld metal cooling time must be greater than five seconds to favor nucleation of acicular ferrite [Ref. 25]. Brownlee, Matlock and Edwards note that as the percentage of acicular ferrite in the microstructure increases, the transition temperature decreases [Ref. 16]. As acicular ferrite increases, the energy absorbed during impact rises, demonstrating the importance of high volume fraction of acicular ferrite on toughness. They also observe a minimum in transition temp near 0.022 w% Al, indicating a change of toughness directly related to the effects of Al on the weld microstructure. Even hardness is determined to be closely controlled by the presence of high volume fractions of acicular ferrite in the microstructure with the optimum at 0.022 w% Al. All of this previous work points to the fact that non-metallic inclusions containing Al, Si, Mn and Ti are responsible for the improvement in mechanical properties through the nucleation of acicular ferrite.

F. SCOPE OF THE PRESENT WORK

The overall objective of the project was to determine how various fluxes affected the microstructure and in turn how this related to the mechanical properties of SAW weldments on HY-100 steel. An evaluation of the effects of variations in flux composition with weld metal microstructure and mechanical properties is necessary. Also necessary is an investigation of the retention of strength and toughness in the multi-run regions that had been remelted and reheated. There are differences in the way that strength and

toughness are affected by the chemical composition and the microstructure. Weld metal composition is controlled by the dilution of the base plate and transfer of elements between the flux, the weld metal and the slag.

The experimental design factors defined by the Annapolis Detachment of the Carderock Division of the Naval Surface Warfare Center, (formerly DTNRC), were intended to ensure equivalent welding conditions to provide the same cooling rate for each weldment. Since welding in a laboratory is better controlled than in an industrial environment, there exists a need to establish improved structure-property correlations in complex weld metal microstructures using variables that are easily controllable. Correlations between flux chemistry and mechanical properties are intended to be used in the optimization of weld metal strength and toughness through a balance of these factors as related to overall flux chemistry. In this steel composite in which slight variations in the molten alloy's composition are reflected in the composition of the precipitated non-metallic inclusions, the shape, size, composition and distribution of the non-metallic inclusions may have a beneficial or deleterious effect on the mechanical properties of the matrix. This observational study attempts to focus on the effects of flux chemistry variations as present in five different commercial fluxes.

III. EXPERIMENTS AND TESTS

A. HY-100 STEELS

Five one inch HY-100 base plates were joined at the Annapolis Detachment of the Carderock Division of the Naval Surface Warfare Center, NSWC, using a single-vee butt weld geometry supported from below by a backing plate. The vee was placed on a similar backing plate and had a 0.5 inch root gap with a 45 degree angle. Table 3-1 below gives further details on the plate chemistry. No alterations were made to the base plate or the consumables used in the welding process.

TABLE 3-1. HY-100 BASE PLATE AND FILLER WIRE CHEMISTRY.

Element Sample↓	C w%	Mn w%	Si w%	P w%	S w%	Ni w%	Mo w%	Cr w%	V w%	Al w%	Ti w%	Zr w%	Cu w%	O w%	N w%	B w%	H ppm
HY-100 Tag 372	0.157	0.33	0.3	0.003	0.005	2.79	0.36	1.46	0.006	0.018	0.004	<.001	0.097	0.0054	0.016	0.001	1.1
L-TEC 120 wire	0.081	1.57	0.4	0.004	0.006	2.25	0.42	0.28	0.001	0.012	0.014	0.012	0.011	0.003	0.004	0.004	2.8

B. SUBMERGED ARC WELDING PROCEDURE

The requirements of MIL-E-23765/2D were adhered to concerning the heat input, the preheat/interpass temperatures and the baking of the flux. The heat input was restricted to 55.3 kJ/inch to achieve the necessary tensile strength in the weld metal. Chromel-alumel thermocouples were plunged into the solidifying weld pools allowing good readings on about 50% of the passes. The cooling rates observed in this manner agreed with those that had been calculated and for which the welding speed had been determined. Table 3-2 shows the control variables that were used by NSWC in the design of this experiment. Note that there was a variation in the number of passes required to join the plates. This lead to a further study to determine if this had an impact on the

strength or toughness of the weld metal samples that were cut from the plates for tensile and Charpy V-notch tests.

TABLE 3-2. WELDING EXPERIMENT CONTROL PARAMETERS.

PROCESS	SAW
BASE PLATE TYPE	HY-100
PLATE THICKNESS	1 inch
ROOT GAP/ ANGLE	0.5" / 45 deg.
NUMBER OF PASSES	21 or 24
GROUND PLACEMENT	Dogged corners and sides on grounded table
WIRE TYPE	L-TEC 120 (HT 120022)
WIRE DIAMETER	3/32"
TIP TO WORK DISTANCE	5/8"
CURRENT	500 amps, DCRP
VOLTAGE	35 V
TRAVEL SPEED	19 in/min
HEAT INPUT	55.3 kJ/in
PREHEAT/INTERPASS TEMP	250-275 °F
COOLING RATE	18-23 °F/sec @ 1000 °F by Plunged thermocouple
POST WELD SOAK	NONE
FLUX RECYCLED	NONE

C. WELDING CONSUMABLES

1. Wire Electrode

The combined electrode/filler wire used in welding the samples was a 3/32 inch diameter L-TEC 120, HT 120022, spooled wire with chemistry as shown in Table 3-1.

2. Fluxes

The purpose of the agglomerated flux is to melt and provide a shielding for the filler wire during metal transfer and the weld pool during solidification. Alloying takes place as a result of the presence of elements intended for deoxidation and slag detachment. This alloying may serve to purposefully alter the mechanical properties of the weldment.

Since mechanical properties are dependent on flux composition the extent of the alloying is very important. Table 3-3 shows the commercial fluxes that were used. Table 3-4 shows the aggregate flux chemistry for each of the fluxes as determined by merging the applicable flux chemistry analysis data provided in Appendix A, Tables A-1 through A-3. Flux composition, when correlated with the factors that affect the weld metal properties, can be used to engineer an optimum flux for SAW application with HY-100 steel.

TABLE 3-3. FLUXES AND DESIGNATIONS USED BY VARIOUS RESEARCHERS .

Sample Designator	FLUX	CDNSWC ID No.	USGS Lab. No.
F289	Oerlikon OP121TT; Lot 047012 (Eisenberg)	S3	D-330827
F292	Oerlikon OP121TT; Lot 1131 (Houston)	H5	D-330819
F293	Kobe PFH80AK; Lot 7DRP810	M2	D-330824
F295	L-TEC 651 VF; Lot 1161 C2115	L2	D-330823
F296	Lincoln MIL800, Lot 317V R29505	R2	D-330826

The values of the basicity, B , and basicity index, BI , for fluxes used in this study are shown in Table 3-5 from the Easterling and Eagar relationships.

$$B = \frac{\text{CaO (+ CaF}_2\text{)} + 1.4\text{MgO} + 0.90\text{Na}_2\text{O} + 0.60\text{K}_2\text{O} + 0.45\text{ZrO}_2}{\text{SiO}_2 + 0.59\text{Al}_2\text{O}_3}$$

$$BI = \frac{\text{CaO (+CaF}_2\text{)} + \text{MgO} + \text{Na}_2\text{O} + \text{K}_2\text{O} + \text{Li}_2\text{O} + .5(\text{MnO} + \text{FeO})}{\text{SiO}_2 + .5(\text{Al}_2\text{O}_3 + \text{TiO}_2 + \text{ZrO}_2)}$$

TABLE 3-4. FLUX CHEMISTRIES IN W% FOR THE FIVE TYPES OF FLUX USED.

FLUX	Al ₂ O ₃	Fe ₂ O ₃	K ₂ O	MgO	Na ₂ O	CaO	CaF ₂	SiO ₂	TiO ₂	MnO
F289	18.139	1.086	0.987	28.804	0.937	10.130	22.113	14.647	0.718	0.887
F292	18.423	1.372	0.682	28.234	0.711	12.479	22.214	13.517	0.701	0.831
F293	13.210	1.200	1.250	28.537	2.007	17.410	14.087	16.638	0.0	0.051
F295	16.868	1.996	0.389	34.934	1.228	8.090	17.224	15.570	0.679	2.515
F296	15.473	1.055	1.346	32.252	1.206	9.896	21.054	14.569	0.523	1.608

FLUX	Ce ₂ O ₃	P ₂ O ₅	BaO	ZrO ₂	V ₂ O ₅	Cr ₂ O ₃	Y ₂ O ₃	Cu ₂ O	NiO	SrO
F289	0.003	0.0	0.044	0.033	0.014	0.019	0.005	0.007	0.003	0.0083
F292	0.006	0.0	0.024	0.029	0.017	0.019	0.004	0.0	0.004	0.0088
F293	0.250	0.0	0.022	0.003	0.006	0.008	0.002	0.005	0.007	0.0114
F295	0.010	0.08	0.026	0.033	0.018	0.051	0.006	0.002	0.004	0.0189
F296	0.004	0.0	0.006	0.059	0.009	0.086	0.004	0.003	0.024	0.0043

FLUX	La	Mo	Nd	Zn	ThO ₂	Pb	Ga	Co	Loss on Ign
F289	0.004	0.0	0.0	0.0	0.0	0.0	0.0	0.001	1.405
F292	0.005	0.0	0.003	0.0	0.0	0.0	0.0	0.001	0.719
F293	0.184	0.005	0.064	0.028	0.0	0.0	0.0	0.006	5.012
F295	0.006	0.0	0.005	0.0	0.004	0.0	0.003	0.002	0.240
F296	0.004	0.0	0.0	0.0	0.0	0.005	0.003	0.003	0.804

TABLE 3-5. BASICITY INDEX FOR FLUXES USED.

FLUX	B	BI	B (w/CaF ₂)	BI (w/CaF ₂)
F289	2.05	1.74	2.92	2.65
F292	2.17	1.87	3.09	2.83
F293	2.45	2.14	3.03	2.75
F295	2.29	1.93	2.96	2.63
F296	2.40	2.04	3.29	2.97

Note that the most basic flux, F296, had the highest basicity in both cases. The other fluxes, however, obviously had distinctions that prevented them from even following a trend. Flux F293 was lowest in Al₂O₃, highest in CaO, highest in SiO₂, had more rare earth elements and lost about 5% of its weight during ignition. This loss on ignition at

900 °C is presumed to be from carbonates. While flux F295 had low weight percent of CaO, it had the most MgO and MnO. The two fluxes that were made by the same manufacturer, F289 and F292, were quite similar in their composition, but did not have a similar basicity using either the Easterling equation, the Eagar equation, or the modified equations. As shown later in the section on mechanical properties, these two fluxes produced very different welds.

D. WELD METAL ALLOYING

1. Chemical Determinations

The weld metal composition was determined for NSWC by another laboratory, and data was obtained by XRF for 16 different elements. The residual hydrogen levels were measured using vacuum hot extraction. The base plate, filler wire and weld metal compositions along with the confidence limits are shown in Table 3-6. No analysis was made of the self peeling flux which may have held clues to some of the complex interactions discovered in these alloys. Although some researchers attempt to relate the chemistry of non-metallic inclusions to the over all weld metal chemistry, it is presently nearly impossible to distinguish the elements of the non-metallic inclusions from the elements in solid solution. Sample F295 was high in sulfur and phosphorus, which could account for the low toughness that will be noted later. Sample F296 had a high amount of residual hydrogen that may in part account for the severe cracking exhibited in that sample. There were also areas of the F296 weldment in which macrosegregation, dendritic structures and solidification cracking were observed, indicating that the sample received for testing may have been a lower quality portion of the weldment that otherwise tested so high in strength and toughness. All samples had oxygen levels between 0.027% and 0.035%; a low oxygen range, which is clean for SAW, and are likely to have significant amounts of acicular ferrite in the microstructures.

2. Dilution

Dilution of the base plate into the weldment is important since it is not just the filler wire-flux interaction that determines the final chemistry of the weld. Based on the available weld metal chemistry, no two elements used for the dilution calculation provided the same result. This is just another indicator as to the complexity of the chemical transfer occurring in the molten weld pool. However, the location from which the mechanical test specimens were taken at the upper central region of the weldment ensured minimal dilution. The tensile specimens were taken longitudinally along the length of the weld, while the Charpy V-notch specimens were taken transversely across the weld with the notch cut in the low dilution volume.

TABLE 3-6. CHEMICAL COMPOSITION OF THE BASE, FILLER, AND WELDMENTS.

	C	Mn	Si	P	S	Ni	Mo	Cr	V	Al	Ti	Zr	Cu	O	N	B	H
	w %	w %	w %	w %	w %	w %	w %	w %	w %	w %	w %	w %	w %	w %	w %	w %	ppm
Filler	0.081	1.57	0.4	0.004	0.006	2.25	0.42	0.28	0.001	0.012	0.014	0.012	0.011	0.003	0.004	0.004	2.8
HY100	0.157	0.33	0.3	0.003	0.005	2.79	0.36	1.46	0.006	0.018	0.004	0	0.097	0.0054	0.016	0.001	1.1
F289	0.062	1.45	0.38	0.007	0.01	2.33	0.46	0.25	0.003	0.013	0.006	0.003	0.02	0.03	0.007	0.004	0.2
F292	0.062	1.49	0.46	0.005	0.006	2.56	0.52	0.43	0.003	0.02	0.008	0.003	0.023	0.027	0.006	0.003	0.4
F293	0.056	1.28	0.42	0.004	0.006	2.51	0.47	0.4	0.002	0.011	0.004	0.003	0.017	0.034	0.006	0.004	0.4
F295	0.064	1.51	0.28	0.015	0.011	2.34	0.47	0.47	0.004	0.011	0.005	0.002	0.021	0.035	0.009	0.004	0.3
F296	0.064	1.54	0.34	0.008	0.007	2.34	0.49	0.5	0.003	0.014	0.006	0.004	0.026	0.032	0.006	0.001	0.8
CL ±	0.001	0.02	0.01	0.002	0.001	0.05	0.01	0.02	0.001	0.002	0.001	0.001	0.002	0.001	0.001	0.001	0.0001

Molybdenum could not be used for determining % Dilution because it has a higher concentration in the weld metal than in either the base plate, filler or flux. This can be accounted for by the reduction of carbon in the weld metal which causes the remaining elements to share a greater weight percent of the chemistry. This in itself indicates that any other element used for % Dilution calculations may not give an expected result. Table 3-7 lists some of the results of the correlations that were considered. Note the agreement between CE and B_S.

The results of the calculations to determine % Dilution bring to light some of the significant changes in filler wire composition that occur from the time the atoms leave the wire in the plasma arc and until they solidify in the weld. Some of the interesting items to note are the losses of alloying elements. F289 lost a significant amount of Cr. F292 and F293 both sustained a significant unexplained increase in Ni accompanied by additional Si probably from the flux. The rise in Si in F293 could be justified from the higher w% SiO₂ in that flux, but this was not so for F292 that was produced with the flux that contained the lowest w% SiO₂. Note however, that F292 had a higher w% Al₂O₃ in the flux. It will be shown later that this along with the higher w% CaO had a role in the increase in Si in the weld metal. Sample F293 also encountered the highest loss in C and Mn. Recall that this flux not only had the lowest Mn and lowest basicity *B*, but had a high percentage loss on ignition and the additional rare earth elements. It seems most probable that the Mn could have been depleted merely by the deoxidation that occurred during formation of non-metallic inclusions.

TABLE 3-7. CORRELATION TOOLS.

FLUX	CE	B _s (°C)	% Dilution Cr	% Dilution Ni	% Dilution Cu
F289	.25	541	-.03	.14	.10
F292	.27	511	.13	.57	.14
F293	.25	540	.10	.48	.07
F295	.26	518	.16	.17	.11
F296	.26	512	.19	.17	.17
Base	.34	-	-	-	-
Filler	.27	-	-	-	-

Note that the most basic flux, F296, which had the highest basicity in both cases suffered the least loss of alloying elements. This as we shall see later will also be evident in the strength of this weldment. While flux F295 had lowest w% CaO and the highest

w% MgO and MnO, it suffered the largest loss of Si in the weld metal. When the basicity is high, there are more hydride formers like Ca and the rare earth elements present, possibly resulting in a higher potential for hydride formation. These hydrides that can not diffuse out of the rapidly cooling weld remain as residual hydrogen. This may explain the trend shown in Figure 3-1, although it should be noted that the levels of residual hydrogen are very low for all the weldments. Since the flux was not tested for sulfur, it is difficult to determine the source of the sulfur that is above the maximum specification, 0.01% in two cases. Figure 3-2 shows the cleaning effect of the higher basicity fluxes on weld metal desulfurization. Samples F289 and F295 which had S and P levels above 0.01% had the lower toughness.

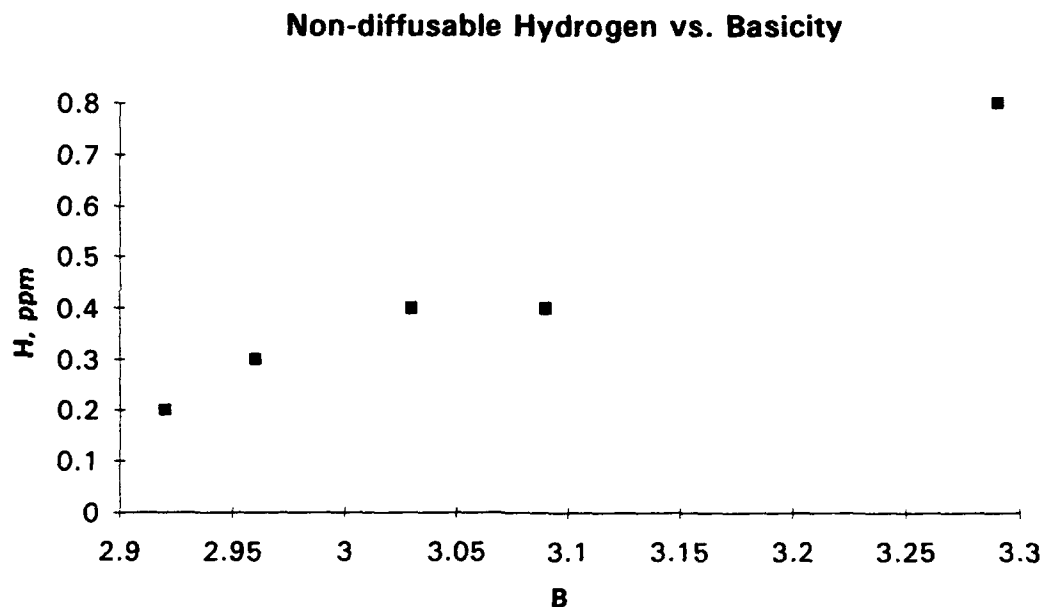


Figure 3-1. Non-diffusible hydrogen versus Basicity.

E. MECHANICAL TESTS

Five weldments were provided by NSWG along with data on mechanical testing that was performed in accordance with MIL-S-24645/2D(SH). Test results for strength and toughness were provided on receipt of the weldments at the Naval Postgraduate School.

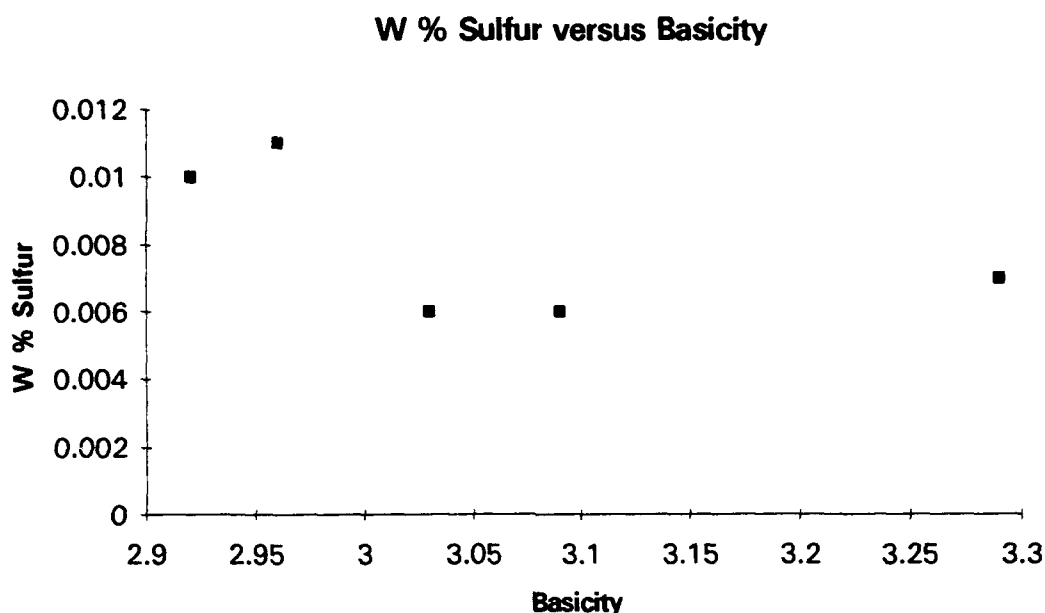


Figure 3-2. Weld metal sulfur versus Basicity.

1. Tensile Test

The purpose of the tensile tests was to measure weld metal strength. Each weldment was sectioned, and two longitudinal 0.505 inch diameter tensile samples of weld metal, taken from a depth 1/8 inch below the surface, were machined and stressed until failure. From this data certain factors can be used for further analysis. These factors include yield strength, YS, ultimate tensile strength, UTS, percent elongation, % EL, and percent reduction of area, % RA.

2. Charpy Toughness Test

The purpose of the Charpy V-notch toughness tests was to measure weld metal impact toughness through absorbed energy measured during fracture. Toughness depends on microstructure, non-metallic inclusions and alloying elements in solid solution. Each weldment was sectioned, and 26 10 mm by 10 mm by 2.5 inch transverse Charpy V-notch samples were machined and fractured. From this test data certain factors can be used for further analysis. These factors include lower shelf energy, LSE, upper shelf energy, USE,

50 percent fracture appearance transition temperature, 50% FATT, ductile to brittle transition temperature, DBTT, and 50 ft-lb transition temperature. The 50% FATT is uniquely different from the other factors, because this method eliminates the effect of variations in strength on toughness since its basis is in the visual appearance of the fractured surface.

3. Dynamic Tear Test

The purpose of the dynamic tear test was to measure overall weld metal and heat affected zone toughness through absorbed energy during fracture. Each weldment was sectioned, and two $1\frac{5}{8}$ by $\frac{5}{8}$ by $7\frac{1}{8}$ transverse dynamic tear test samples were machined and fractured. From this test data the absorbed energy was used for further analysis.

4. Microhardness Test

The purpose of the diamond pyramid hardness tests was to measure overall weld metal hardness. A series of micro hardness tests was performed on each of the samples and the base plate, all of which had been polished to a one micron finish. Measurements were taken at random locations in the weldment with a Micromet® microhardness tester using a 100 gm impression weight and a Vickers diamond indenter. The area covered during these tests was limited to the general location for which the chemical compositions had been determined and mechanical tests had been performed. This was necessary to ensure that attempts to determine the cause for the variations in the strength and toughness would be focused on the same representative portion of the weld.

F. SCANNING ELECTRON MICROSCOPY

A Cambridge Stereo Scan S200 scanning electron microscope was used with a LaB₆ filament energized to 20,000 volts. The non-metallic inclusions were small enough to border on the limits of resolution of the SEM, requiring a special procedure to analyze

compositions. Since mechanical properties and chemistry were only known for a certain volume of the weldment, care was taken to ensure that observations were restricted to the same general area on the specimen.

1. Inclusion Analysis

Each sample was polished to a one micron finish and examined at a working distance of 9 mm and a magnification of 7.04K times using back scatter imaging. The resultant field of view was 15 microns by 12 microns in size. The inclusions were counted and sized using 100 random fields for each sample.

2. Energy Dispersive X-Ray Analysis

To further characterize the inclusions present in each of the welds, a study of the non-metallic inclusions was conducted. A unique technique with the EDX permitted a detailed analysis of inclusion composition. This process was accomplished on the Kevex 8000 in the following manner. The inclusions and the matrix were both separately acquired at a 18 mm working distance with a LaB₆ filament at 20.0 Kv. The energy dispersive x-rays were first counted for the background matrix region directly adjacent to an inclusion. This data was held temporarily for later use in determining the elements present in the inclusion. The x-rays emitted from the inclusion were then acquired at a count rate and total x-ray count consistent with that of the background matrix. The data for the background matrix was then subtracted from the inclusion data to eliminate the effect of the matrix 'noise' on the analysis of the inclusion. This was certainly necessary because the bulb of interaction went well below the inclusion. The remaining x-ray data was then analyzed to identify the elemental constituents of the inclusion. Through this process, the atomic percentages and weight percentages of the elements present in the oxide type inclusions could be determined and categorized.

G. OPTICAL MICROSCOPY

Optical metallography was performed on transverse weld metal sections that were polished to a one micron finish and etched for 15 seconds with 5% Nital. The weld metal area and HAZ were examined for evidence of cracking. Micrographs were taken at 1000x magnification. The specimens were examined to determine the type of microstructures. The weldments were also etched for 400 seconds with a solution of 5 grams sodium hydroxide per 100 ml of 1% aqueous picric acid to etch the inclusions.

A weld metal reheat study was performed by taking macrographs of the whole weldment at 8x magnification. The samples were polished to a one micron finish and etched for 15 seconds with 5% Nital. Because the effects of weld metal reheat were only visible under direct light and ordinary camera lighting was not sufficient for this photography, the photographs were taken under high intensity 1000 watt tungsten lamps. These photographs were scanned into a computer and processed using an image analysis program to determine the representative areas of columnar grain regions, coarsened grain regions and refined grain regions. It is understood that these regions can be broken down into possibly four or five regions, but these were not clearly visible in these multi-run weldments.

IV. EXPERIMENTAL RESULTS AND DISCUSSION

A. MECHANICAL TESTS

Five weldments were provided by NSWC with data on mechanical testing that had been performed in accordance with MIL-S-24645(SH). The completed test results for tensile strength, Charpy V-notch impact toughness and dynamic tear toughness were provided with weldments to the Naval Postgraduate School for further evaluation.

1. Tensile Test

The purpose of the tensile tests was to measure weld metal yield strength, YS, ultimate tensile strength, UTS, percent elongation, % EL, and percent reduction of area, % RA. Table 4-1 shows averaged results of the tensile test. Notice that samples F289 and F293 did not meet the *minimum strength requirement*, and that sample F295 was near the minimum strength requirements. Sample F296 exhibited extremely low ductility during one test, resulting in the low average value for % RA. The % RA is not a value that must meet certain military specifications, but it does provide some insight into the ductility of the weld metal. Sample F296 which had the highest BI had the highest strength; this can be accounted for by noticing the least loss of alloying elements in that sample. This high strength was consistent with later findings of severe cracking in that specimen during visual inspection of the polished sample. It is also possible that specimen F296 was taken from a bad part of the weld arising from welding process control errors. This is proposed since the high quality of the reported mechanical properties was not reflected in the sample analyzed at NPS.

TABLE 4-1. TENSILE TEST DATA.

SAMPLE	YS, Avg. (ksi)	UTS, Avg. (ksi)	El, Avg. (%)	RA, Avg. (%)
F289	100.7	118.8	22.0	62.5
F292	109.1	124.4	19.5	63.0
F293	99.7	114.6	22.5	69.5
F295	102.3	119.4	21.0	63.5
F296	119.7	126.6	16.5	39.5
SPEC.-min	102		14	
SPEC. -max.	123			

Yield Strength vs. Weld Metal Residual Hydrogen

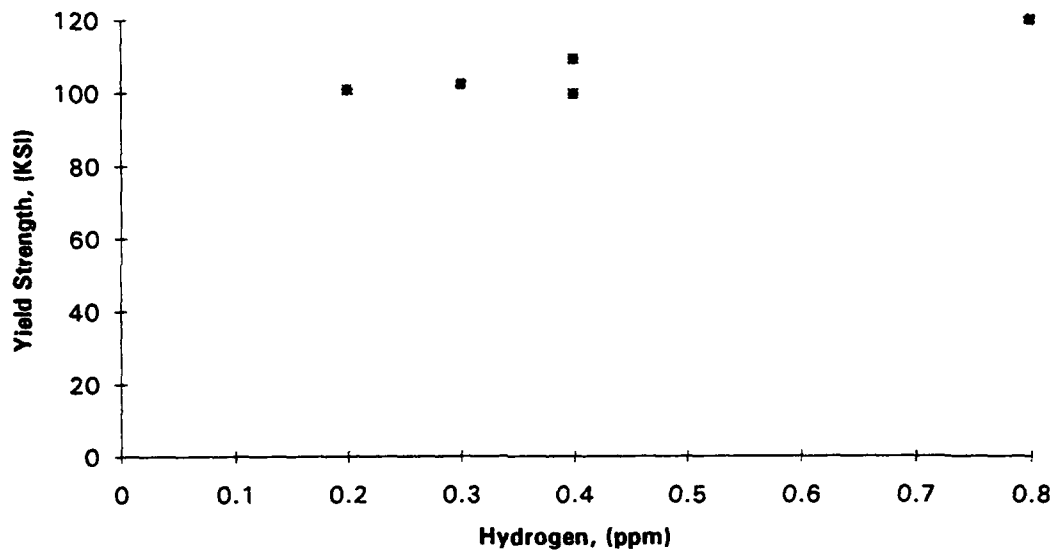


Figure 4-1. Yield Strength vs. Weld metal residual hydrogen.

Note in Figure 4-1 the rise in strength that accompanies the residual or non-diffusible hydrogen. As the CE becomes higher and the martensite and bainite start temperatures are lowered, the weld metal is more likely to form a stronger and tougher microstructure. Accompanying this transformation is the retention of non-diffusible hydrogen which would have otherwise been able to diffuse out of the cooling weldment. This retention may be in the form of hydrides which served as nucleants for inclusions that did not escape to the slag. It is possible that these too helped nucleate acicular ferrite.

Figures 4-2 and 4-3 below show a certain relationship between the flux chemistry and the resultant yield strength. This was expected since the fluxes with higher basicity are more efficient at scavenging oxygen so that atoms responsible for solid solution strengthening are less likely to be denuded from the weld metal matrix as the basicity is increased.

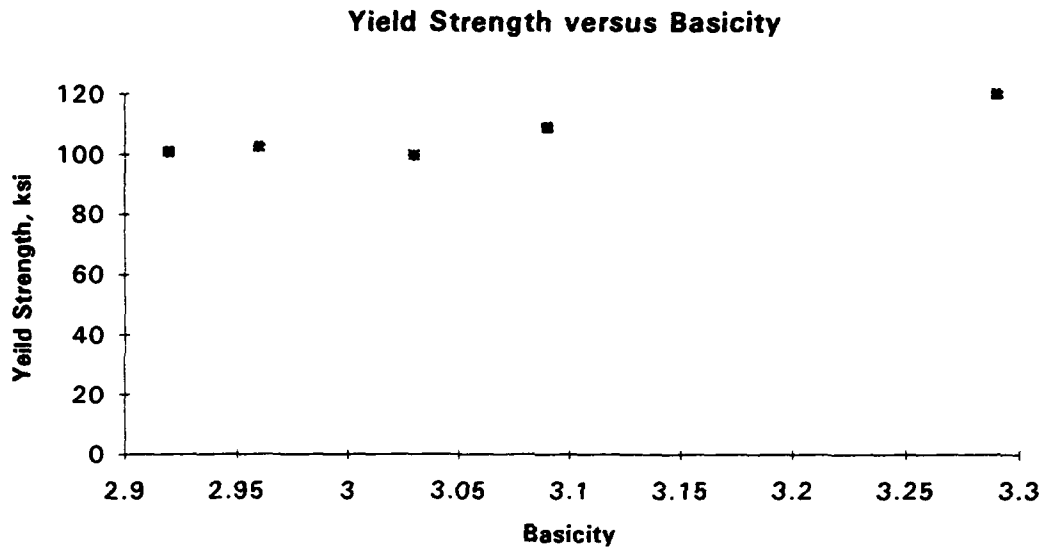


Figure 4-2. Yield Strength vs. Basicity (w/CaF₂) by the Easterling relationship.

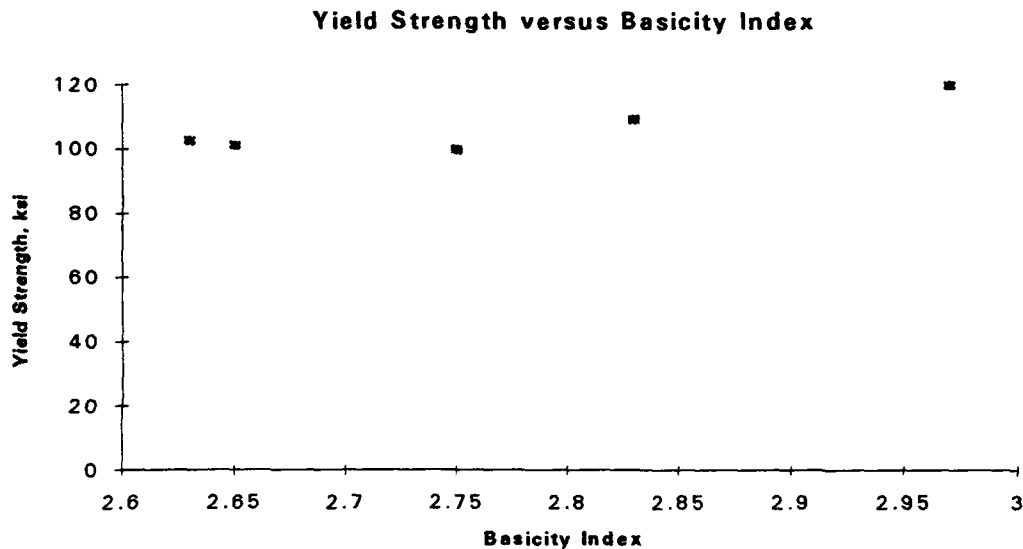


Figure 4-3. Yield Strength vs. Basicity Index (w/CaF₂) by the Eagar relationship.

Figures 4-4 and 4-5 show an expected trend with one sample that did not conform. This was sample F293 which had the lowest MnO and Al₂O₃ and highest SiO₂, giving a false indication of its actual ability to clean the weld metal without denuding it of the solid solution strengtheners. Consequently, this sample had the lowest percentages of C and Mn in the weld metal and thus the lowest ultimate tensile strength.

Ultimate Tensile Strength vs Basicity

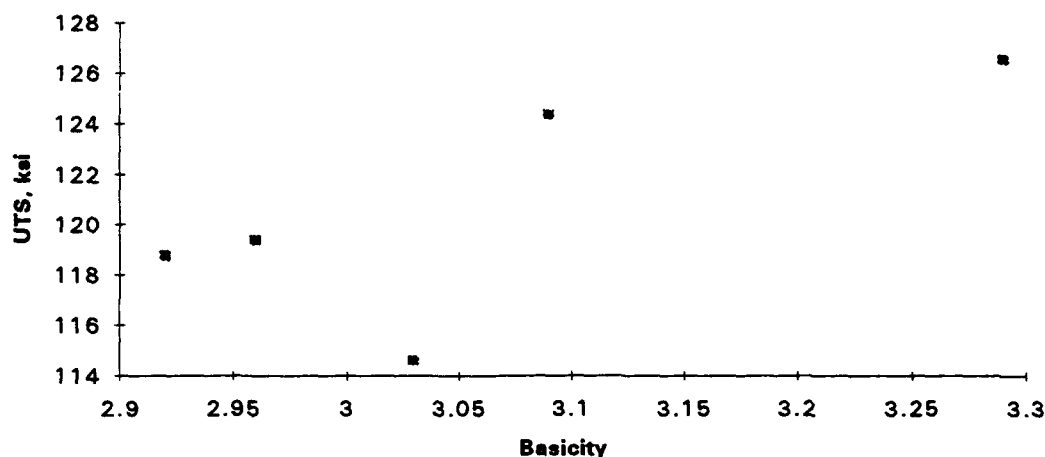


Figure 4-4. UTS vs. Basicity (w/CaF₂) by the Easterling relationship.

Ultimate Tensile Strength versus Basicity Index

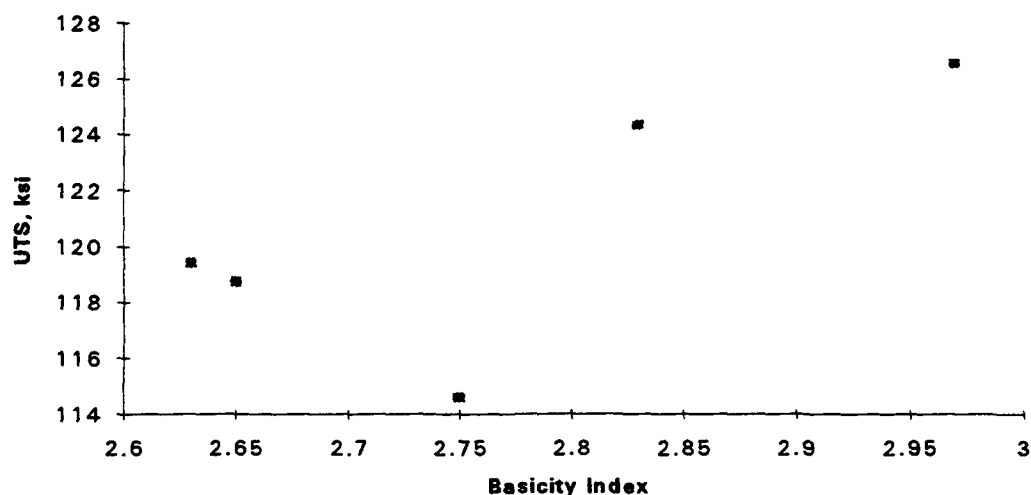


Figure 4-5. UTS vs. Basicity Index (w/CaF₂) by the Eagar relationship.

2. Charpy Toughness Test

The purpose of the Charpy V-Notch toughness tests was to measure weld metal impact toughness through absorbed energy measured during fracture and through fracture appearance. Tables 4-2 through 4-4 show averaged results of the Charpy toughness tests. Figures B-1 through B-5 in Appendix B show the Charpy and FATT curves. The reference transition temperature, RTT, varied for each weldment showing that it is important to perform tests at various temperatures to see the effect of any relationships pertinent to ductility and temperature. It is usually suggested that strength be lowered to increase toughness, but the data reflects an inconsistent effect of strength on toughness due to either too few data points, the effect of multi-run weld reheat or the role of inclusions in the nucleation of acicular ferrite. Notice that sample F295 did not even meet the minimum Charpy V-notch energy specification for toughness at - 60 °F, since two samples failed at 27 and 42 ft-lb. Additionally F293 did not meet the minimum specifications for toughness at -60 °F for one of the individual tests, which are not apparent in this averaged value, failed at 21 ft-lb. The characteristics of F293 were unique in that it had the best upper shelf energy, but it had the lowest 50% fracture appearance transition temperature. Usually there is an inverse relationship between strength and toughness; in this case F296 had the highest strength and the highest toughness.

TABLE 4-2. CHARPY TOUGHNESS TEST DATA.

SAMPLE	CVN LSE (ft-lb)	CVNE -240 F (ft-lb)	CVNE -180 F (ft-lb)	CVNE -120 F (ft-lb)	CVNE -60 F (ft-lb)	CVNE 0 F (ft-lb)	CVNE 60 F (ft-lb)	CVNE 120 F (ft-lb)	CVNE 180 F (ft-lb)	CVNE 240 F (ft-lb)	CVN USE (ft-lb)
F289	8	9	14	38.6	70.7	90.6	104.8	105.3	104.8	106	106
F292	3.5	3.5	14	31.6	62.5	85.3	91.4	94.8	95	98.5	95
F293	12	---	12.5	19.3	48.7	86.1	103.4	113.9	122.8	122.5	120
F295	5	5.5	8	28.5	44	62.8	75.8	86.8	91.5	96	94
F296	7	8	22	46.7	66.2	86.6	86	92	95.5	103	92
Spec.-min.					45	60					

TABLE 4-3. FRACTURE APPEARANCE TEST DATA.

SAMPLE	FATT -240 F (%BF)	FATT -180 F (%BF)	FATT -120 F (%BF)	FATT -60 F (%BF)	FATT 0 F (%BF)	FATT 60 F (%BF)	FATT 120 F (%BF)	FATT 180 F (%BF)	FATT 240 F (%BF)
F289	95	90	67.5	44	30	5	1.67	0	0
F292	100	100	87.5	46	14	0	0	0	0
F293	100	100	83.3	54	28	12.5	1.67	0	0
F295	100	90	63.3	53.3	36.7	10	1.67	0	0
F296	95	80	60	30	10	3	2.5	0	0

TABLE 4-4. TRANSITION TEMPERATURE DATA.

SAMPLE	50 ft-lb TT °F	DBTT °F	50% FATT °F
F289	-99	-84	-65
F292	-85	-85	-65
F293	-62	-62	-49
F295	-44	-44	-52
F296	-108	-108	-99

Basicity vs. 50% Fracture Appearance Transition Temperature

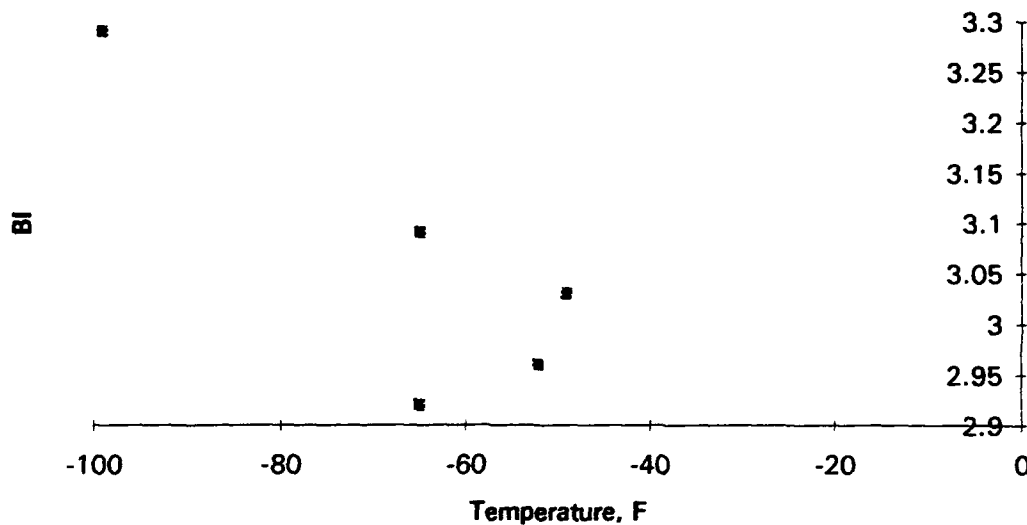


Figure 4-6. Basicity versus 50% Fracture Appearance Transition Temperature.

In Figures 4-6 and 4-7 one can see the toughening effect of the higher basicity fluxes. Note that there is an outlier, F289, which shows higher toughness than would be expected by its low value of basicity. This sample had the lowest w% Cr and hence had the highest bainite start temperature. It is noteworthy that F289 and F295 followed the normal expectation that, if strength were low, the toughness would be higher. The reasoning behind the others not following this trend can only be attributed to a microstructure toughened through acicular ferrite. Although sulfur is often blamed for reduction in toughness, the S content was too low to reproduce that effect here especially since F289 and F295 had the highest levels of sulfur in the weld metal.

Looking ahead to the results of a future section, the author would like to comment here that sample F289 also had the lowest amount of residual hydrogen, 0.2 ppm, and under the optical microscope showed no hairline cracks such as had been present to some extent in all the other samples. Recalling that these welds were not subjected to the customary post weld soak, it is expected that the results may have varied had that procedure been accomplished.

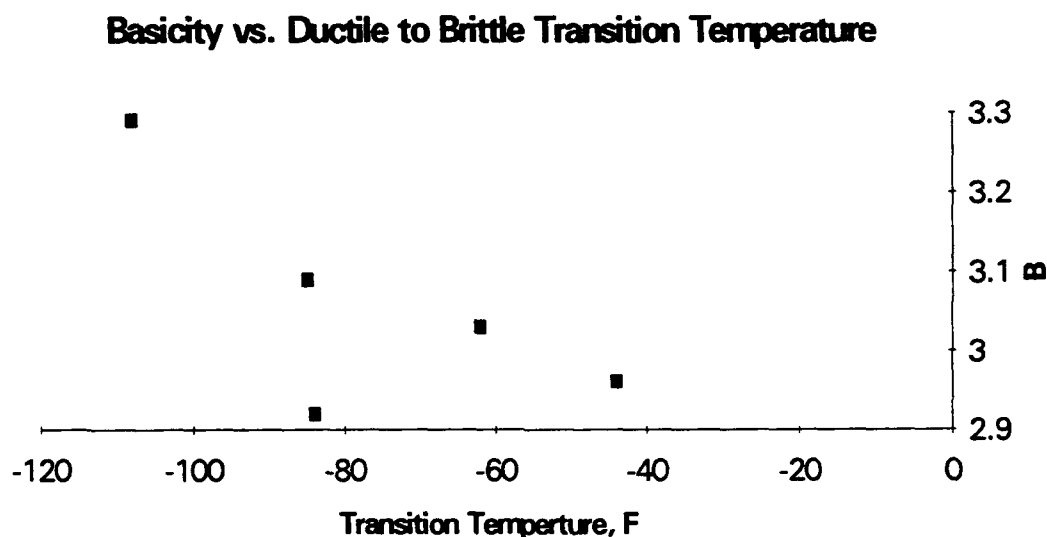


Figure 4-7. Basicity versus Ductile to Brittle Transition Temperature.

3. Dynamic Tear Test

The purpose of the dynamic tear tests was to measure overall weld metal and heat affected zone, HAZ, toughness through absorbed impact energy during fracture. Table 4-5 shows averaged results of the dynamic tear tests. Notice that samples F293 and F295 did not meet the specifications for minimum absorbed energy. This confirmed the lower energy absorbed in each those weld metal samples in the Charpy V-notch impact toughness tests. F293 during those tests dropped an incredible 1000 ft-lb span over just a 50°F drop in temperature. These test results show the importance of performing the dynamic tear test at the two different temperatures. Figure 4-8 is included as a reminder that the effect of the flux basicity in the weld metal center, which was obvious in the Charpy tests, does not extend to the whole weldment.

TABLE 4-5. DYNAMIC TEAR TEST DATA.

SAMPLE	DTE @ -20°F (ft-lb)	DTE @ 30°F (ft-lb)
F289	1074	1119
F292	684	972
F293	209	1235
F295	366	757
F296	880	1035
SPEC.-min	400	575

Dynamic Tear Test (30F) Energy vs Basicity

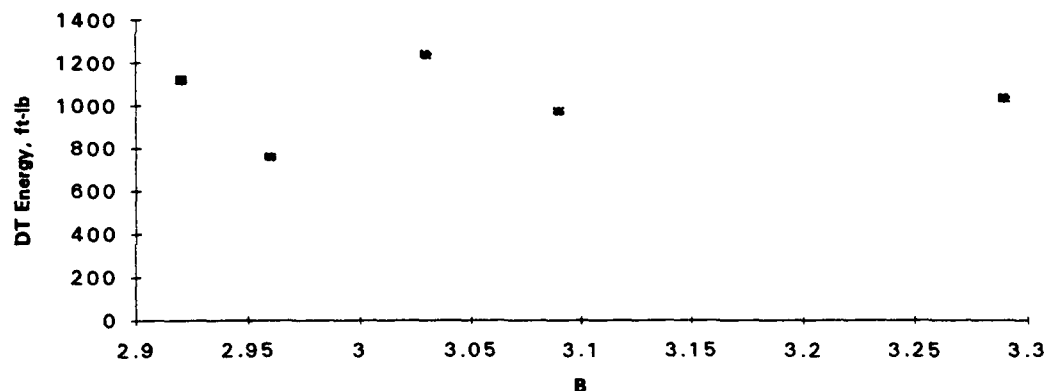


Figure 4-8. Dynamic Tear Test Energy vs. Basicity.

4. Microhardness Test

The purpose of the diamond pyramid hardness tests was to measure overall weld metal hardness. A series of ten micro hardness tests was performed on each of the samples and the base plate with a 100 gm impression weight. Measurements were taken at random locations in the weldment and good reproducibility of results was obtained. The area covered during these tests was limited to that location for which the mechanical tests had already been performed. This was necessary to ensure that attempts to determine the cause for the variations in the strength and toughness would be focused on the same representative portion of the weld. The HY-100 weld metal has a higher hardness than the HY-100 base metal and a lower hardness than the HAZ for each flux variation. Table 4-6 shows those test results which also agree nicely with the variations in strength shown in Table 4-1. That the DPH values were consistent with the tensile strengths provided assurance that the samples provided by NSWC were labeled correctly. Figure 4-9 shows the relationship that higher basicity certainly promotes hardness through less loss of alloying elements. Note how the DPH values in the base plate are very similar, with a small standard deviation; but those areas in which the grain sizes varied considerably had a larger standard deviation.

TABLE 4-6. DIAMOND PYRAMID HARDNESS VALUES.

SAMPLE	Base plate	Base Plate HAZ	F289	F292	F293	F295	F296
DPH value	259	367	252	303	266	274	333
Std. Dev	5.6	21.6	14.1	21.6	16.3	18.2	25.6

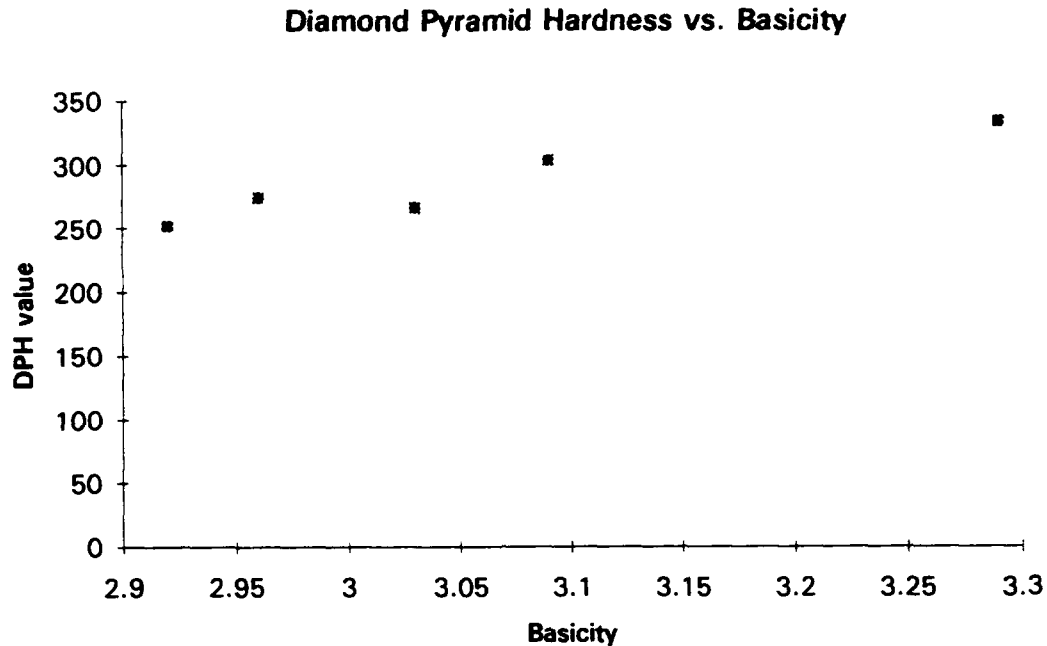


Figure 4-9. Diamond Pyramid Hardness vs. Basicity.

B. SCANNING ELECTRON MICROSCOPY

1. Non-Metallic Inclusions

Each sample was examined at a working distance of 9 mm and a magnification of 7.04K times. The field of view size was 15 microns by 12 microns. The inclusions were counted and sized using 100 random fields for each sample. Each inclusion was categorized by bin size from 0.15 micron to 1.5 micron with the bins being ± 0.05 microns in width except for the smallest bin which was ± 0.1 microns in width. Figure 4-10 is a SEM micrograph of a typical field of view using back scatter emissions. Tables 4-7a and 4-7b list some of the statistical data that was obtained during the analysis. Figure 4-11 shows graphically the data of Table 4-7a in the inclusion diameter range to 0.9 microns. Note that F296 has significantly more inclusions in every size bin. This is not consistent with the expectation that a higher basicity flux would produce the cleanest weld.

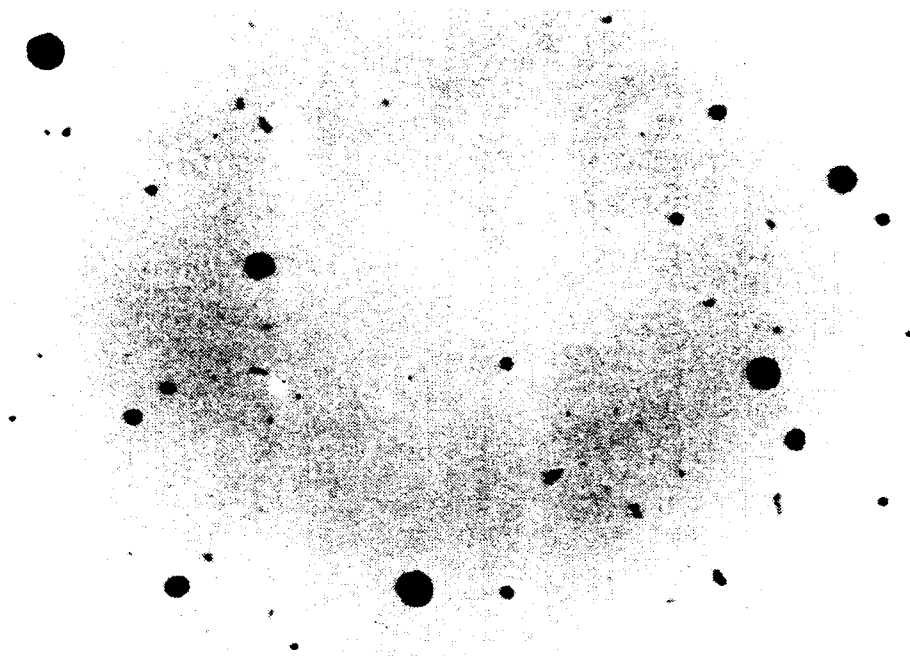


Figure 4-10. SEM micrograph of non-metallic inclusions using BSE imaging.

TABLE 4-7a. INCLUSION QUANTITIES CATEGORIZED BY SIZES.

Inclusion Size (micron)	0.15 μ	0.3 μ	0.4 μ	0.5 μ	0.6 μ	0.7 μ	0.8 μ	0.9 μ	1.0 μ	1.1 μ	1.2 μ	1.3 μ	1.4 μ	1.5 μ
F289	161	146	100	40	18	8	3	3	0	0	2	1	1	0
F292	84	74	55	35	20	11	5	3	3	4	1	0	1	1
F293	163	110	62	25	14	14	10	3	2	4	0	1	0	0
F295	130	115	45	34	18	10	7	1	1	3	0	0	0	0
F296	1870	464	199	96	57	27	24	4	4	3	2	1	1	2

TABLE 4-7b. INCLUSION STATISTICS BASED ON 100 RANDOM FIELDS.

SAMPLE	F289	F292	F293	F295	F296
Inclusion count	483	297	408	364	2754
Mean incl. size	0.320	0.378	0.322	0.323	0.232
Volume %	1.12	1.01	1.03	0.877	3.68

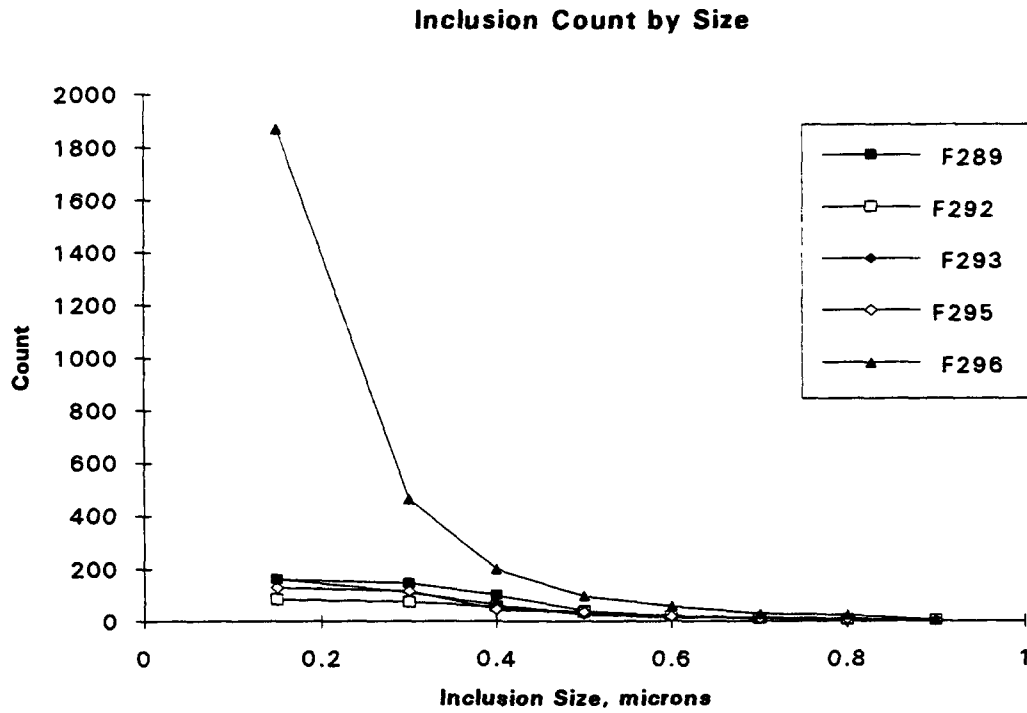


Figure 4-11a. Non-metallic inclusions categorized by size and quantity.

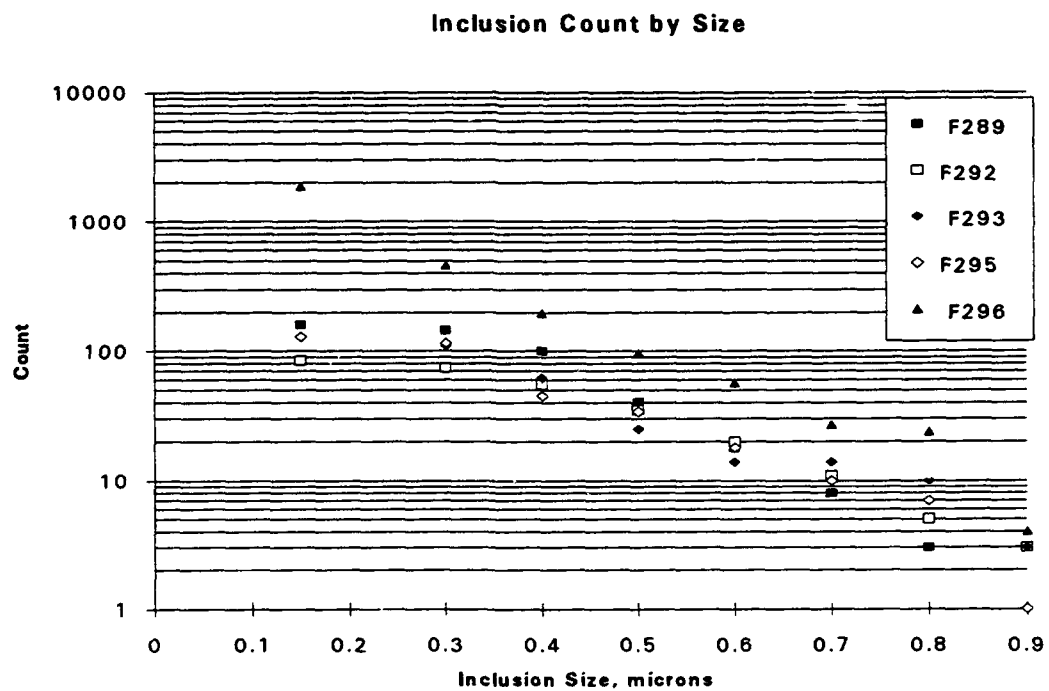


Figure 4-11b. Non-metallic inclusions categorized by size and quantity.

Figure 4-11 shows that the formation of inclusions is a phenomenon which occurs in an exponential manner.

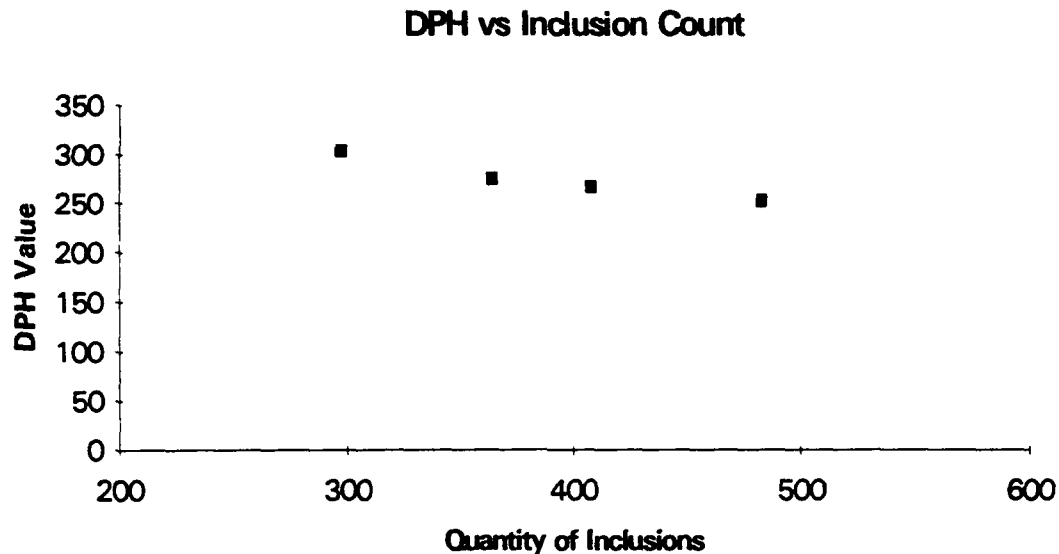


Figure 4-12. Diamond Pyramid Hardness versus the quantity of inclusions per 100 random fields of view.

In Figure 4-12 note that the harder weldments have fewer inclusions with the exception of F296 which was the hardest and had by far the most inclusions. That sample which is off the scale was not included in this figure even though it still exhibited that phenomenon. This figure concurs with the results of the tensile tests and the expectation that as the quantity of inclusions in the matrix rises, the size would decrease. This obviously has to be the case since buoyancy increases as the size increases, and an inclusion of higher buoyancy in the molten weld pool will more easily escape to the slag on the surface. Because Stokes hypothesis was accurate for these weldments, we see that the buoyancy of the non-metallic inclusions and viscosity of the weld pool is important for obtaining a clean weldment. This is shown in Table 4-8 and Figure 4-13 for inclusions that have a mean diameter greater than 0.25 microns. The figure is similar for all the inclusions studied, but the scale needed to show all the inclusions obscures the Stokes effect.

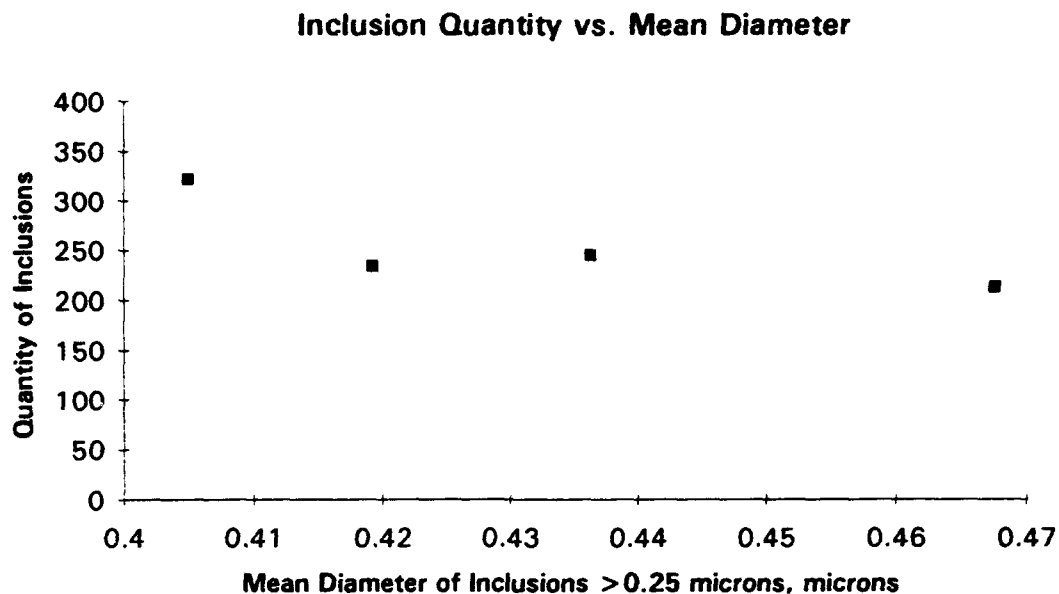


Figure 4-13. Buoyancy effect shown by fewer inclusions as their size increases.

TABLE 4-8. INCLUSION STATISTICS BASED ON INCLUSIONS ≥ 0.25 MICRONS.

SAMPLE	F289	F292	F293	F295	F296
Inclusion count	322	213	245	234	884
Mean incl. size	.405	.468	.436	.419	.405

In general, quantity and volume percent of inclusions could not be directly correlated with O_2 in the weld metal. But, Figure 4-14 shows the effect of flux basicity on the quantity of inclusions. Since all samples were near 0.03 % oxygen, the flux basicity had little effect on the variation in the volume percentage of inclusions in the weld metal. This may also be a result of variations in CaF_2 and other compounds that had served to alter the viscosity of the flux. Figure 4-15 shows the toughening effect of a higher volume fraction of weld metal inclusions on the lowering of the DBTT. Note how the effect of nucleating more acicular ferrite helped to toughen the F296 weld which would have otherwise been more brittle because of its high strength.

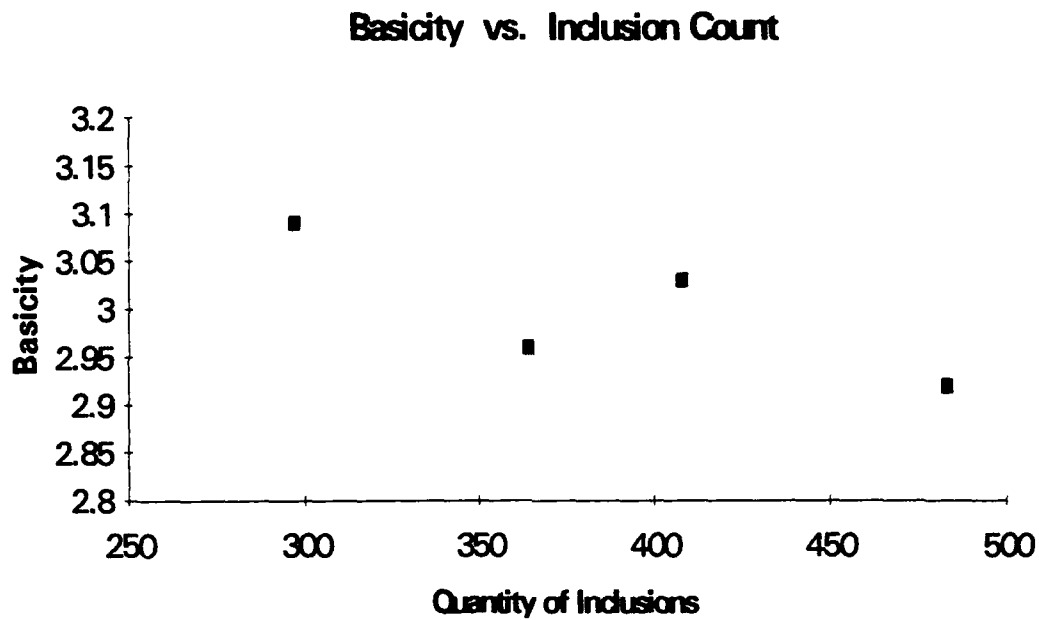


Figure 4-14. Effect of flux basicity on quantity of inclusions.

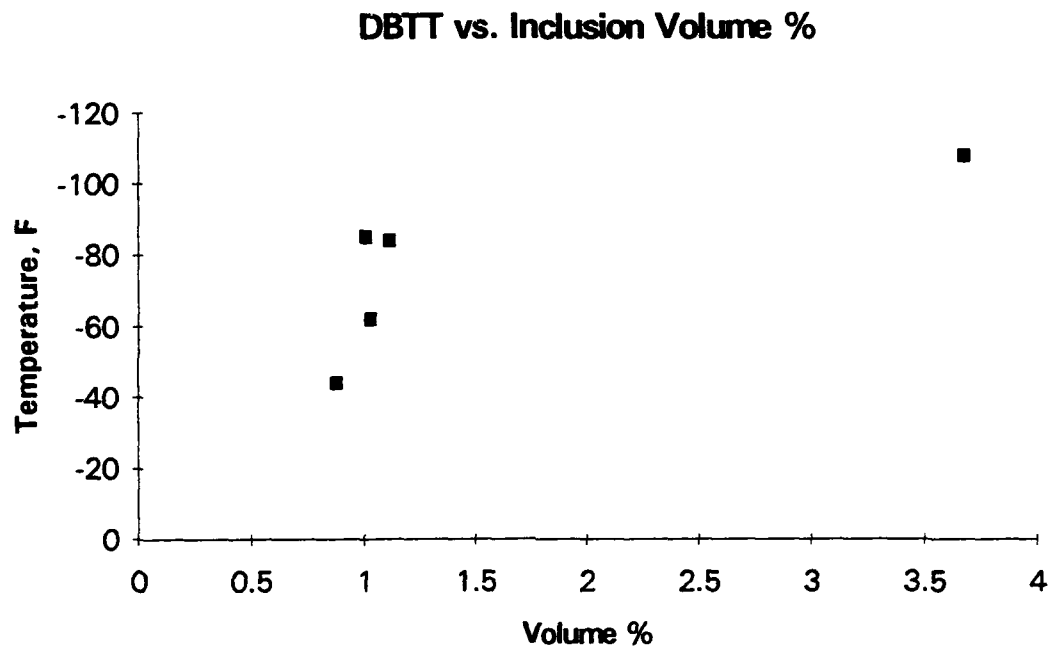


Figure 4-15. Effect of inclusion volume % on DBTT.

2. EDX Analysis of Inclusions

To further characterize the inclusions present in each of the welds, an extensive study of the inclusions was conducted. Through the process described in Section III, the weight percent of the oxides present in each non-metallic inclusion was determined and categorized. The primary elements present in the inclusions were Al, Si, Ti, and Mn. The Ti was present in small amounts, and it is probable based on the thermodynamics of the weld pool chemistry that the Ti was present as TiN. One indication of this was that over 90% of the inclusions had a stoichiometric character when the Ti was assumed to be a nitride and not considered in the oxide calculations. The cases in which a stoichiometric ratio did not exist were cases which the inclusions contained a high percentage of manganese or significant amounts of calcium, sulfur or phosphorus. Microprobe examination did not reveal the presence of any rare earth compounds in the weld metal other than Ce that was present in trace amounts in some of the F293 inclusions.

As shown in Table 4-9 manganese anorthite is the predominant inclusion present in these samples. It forms near 1530 °C in a ratio of 1 MnO, 1 Al₂O₃, and 2 SiO₂. Kiessling's work [Ref. 24] was very useful in this portion of the study. The temperature data was abstracted from Maun and Osborn [Ref. 18], and is shown in Figure 4-16. These two books were extremely helpful in understanding the complex chemical relationships that exist in the precipitation of non-metallic inclusions during solidification of the weld.

TABLE 4-9. INCLUSION CHEMISTRY.

# MnO	# Al ₂ O ₃	# SiO ₂	COMMON NAME	MnO w%	Al ₂ O ₃ w%	SiO ₂ w%	Approximate Solidification Temp°(C)	F289	F292	F293	F295	F296
0	0	1	Quartz	0.00	0.00	100.0	1700					
0	1	0	Corundum	0.00	100.0	0.00	2100					
0	3	2	Mullite	0.00	71.79	28.21	1870	1				
1	0	0	Manganosite	100.0	0.00	0.00	1800					1
1	0	1	Rhodonite	54.14	0.00	45.86	1420	1		1		1
1	1	0	Galaxite	41.03	58.97	0.00	1790		31	2	3	4
1	1	2	Mn-anorthite	24.21	34.79	41.00	1530	78	10	58	26	50
2	0	1	Tephroite	70.25	0.00	29.75	1400	1	1		6	3
2	1	1		46.68	33.55	19.77	1530	3				
2	1	4		29.30	21.06	49.64	1140	1			20	4
2	2	1		34.95	50.24	14.80	1720	1	1			
2	2	5	Mn-cordierite	21.95	31.56	46.49	1520					
2	3	0		31.69	68.31	0.00	1850		16			
2	5	0		21.77	78.23	0.00	1940		1			
3	1	3	Spessartite	42.99	20.60	36.41	1100			1		1
3	1	4		38.34	18.37	43.30	1100				2	4
3	2	6		27.38	26.24	46.38	1250	3	1	1	33	13
3	3	5		25.98	37.34	36.68	1500	2	17	1	1	5
3	5	0		29.45	70.55	0.00	1865		7			
4	2	1		51.80	37.23	10.97	1600			1	1	1
4	2	5		36.00	25.88	38.12	1250		1		1	1
4	4	3		32.55	46.78	20.67	1680					3
4	4	5		28.60	41.11	30.28	1600	1	13		4	4
5	3	5		36.91	31.83	31.26	1450				1	
6	1	6		47.93	11.48	40.59	1100				2	
7	1	1		75.40	15.48	9.12	1530	1				
8	2	2		63.65	22.87	13.48	1450			3		
10	1	1		81.40	11.70	6.90	1600	3		28		

The ternary in Figure 4-16 was used in estimating a mean solidification temperature for the inclusions present in each of the weld metals. The results are shown in Table 4-10. The results of this portion of the study are shown in Figures 4-17 through 4-22 and Tables 4-11 through 4-16. The titanium values presented in Table 4-17 are the mean values of titanium present in the inclusions with TiN probably the nucleation site for the inclusion based on the energetics of the solution [Ref. 18:pp. 3-9].

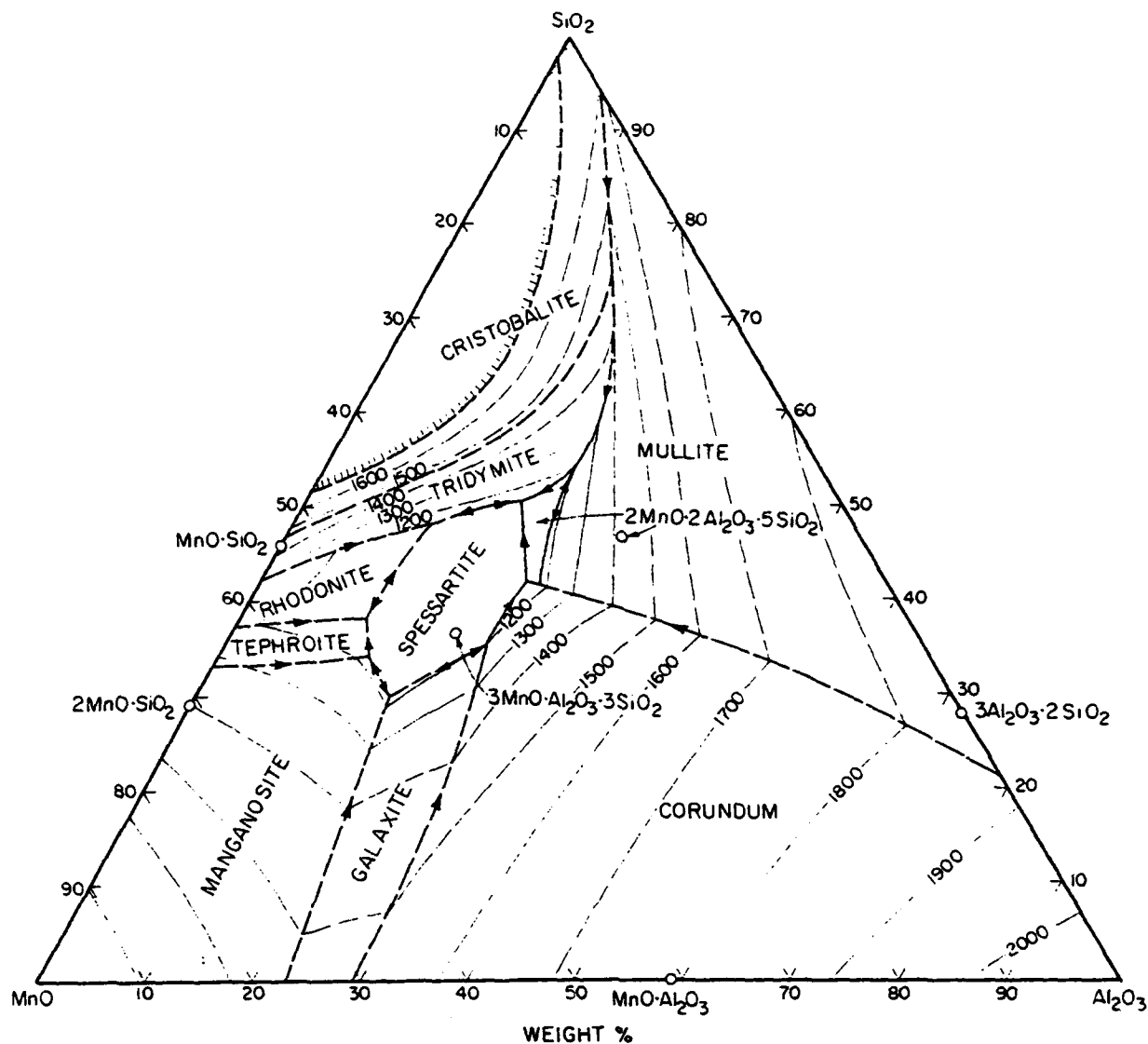


Figure 4-16. Phase relations at liquidus temperatures in the $\text{MnO-Al}_2\text{O}_3\text{-SiO}_2$ system [Ref. 17].

TABLE 4-10. MEAN INCLUSION SOLIDIFICATION TEMPERATURES.

Sample	F289	F292	F293	F295	F296
Mean Solidification Temp (C)	1523	1690	1545	1342	1465

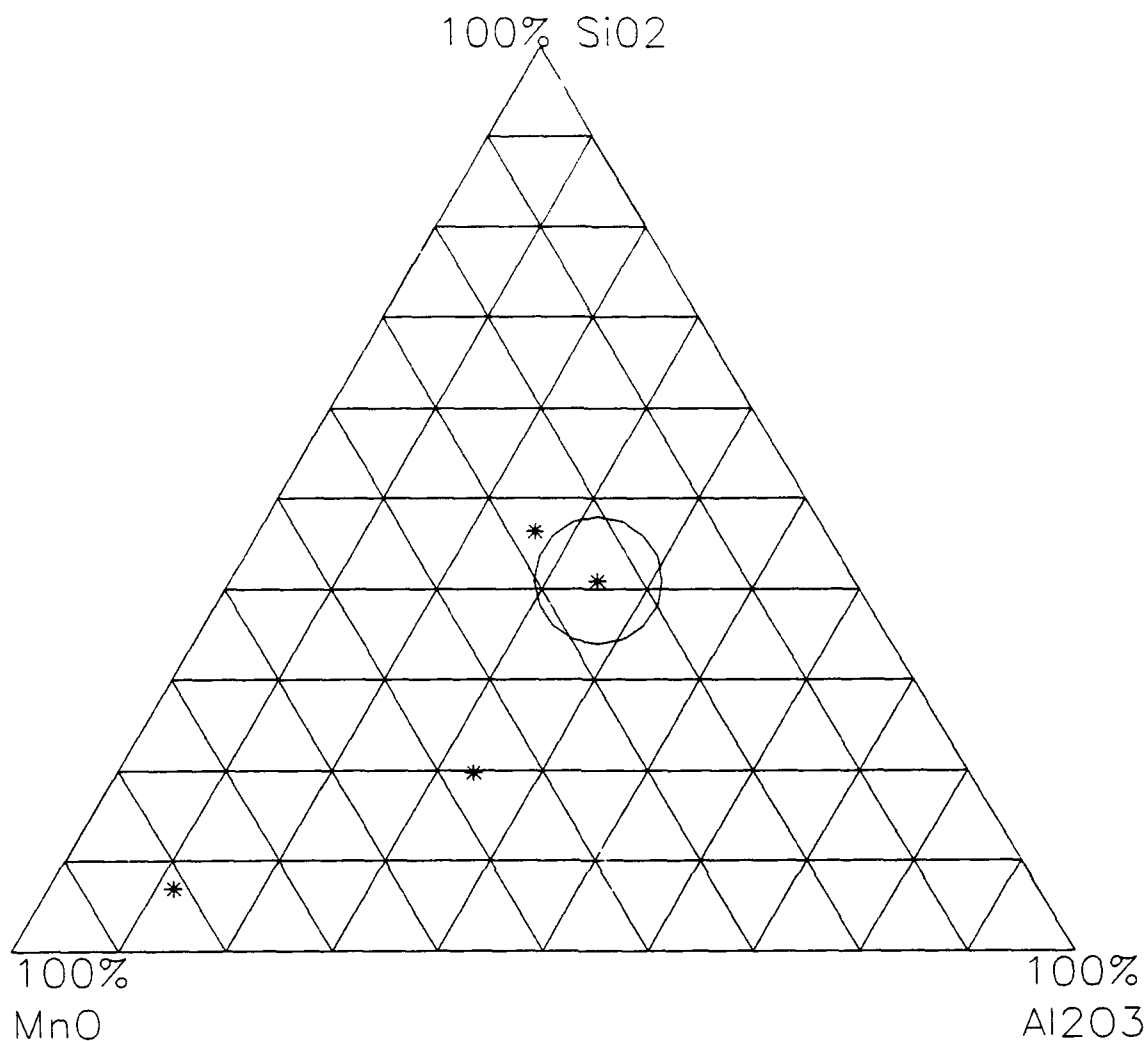


Figure 4-17. Ternary diagram for inclusions in F289 weld metal.

TABLE 4-11. F289 WELDMENT INCLUSION CHEMISTRY CORRELATION DATA.

	Base w %	Filler w %	Flux Ox %	Weld w %	#1 Incl. Ox %
Al	0.018	0.012	18.14	0.013	34.79
Si	0.30	0.40	14.65	0.38	41.0
Mn	0.33	1.57	0.89	1.45	24.21
Ti	0.004	0.014	0.72	0.006	7.22 (N)
O	0.0054	0.003	0.03	---	stoich.

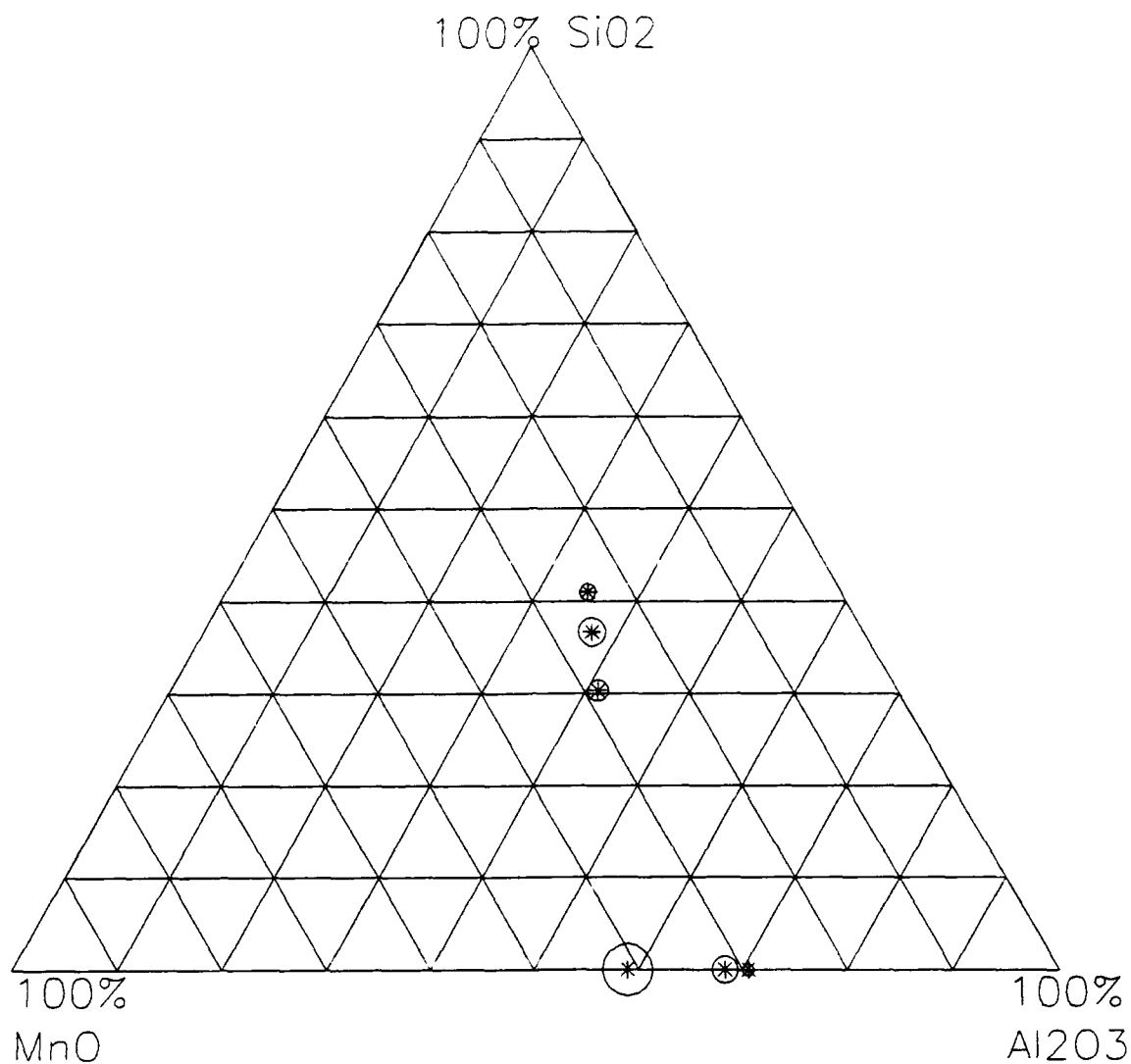


Figure 4-18. Ternary diagram for inclusions in F292 weld metal.

TABLE 4-12. F292 WELDMENT INCLUSION CHEMISTRY CORRELATION DATA.

	Base w %	Filler w %	Flux Ox %	Weld w %	#1 Incl. Ox %	#2 Incl. Ox %	#3 Incl. Ox %	#4 Incl. Ox %	#5 Incl. Ox %
Al	0.018	0.012	18.42	0.020	58.97	37.34	68.31	41.11	34.97
Si	0.30	0.40	13.52	0.46	0.0	36.68	0.0	30.28	41.0
Mn	0.33	1.57	0.83	1.49	41.03	25.98	31.69	28.6	24.21
Ti	0.004	0.014	0.701	0.008	11.1 (N)				
O	0.0054	0.003	---	0.027	stoich.				

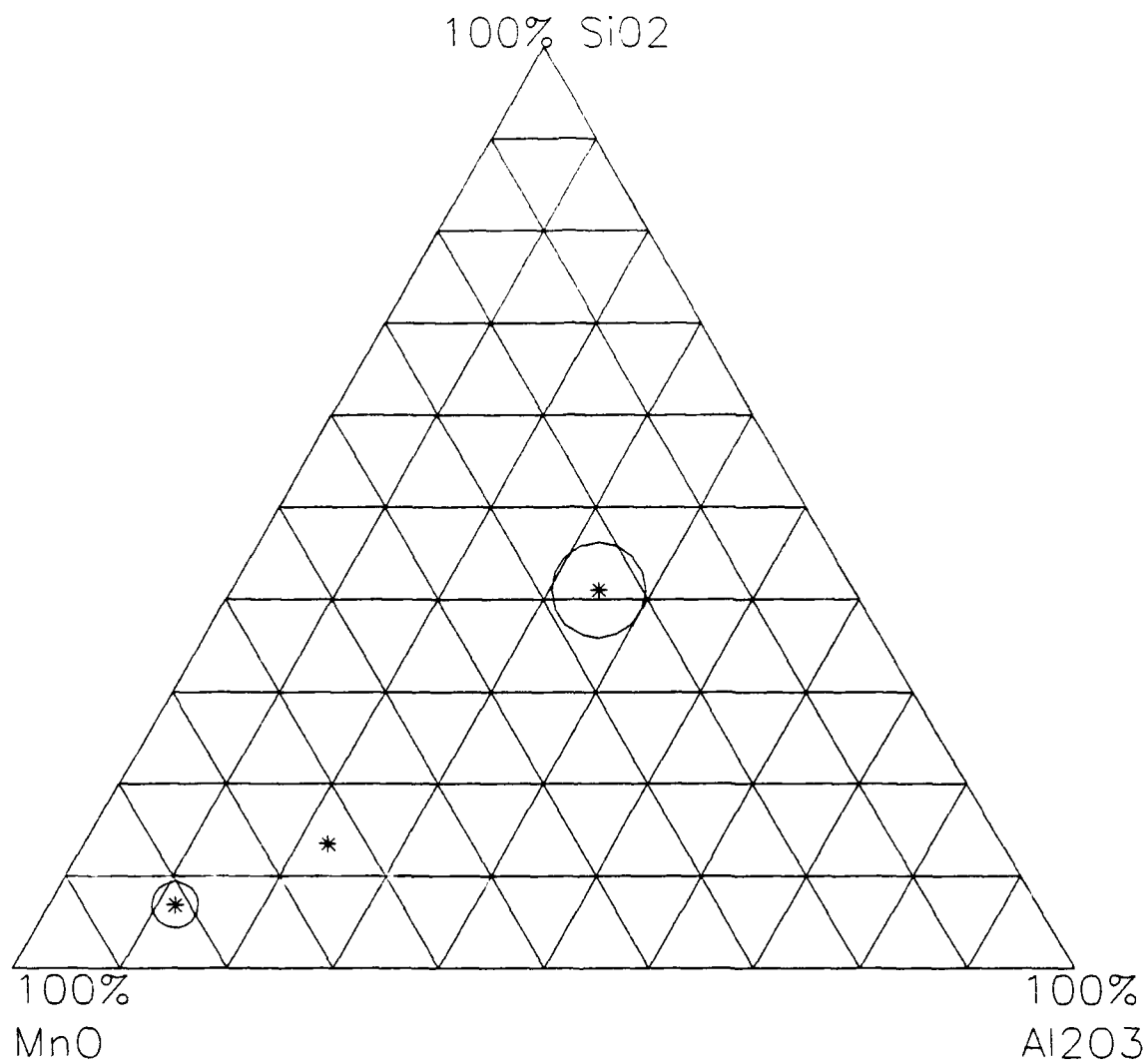


Figure 4-19. Ternary diagram for inclusions in F293 weld metal.

TABLE 4-13. F293 WELDMENT INCLUSION CHEMISTRY CORRELATION DATA.

	Base w %	Filler w %	Flux Ox %	Weld w %	#1 Incl. Ox %	#2 Incl. Ox %
Al	0.018	0.012	13.21	0.011	34.79	11.7
Si	0.30	0.40	16.64	0.42	41.00	6.9
Mn	0.33	1.57	0.051	1.28	24.21	81.4
Ti	0.004	0.014	0.000	0.004	5.28 (N)	
O	0.0054	0.003	---	0.034	stoich.	

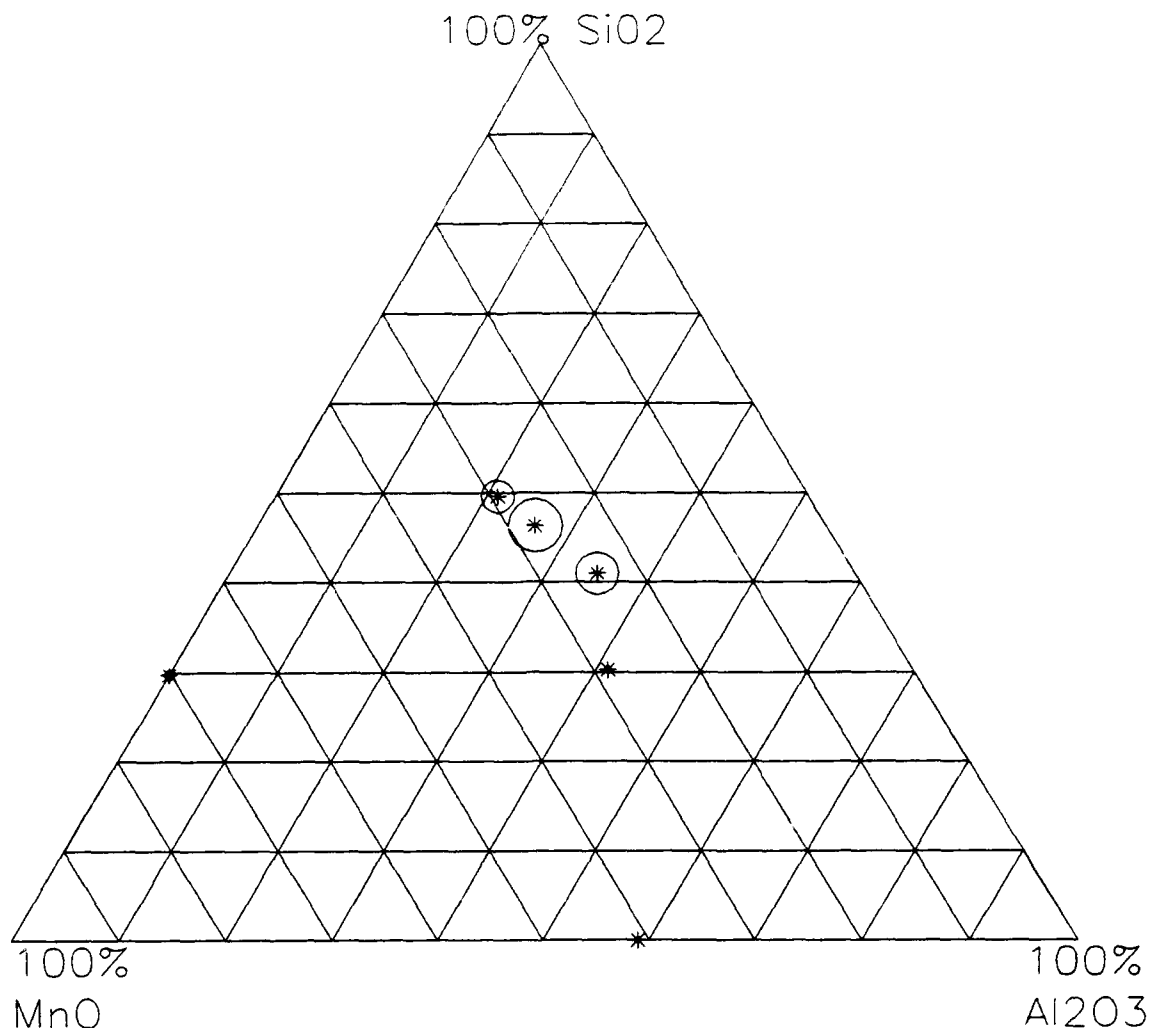


Figure 4-20. Ternary diagram for inclusions in F295 weld metal.

TABLE 4-14. F295 WELDMENT INCLUSION CHEMISTRY CORRELATION DATA.

	Base w %	Filler w %	Flux Ox %	Weld w %	#1 Incl. Ox %	#2 Incl. Ox %	#3 Incl. Ox %
Al	0.018	0.012	16.87	0.011	26.24	34.79	21.06
Si	0.30	0.40	15.57	0.28	46.38	41.00	49.64
Mn	0.33	1.57	2.52	1.51	27.38	24.21	29.30
Ti	0.004	0.014	0.679	0.005	4.34 (N)		
O	0.0054	0.003	---	0.035	stoich.		

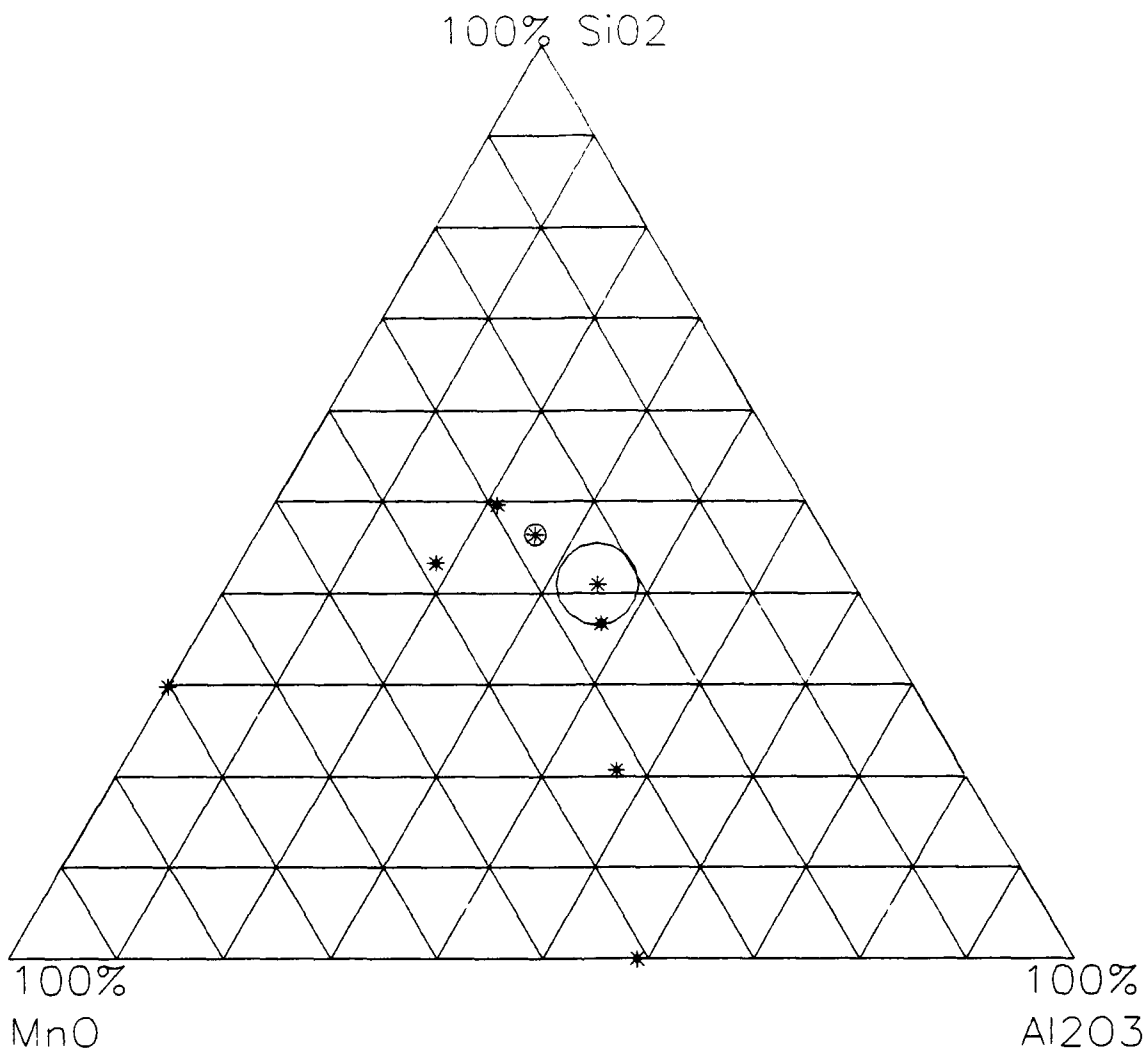


Figure 4-21. Ternary diagram for inclusions in F296 weld metal.

TABLE 4-15. F296 WELDMENT INCLUSION CHEMISTRY CORRELATION DATA.

	Base w %	Filler w %	Flux Ox %	Weld w %	#1 Incl. Ox %	#2 Incl. Ox %
Al	0.018	0.012	15.47	0.014	34.79	26.24
Si	0.30	0.40	14.57	0.34	41.00	46.38
Mn	0.33	1.57	1.61	1.54	24.21	27.38
Ti	0.004	0.014	0.52	0.006	6.72 (N)	
O	0.0054	0.003	---	0.032	stoich.	

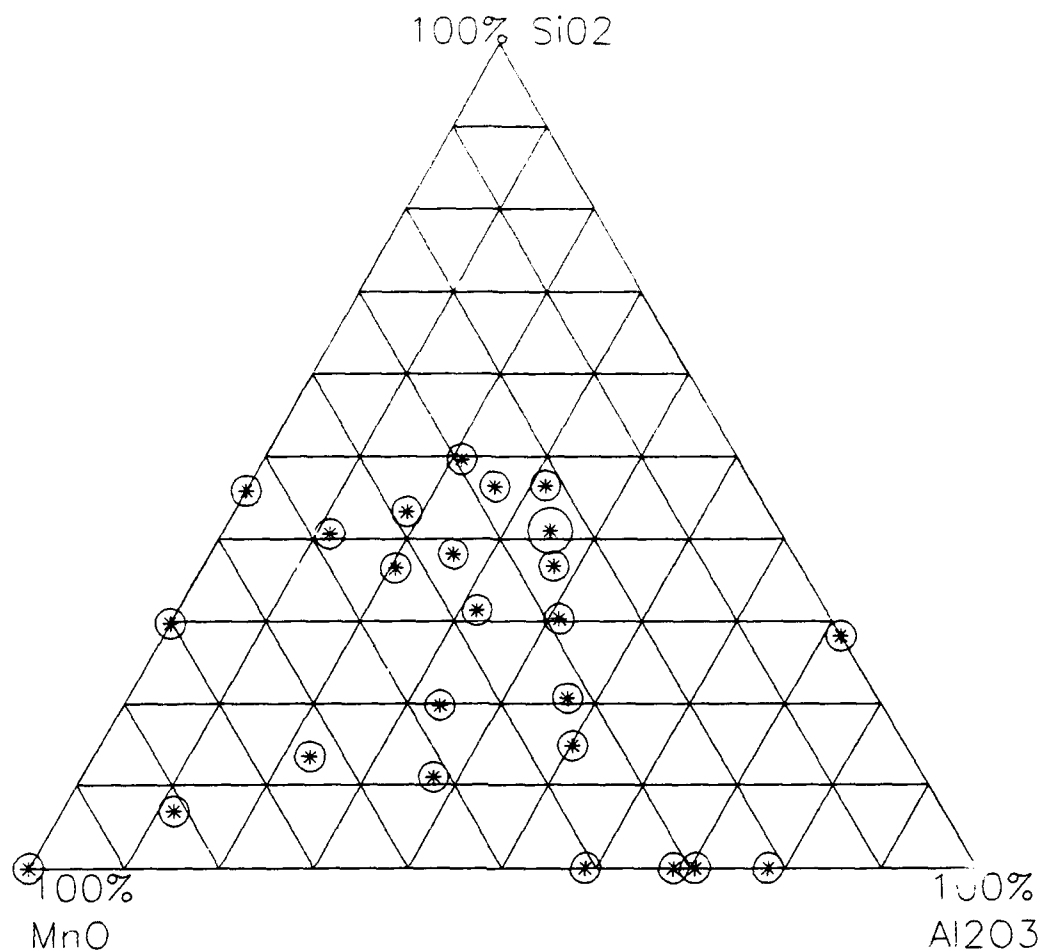


Figure 4-22. Ternary diagram for inclusions in all the weldments studied.

TABLE 4-16. INCLUSION CHEMISTRY CORRELATION DATA FOR ALL WELDMENTS.

	Mn	MnO	Si	SiO ₂	Al	Al ₂ O ₃	Ti	TiO ₂	O
	w %	w %	w %	w %	w %	w %	w %	w %	w %
Filler	1.57		0.4		0.012		0.014		0.003
HY100	0.33		0.3		0.018		0.004		0.0054
	weld metal	flux	weld metal	flux	weld metal	flux	weld metal	flux	weld metal
F289	1.45	0.887	0.38	14.647	0.013	18.139	0.006	0.718	0.03
F292	1.49	0.831	0.46	13.517	0.020	18.423	0.008	0.701	0.027
F293	1.28	0.051	0.42	16.638	0.011	13.210	0.004	0.000	0.034
F295	1.51	2.515	0.28	15.570	0.011	16.868	0.005	0.679	0.035
F296	1.54	1.608	0.34	14.569	0.014	15.473	0.006	0.523	0.032

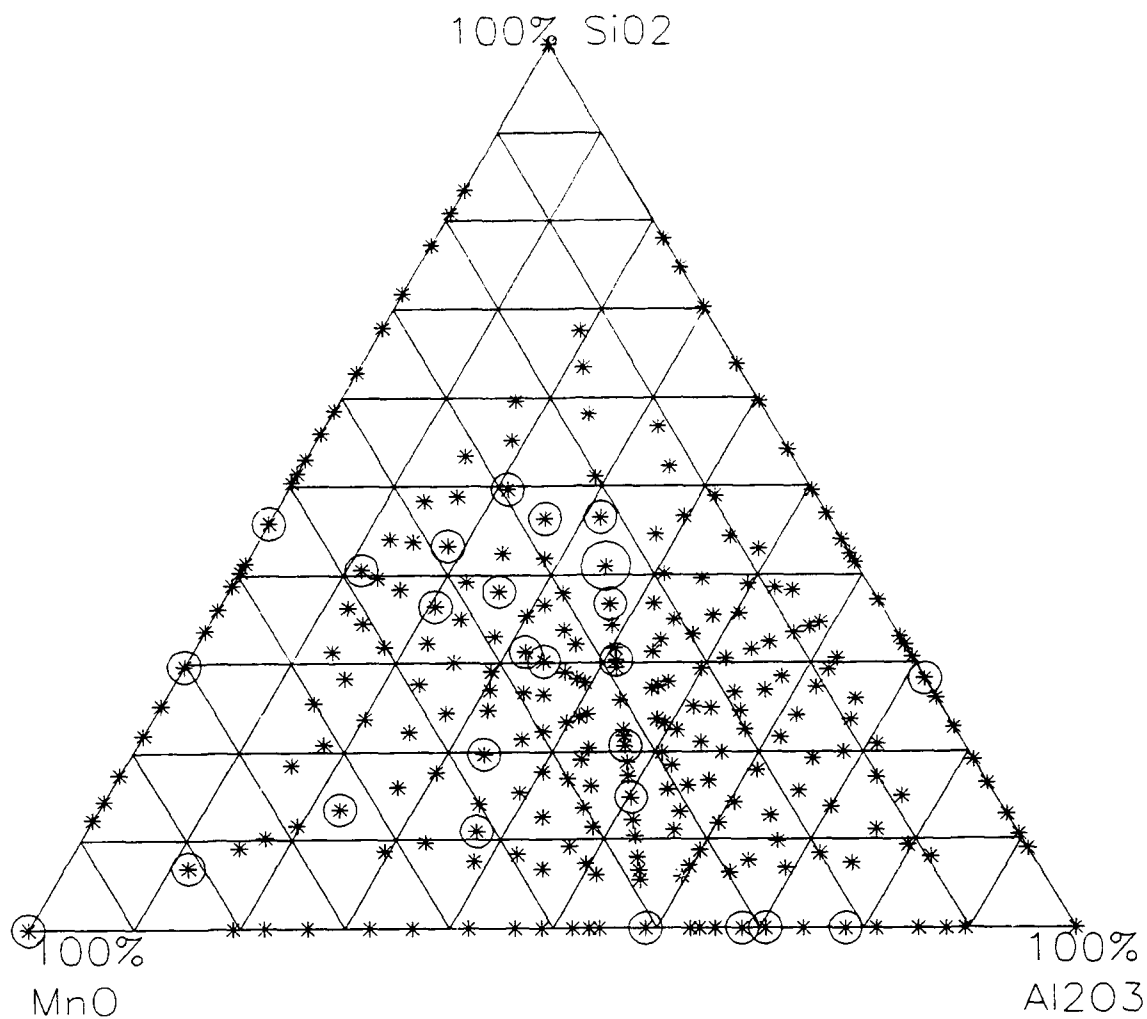


Figure 4-23. Ternary diagram for inclusions in all weld metals.

TABLE 4-17. TITANIUM RELATED INCLUSION DATA FOR ALL WELDMENTS.

W% TiN in Inclusions	F289	F292	F293	F295	F296
Mean	7.2	11.1	5.3	4.3	6.7
Standard Deviation	3.1	4.1	2.6	1.3	3.3
Variance	9.6	16.9	6.8	1.8	11.0

C. CHEMICAL COMPOSITION

The chemical composition of the inclusions in submerged-arc welds is primarily driven by the elements present in the flux. High basicity alone is not sufficient. Welding fluxes must be engineered to provide the optimum amount of weld metal deoxidation and cleaning while minimizing the loss of elements that have been added to the base or filler wire as strengthening or toughening agents. As pointed out earlier, the higher basicity fluxes had a greater influence on cleaning sulfur from the weld metal. Aluminum was significantly higher in the weldment in which the inclusions formed were primarily galaxite. The HY-100 steel base plate and filler wire were each analyzed for 17 alloying elements, while the fluxes were analyzed for 28 elements. Since the analyses of chemical composition for the metals do not completely coincide with the fluxes, it is difficult to claim why certain elements stand out as having changed significantly. However, some inferences can be made with the data that is known.

It is proposed in Figures 4-24 and 4-25 that the final weld metal chemistry is related to the temperature at which the inclusions solidify under equilibrium conditions. As noted earlier, nearly all of the inclusions analyzed were composed of stoichiometric Al-Mn-Si oxides. The temperature at which the oxides solidify under equilibrium conditions is dependent on the transformation kinetics of the molten weld pool. Since the inclusions are present in stoichiometric amounts, we know that the cooling rate was sufficiently slow to permit the inclusions to form prior to the steel entering the delta phase. Had this not been the case, it is probable that the inclusions would have precipitated with non-equilibrium compositions. This probably the case in welds for which the cooling rate is above some level. While there are critical cooling rates for other phenomenon, it has not been determined how and if these cooling rate limits are related.

**Inclusion Solidification Temperature vs. Weld
Metal Mn/Si Ratio**

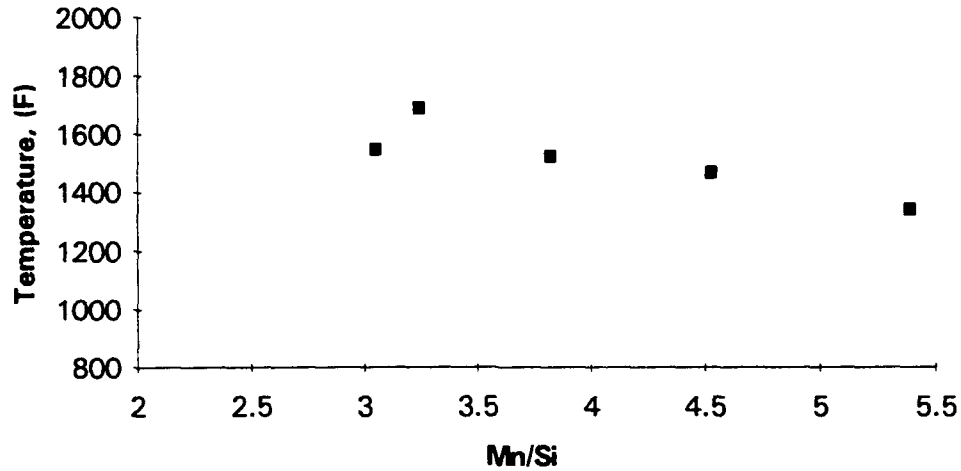


Figure 4-24. Correlation of Mn/Si ratio in weld metal with the average solidification temperature of the 100 inclusions analyzed for each sample.

**Inclusion Solidification Temperature vs. Weld Metal
Al/O Ratio**

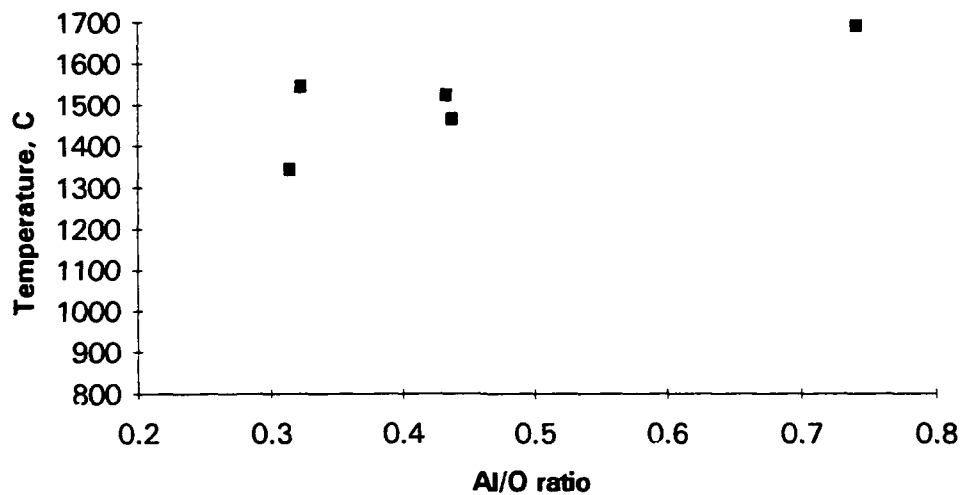


Figure 4-25. Correlation of Al/O ratio in weld metal with the average solidification temperature of the 100 inclusions analyzed for each sample.

There was no correlation between weld metal w% Al and 50% FATT is observed by other researchers, indicating that other effects were present in these welds and that the amount of aluminum in the weld metal was not sufficient to cause deleterious effects. It was possible to confirm the postulation for low Al/O ratios that the effects of aluminum on the composition, volume percentage and size of inclusions would be small in comparison with the effects of the other deoxidizers such as Si, Ti, and Mn [Ref. 16]. However, in sample F292, which had an Al/O ratio of 0.74, it was noted that there were the fewest and largest inclusions. This may be due to the fact that the inclusions with higher concentrations of aluminum in the form of galaxite solidify at higher temperatures than the manganese anorthite and have more time to grow and or escape before the molten weld pool solidifies. Also confirmed is the effect of increasing the Al/O ratio is to decrease the overall number of inclusions while increasing their size [Ref. 16].

The combination of trends shown in Figures 4-24 and 4-25 suggests those weld metals that have a low Al/O ratio are inclined to have a higher Mn/Si ratio. This is consistent with sample F295 that had the highest Mn/Si ratio and lowest Al/O ratio while having the lowest volume percentage of inclusions, 0.88%. Thus the toughening afforded through the nucleation of acicular ferrite was not achieved as noted in the low toughness of this sample in both series of impact tests. A thorough review of the flux compositions does not reveal a specific reason for the higher weld metal Al/O ratio in F292, especially when compared to the similar flux made by the same company used in F289. However, when all the chemistry results are analyzed, it is clear in the comparison of these two, that the flux with the higher basicity had the highest toughness and strength. These trends, however, do not always carry over to the other samples because of the loss of filler wire alloying elements when certain chemical combinations are present. The Al/O and Mn/Si ratios may be the result of other factors which are the drivers in the formation of the non-metallic inclusions which are responsible for the finer microstructure of acicular ferrite.

There also proved to be no tangible correlation between the Mn/Si ratio and the inclusion size or the inclusion volume percentage of the weld metal.

One such factor may be the nucleation and growth of the inclusions themselves. Of concern here is the issue of whether the inclusions contain titanium present as TiO_2 in solution or as a separate TiN phase. If it were present as TiN, it would have been formed as fine particles onto which the remainder of the inclusion oxide nucleated. If it were present as TiO_2 , then it would not necessarily have been responsible for the nucleation of the inclusion, but could have been part of a quaternary equilibrium relationship. The EDX analyzer attached to the SEM was not capable of showing the low energy level and counts emitted from the nitrogen as characteristic x-rays. Peters, however, was able to determine the nature of the titanium through the use of Auger electron spectroscopy [Ref. 26:p. 69]. He reports that the small faceted particles within the inclusion did contain nitrogen.

Based on Peters' finding, four reasons are given to confirm the postulate that the titanium is present as a precipitated TiN type intermetallic, which served as the nucleation site for the Al-Si-Mn oxide inclusions. This would also give balance to the earlier portion of the study in which the inclusions were found to have stoichiometric compositions when the titanium was treated as the nucleation site rather than a part of the oxide.

The stoichiometric nature of the inclusions, the % titanium within each inclusion, the presence of the faceted particle within the inclusion, and the presence of various oxides with a lower free energy of formation for forming oxides. When analyzed as an Al-Si-Mn-Ti quaternary, none of the inclusions had a stoichiometric nature. However, when only the dispersive x-rays of the Al, Si and Mn were analyzed, the results were amazingly stoichiometric; such that sample F289 had 78% of its non-metallic inclusions characterized as primarily manganese anorthite. When the variation of the amount of titanium present in the inclusions was analyzed, there was no correlation between the amount of titanium and the type of inclusion. Some of that data was shown in Table 4-17. When the matrix and inclusions were etched with a sodium-picrate solution, there were faceted structures

present in the interior of the inclusion. An example of this is shown in Figure 4-26, a micrograph of a faceted particle interior to an inclusion in sample F293. To ensure that the TiN particles were present as a result of the molten weld pool interaction and not from the flux, this example was used since sample F293 did not have any titanium detected in its flux. Finally, since the flux basicity was high, the weld pool thermodynamics were favorable for the formation of TiN.

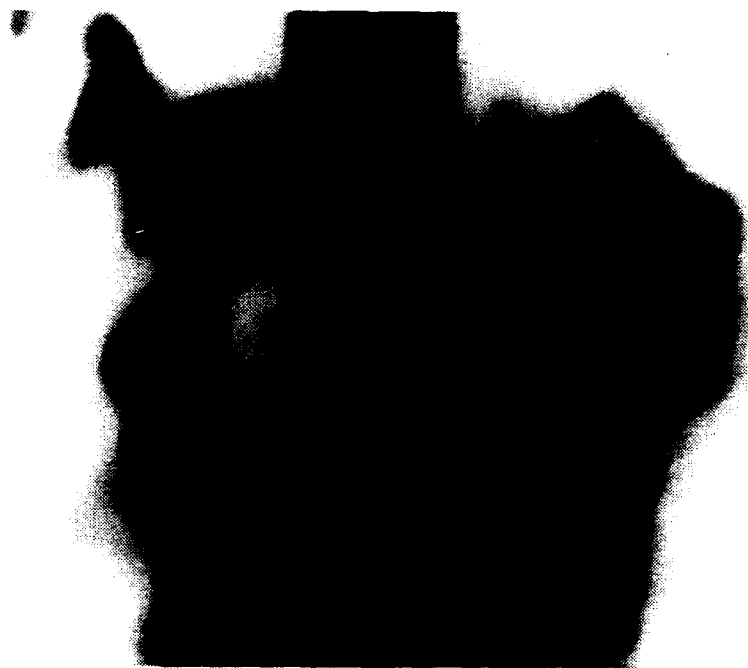


Figure 4-26. SEM micrograph of F293 weldment inclusion with faceted TiN particle etched with Sodium-picrate under 43100x magnification with BSE.

Other relationships between the titanium present in the inclusions and the final weld metal chemistry can be addressed. Figure 4-27 shows that the titanium variation in the weld metal is primarily due to the faceted TiN particles within the inclusions. As shown in Figure 4-28, it is possible that the titanium was directly responsible for reduction in the weld metal oxygen. The inclusions that had the largest titanium presence performed the best deoxidation of the weld. The larger TiN particles enhanced nucleation of non-

metallic inclusions which could then rise to the slag and deoxidize the weld metal. This could have been due in part to the early nucleation and growth of aluminum rich inclusions as shown in Figure 4-29 and discussed earlier in correlation with Figure 4-25. It is postulated that conditions favorable for titanium nitride formation will promote inclusion formation at higher temperatures, preserving the alloying of the matrix, enhancing deoxidation of the weld, and promoting the nucleation of acicular ferrite through sufficient non-metallic inclusions. Based on the limited number of samples examined, it seems that at least 0.006 weight percent titanium in the weld metal is necessary for good deoxidation of the weld.

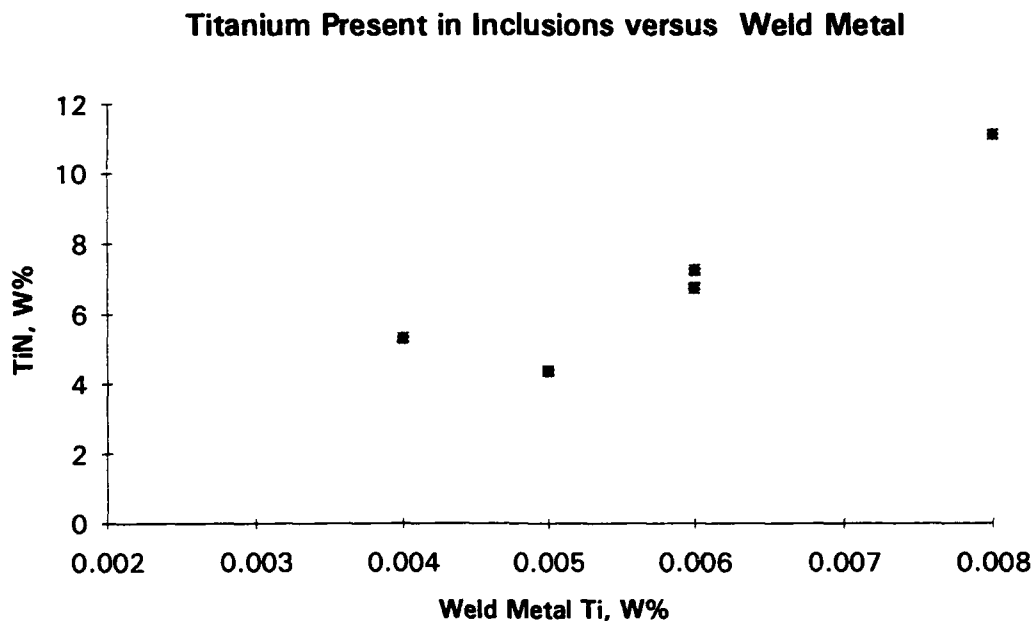


Figure 4-27. Correlation of weld metal titanium versus titanium in the inclusions.

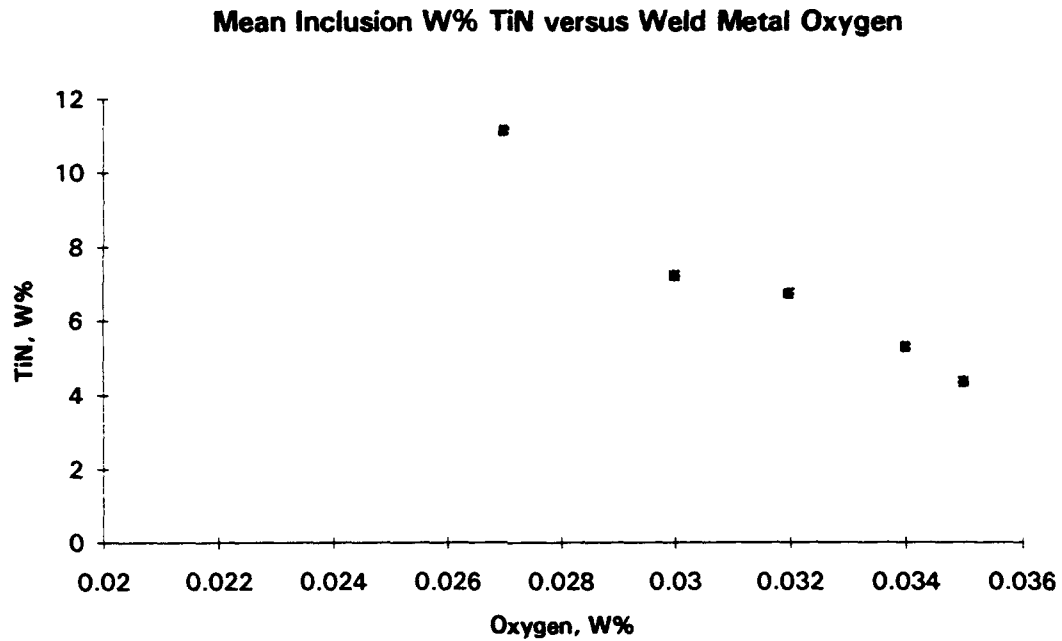


Figure 4-28. Correlation of weld metal oxygen versus titanium in the inclusions.

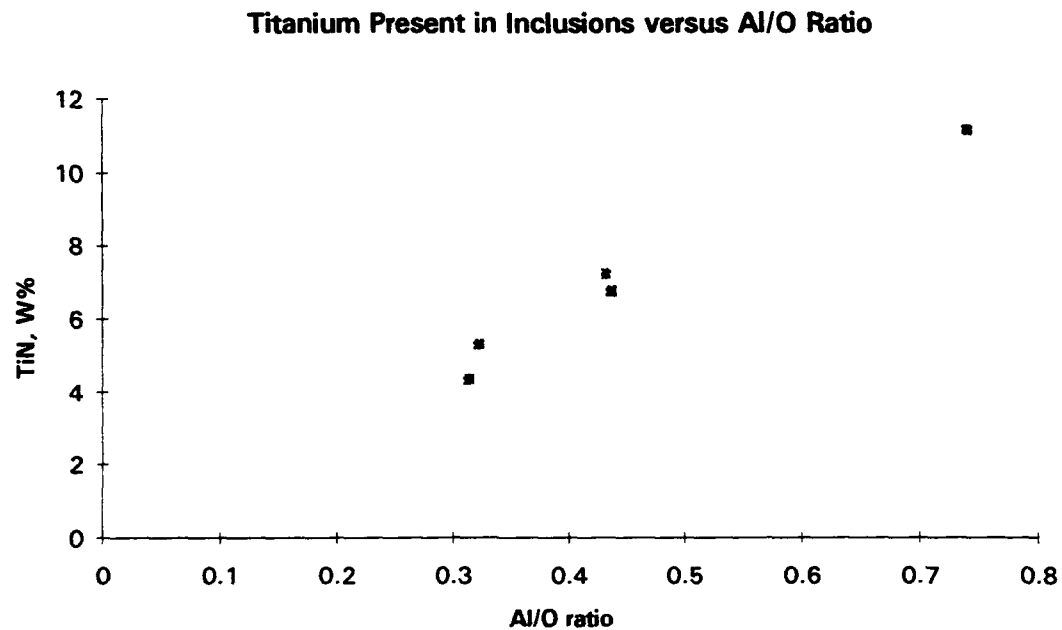


Figure 4-29. Correlation of weld metal Al/O ratio versus titanium in the inclusions.

D. METALLOGRAPHY

1. Weld Metal Reheat

A weld metal reheat study was performed by taking macrographs of the whole weldment at 8x magnification. The portion of the weld used for the mechanical testing was the focus of this part of the study. The results of the computer aided image analysis are shown in Table 4-18. Many attempts were made to correlate this data to show some effect of weld metal reheat, but there seems to be none. The sample with the highest percentage of columnar grains in the upper region was F292. It would seem that this sample would have had poor toughness, but that was not the case. It appears that the use of the 3/32 inch filler wire combined with the 55.3 kJ/inch heat input provide sufficient tempering for the weld metal in these multi-run welds. There also was not any correlation between the samples that were made with 21 and 24 passes and their respective microstructures or mechanical properties.

TABLE 4-18. RESULTS OF REHEAT ANALYSIS.

SAMPLE	F289	F292	F293	F295	F296
% Top Lvl Col Grains	0.04	0.21	0.09	0.18	0.01
% Columnar Grains	0.29	0.37	0.26	0.33	0.29
% Coarse Grain Region	0.29	0.24	0.35	0.31	0.32
% Fine Grain Region	0.42	0.39	0.39	0.36	0.39
Col\CsGR	1.00	1.54	0.74	0.97	0.91

2. Microscopy

Optical and SEM metallography were performed on transverse weld metal sections that were polished to a one micron finish and etched for 15 seconds with 5% Nital. The weld metal area and HAZ were examined for evidence of cracking. Optical micrographs were taken at 1000x magnification and are displayed in Appendix C. Scanning electron micrographs taken at 4000x magnification were taken and are also displayed in Appendix C. The microstructure of the samples were all very similar with

various amounts of bainite, grain boundary ferrite, side plate ferrite and acicular ferrite. Every specimen had micro cracks in the weld metal and HAZ. This is probably related to hydrogen since the weldments did not receive a post weld soak. Micrographs are also included in Figures C-26 through C-29 to show the nature of the F296 specimen which had such a high inclusion count.

V. CONCLUSIONS

Although the chemical properties of the base plate, filler wire and deposited weld metal were in conformance with MIL-E-23765 requirements, variations in the flux basicity had diverse impacts on the strength and toughness of the weldments. A more basic flux results in higher weld metal strength and toughness through efficient deoxidation, non-metallic inclusion formation and nucleation of acicular ferrite. A higher volume % of inclusions enhanced the nucleation of acicular ferrite which is known to be beneficial for increasing toughness through a lowering of the DBTT. The higher percentage of rare earth elements used in the F293 flux of did not appear to improve strength or toughness. Poor weld pool mixing in F296 caused segregation of alloy elements, resulting in solidification cracking and the prevention of inclusions surfacing to the slag.

Titanium was observed to enhance the nucleation and growth of non-metallic inclusions that solidify at higher temperatures. This resulted in the retention of more silicon in the matrix since less silicon was present in these inclusions.

The author's recommendation for further study of these effects is that a quantitative metallographic analysis be performed to determine weld metal microconstituent volume fractions for correlation with the presented data. Additionally, it is recommended that fluxes be tested for lead, sulfur and phosphorus to insure that the weld metal is does not become contaminated.

APPENDIX A. FLUX CHEMISTRY DATA

TABLE A-1. RESULT OF XRF ANALYSIS ON THE FLUXES.

	H5	L2	M2	R2	S3
SiO ₂	13.5	15.6	16.5	14.5	14.7
Al ₂ O ₃	18.4	16.9	13.1	15.4	18.2
Fe ₂ O ₃	1.37	2.00	1.19	1.05	1.09
MgO	28.2	35	28.3	32.1	28.9
CaO	28.4	20.5	27.3	24.9	26.1
Na ₂ O	0.71	1.23	1.99	1.20	0.94
K ₂ O	0.68	0.39	1.24	1.34	0.99
TiO ₂	0.70	0.68	<0.02	0.52	0.72
P ₂ O ₅	<0.05	0.08	<0.05	<0.05	<0.05
MnO	0.83	2.52	0.05	1.60	0.89
F	10.8	8.4	6.8	10.2	10.8
LOI(900C)	0.71	0.24	4.97	0.80	1.41

TABLE A-2. RESULT OF OES ANALYSIS ON THE FLUXES.

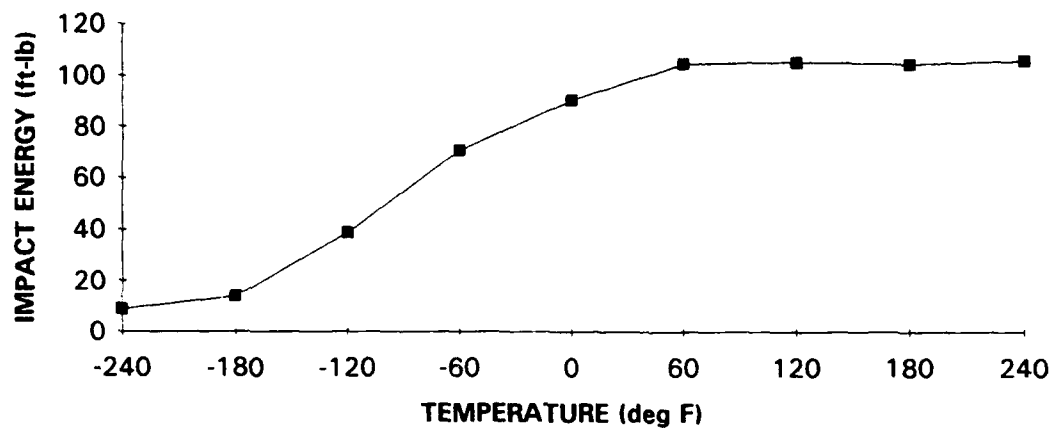
	H5	L2	M2	R2	S3
Ca	>20	15	>20	>20	>20
Fe	2.0	3.0	1.5	1.5	1.5
Mg	>10	>10	>10	>10	>10
Na	1.5	2.0	>5	3.0	2.0
P	>0.2	>0.2	>0.2	>0.2	>0.2
Ti	1.0	1.0	0.05	0.7	>1
B	0.001	0.001	0.02	<0.001	<0.001
Ba	0.05	0.07	0.05	0.01	0.03
Bi	0.007	<0.001	<0.001	<0.001	0.01
Co	0.0015	0.003	0.003	0.007	0.0015
Cr	0.02	0.07	0.01	0.07	0.02
Cu	0.0015	0.0015	0.002	0.003	0.002
Ga	0.015	0.01	0.007	0.007	0.01
La	0.007	0.005	>0.1	0.007	0.007
Mn	>0.5	>0.5	0.1	>0.5	>0.5
Mo	<0.0005	<0.0005	0.007	<0.0005	<0.0005
Ni	0.002	0.005	0.005	0.02	0.002
Pb	<0.001	0.003	0.0015	0.015	0.002
Sc	0.0007	0.001	<0.0005	0.0005	0.0005
Sn	<0.001	<0.001	0.003	<0.001	<0.001
Sr	0.015	0.015	0.015	0.01	0.01
V	0.007	0.01	0.003	0.003	0.007
Y	0.005	0.003	0.003	0.005	0.005
Zr	0.02	0.02	0.05	0.03	0.05

TABLE A-3. RESULT OF ICP ANALYSIS ON THE FLUXES.

	H5	L2	M2	R2	S3
Al	10.3	11.4	8.45	11.1	11.0
Ca	21.8	19.1	24.4	24.5	21.2
Fe	1.08	1.84	1.1	1.1	0.88
K	0.7	0.5	1.4	1.7	1.0
Mg	18.8	28	1.9	27.4	20.3
Na	0.65	1.32	2.06	1.4	0.91
P	<0.04	0.05	<0.04	<0.04	<0.04
Ti	0.47	0.56	<0.04	0.46	0.52
Mn	0.667	2.53	0.063	1.63	0.767
Ag	<0.002	<0.002	<0.002	<0.002	<0.002
As	<0.008	<0.008	<0.008	<0.008	<0.008
Au	<0.006	<0.006	<0.006	<0.006	<0.006
Ba	0.0232	0.031	0.0242	0.0076	0.0453
Be	<0.0008	<0.0008	<0.0008	<0.0008	<0.0008
Bi	<0.008	<0.008	<0.008	<0.008	<0.008
Cd	<0.002	<0.002	<0.002	<0.002	<0.002
Ce	0.005	0.011	0.265	0.005	0.003
Co	0.0015	0.0024	0.0078	0.0047	0.0013
Cr	0.014	0.0461	0.007	0.0811	0.0149
Cu	<0.0008	0.0017	0.0052	0.003	0.0067
Eu	<0.002	<0.002	<0.002	<0.002	<0.002
Ga	<0.003	0.004	<0.003	0.004	<0.003
Ho	<0.003	<0.003	<0.003	<0.003	<0.003
La	0.005	0.008	0.229	0.006	0.005
Mo	<0.002	<0.002	0.006	<0.002	<0.002
Nb	<0.003	<0.003	<0.003	<0.003	<0.003
Nd	0.003	0.006	0.08	<0.003	<0.003
Ni	0.003	0.004	0.007	0.026	0.003
Pb	<0.003	<0.003	<0.003	0.006	<0.003
Sc	<0.002	<0.002	<0.002	<0.002	<0.002
Sr	0.008	0.021	0.012	0.005	0.008
Ta	<0.03	<0.03	<0.03	<0.03	<0.03
Th	<0.003	0.005	<0.003	<0.003	<0.003
U	<0.08	<0.08	<0.08	<0.08	<0.08
V	0.01	0.013	0.004	0.007	0.009
Y	0.003	0.005	0.002	0.004	0.004
Yb	<0.0008	<0.0008	<0.0008	<0.0008	<0.0008
Zn	<0.002	<0.002	0.028	<0.002	<0.002
Zr	0.023	0.032	0.003	0.06	0.028

APPENDIX B. CHARPY AND FATT CURVES

F289 CVN TEST



F289 FATT

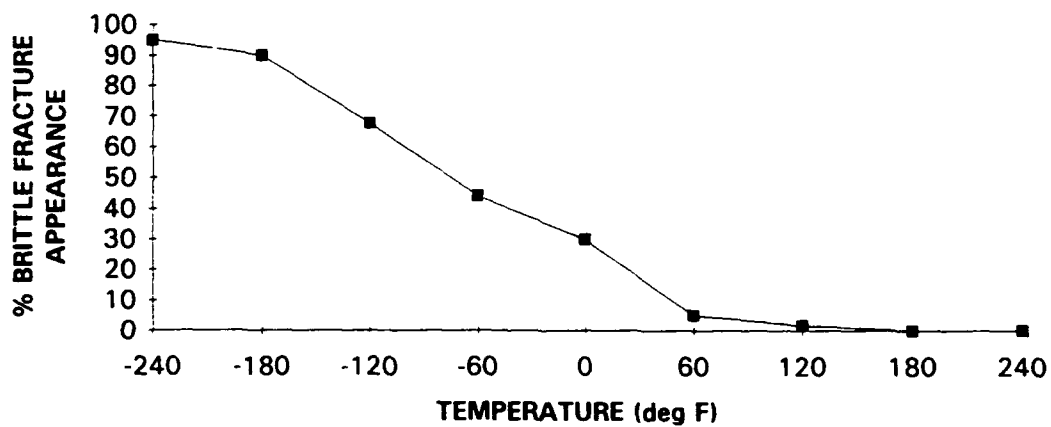


Figure B-1. Sample F289 toughness curves.

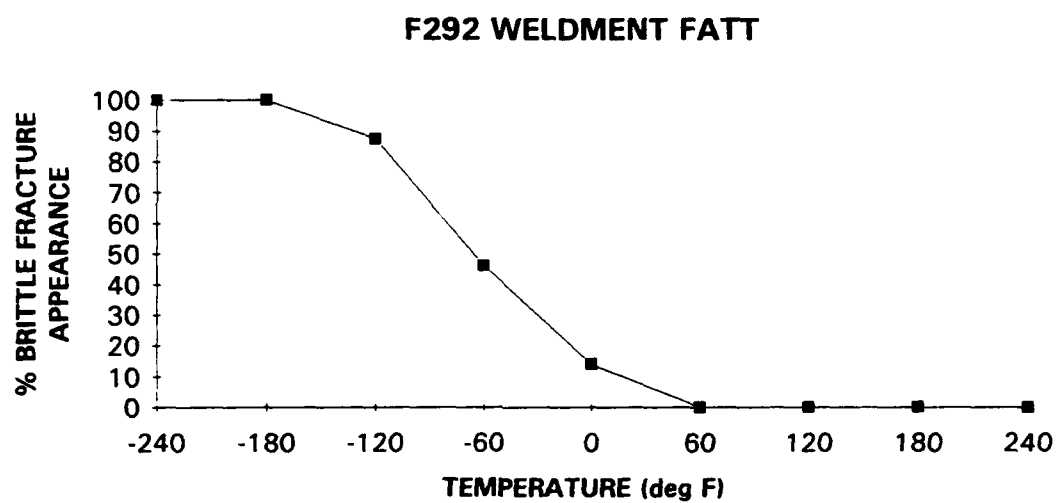
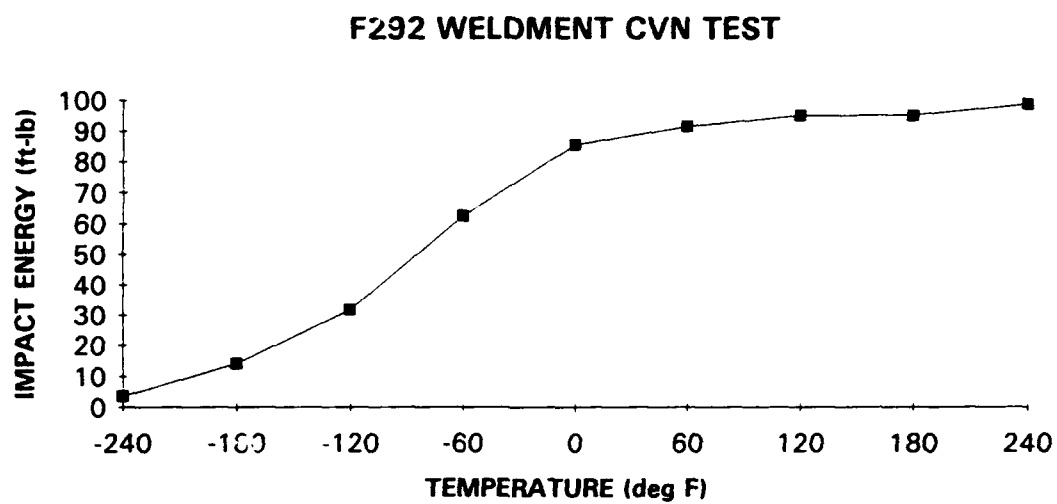
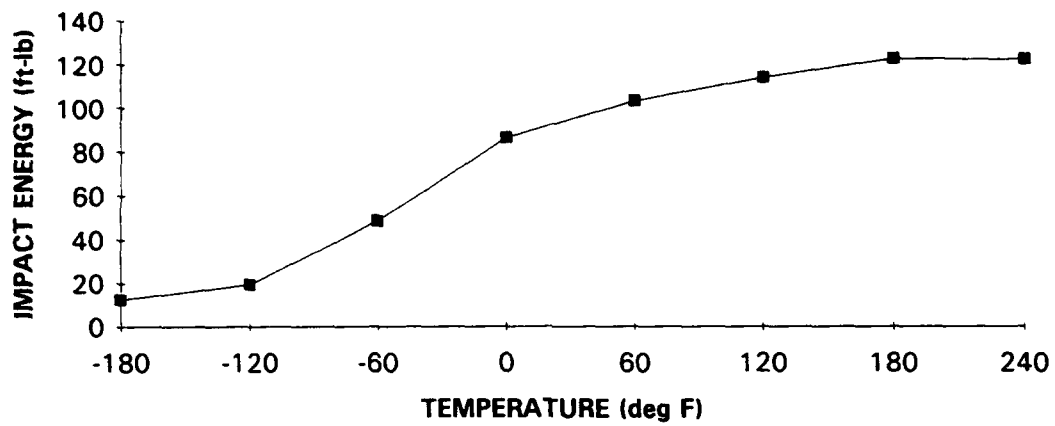


Figure B-2. Sample F292 toughness curves.

F293 WELDMENT CVN TEST



F293 WELDMENT FATT

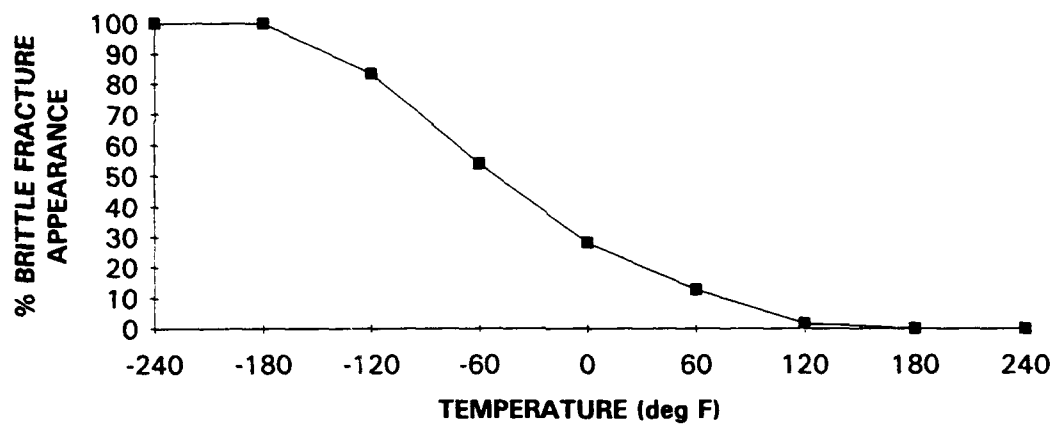


Figure B-3. Sample F293 toughness curves.

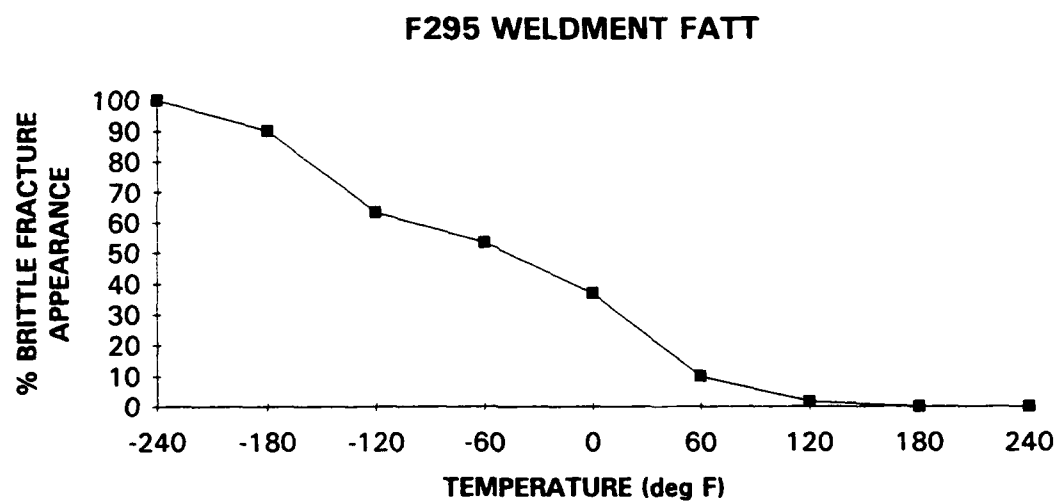
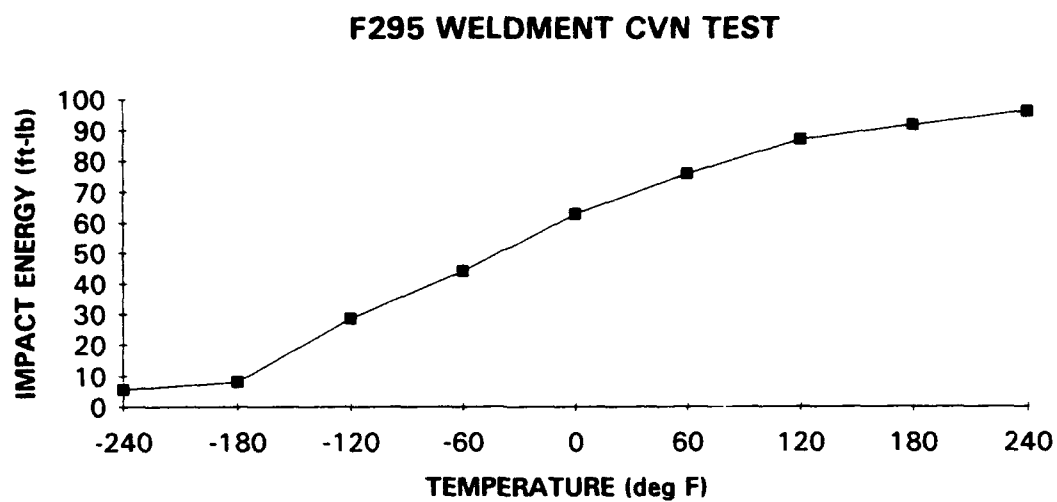
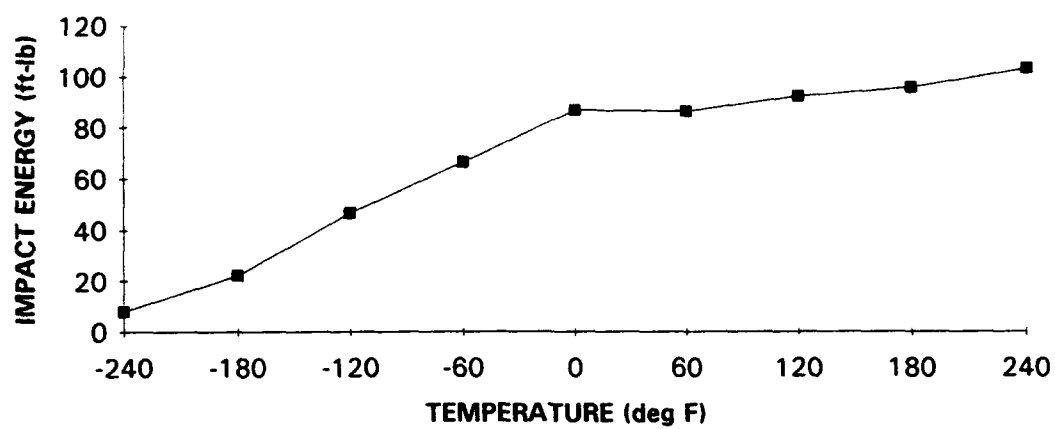


Figure B-4. Sample F295 toughness curves.

F296 WELDMENT CVN TEST



F296 WELDMENT FATT

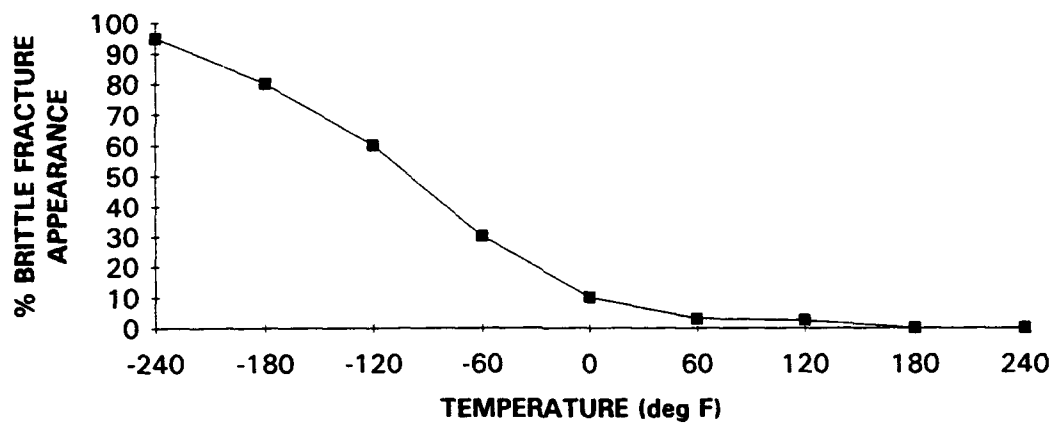


FIGURE B-5. SAMPLE F296 TOUGHNESS CURVES.

APPENDIX C. PHOTOGRAPHS AND MICROGRAPHS

F289



Figure C-1. Photograph of sample F289 weldment etched with 5% Nital.

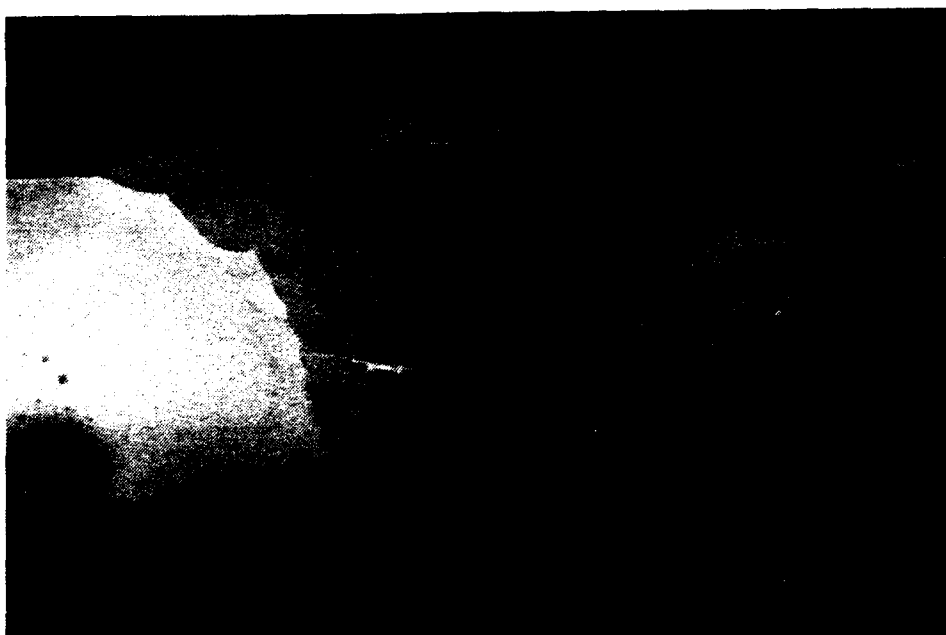


Figure C-2. Macrograph of F289 weld metal etched with 5% Nital.

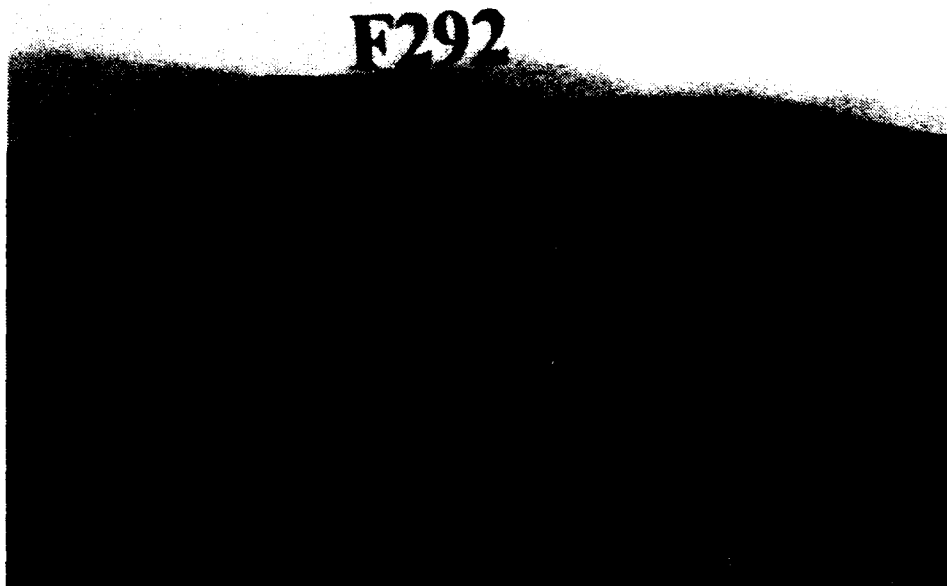


Figure C-3. Photograph of sample F292 weldment etched with 5% Nital.

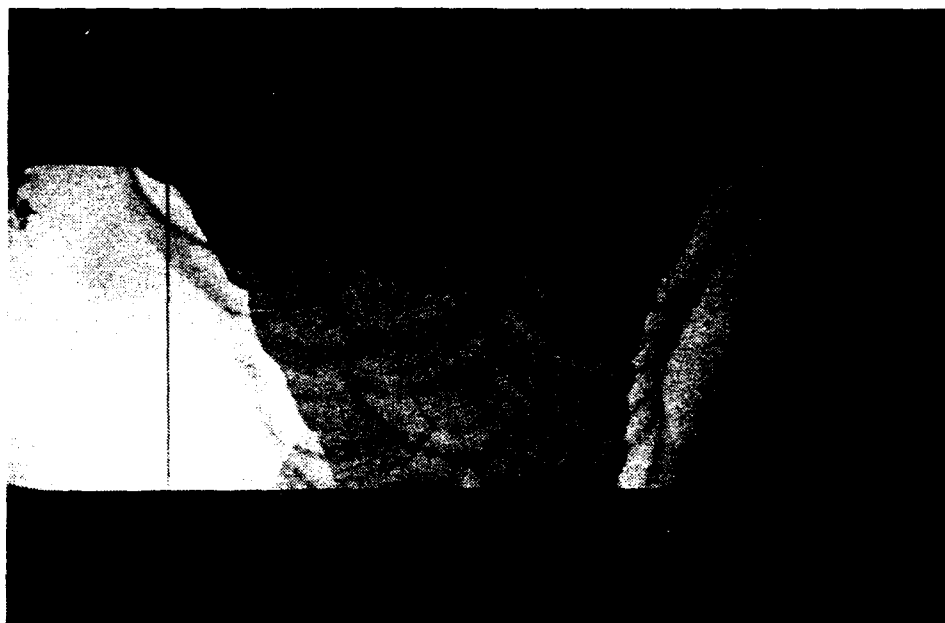


Figure C-4. Macrograph of F292 weld metal etched with 5% Nital.

F293



Figure C-5. Photograph of sample F293 weldment etched with 5% Nital.



Figure C-6. Macrograph of F293 weld metal etched with 5% Nital.

F295



Figure C-7. Photograph of sample F295 weldment etched with 5% Nital.

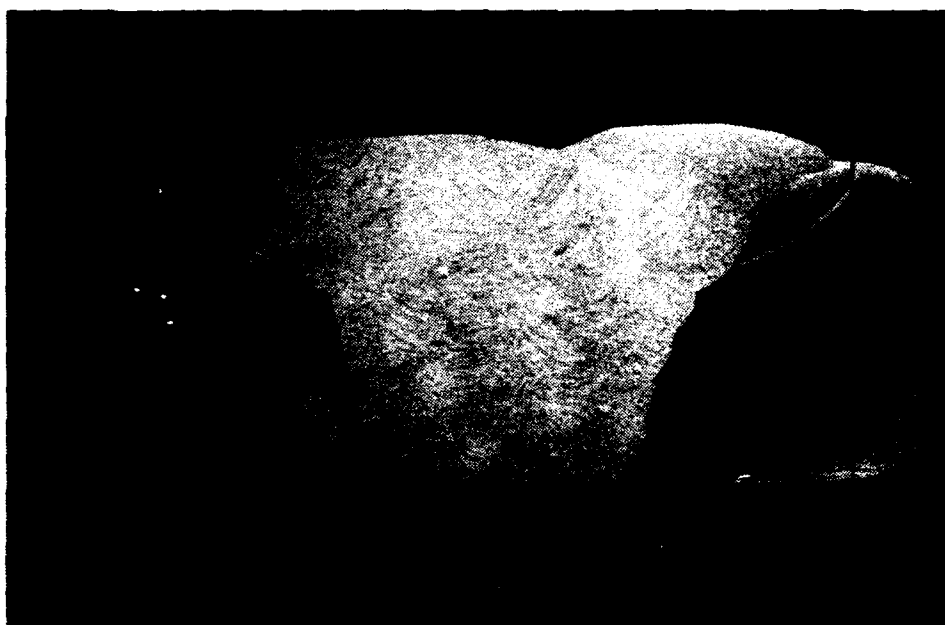


Figure C-8. Macrograph of F295 weld metal etched with 5% Nital.

F296

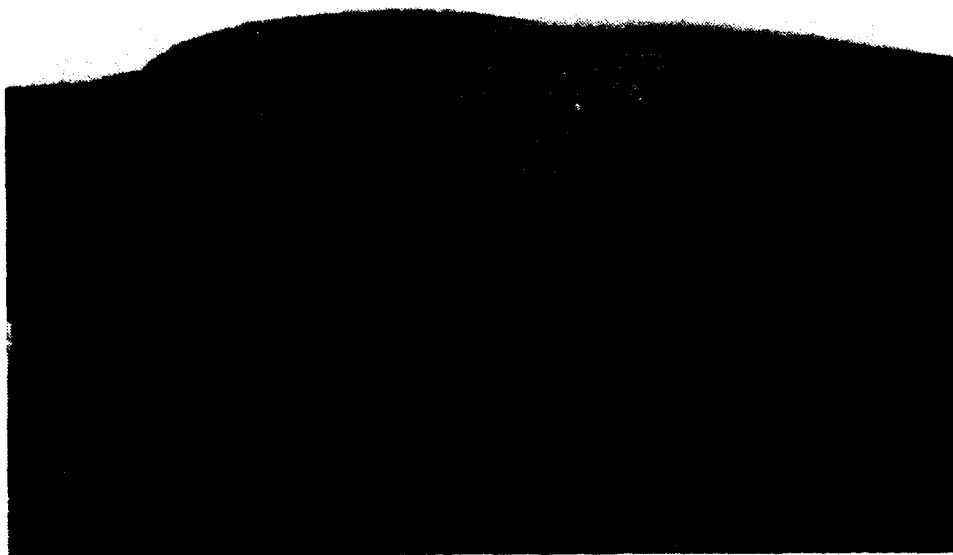


Figure C-9. Photograph of sample F296 weldment etched with 5% Nital.

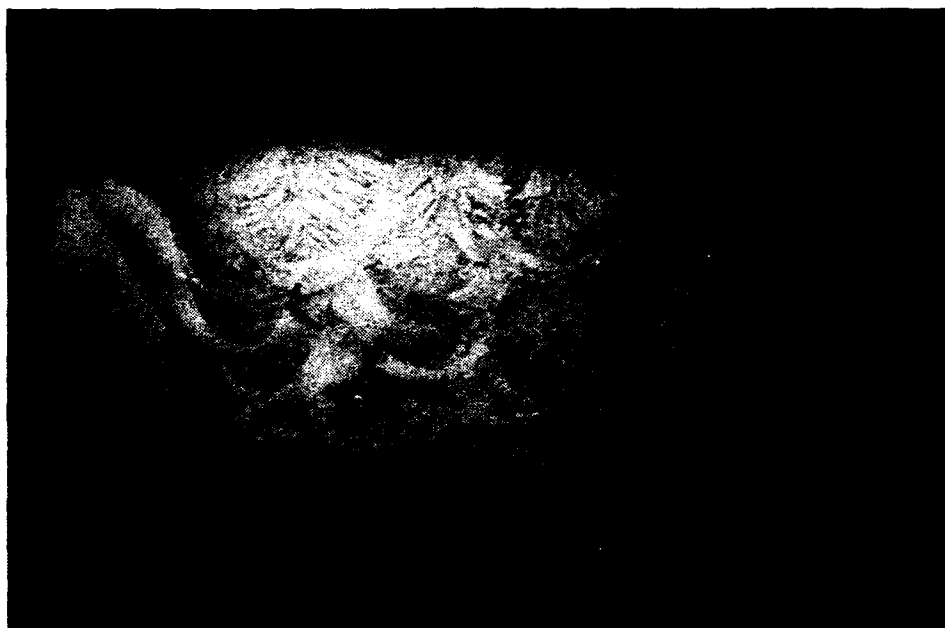


Figure C-10. Macrograph of F296 weld metal etched with 5% Nital.

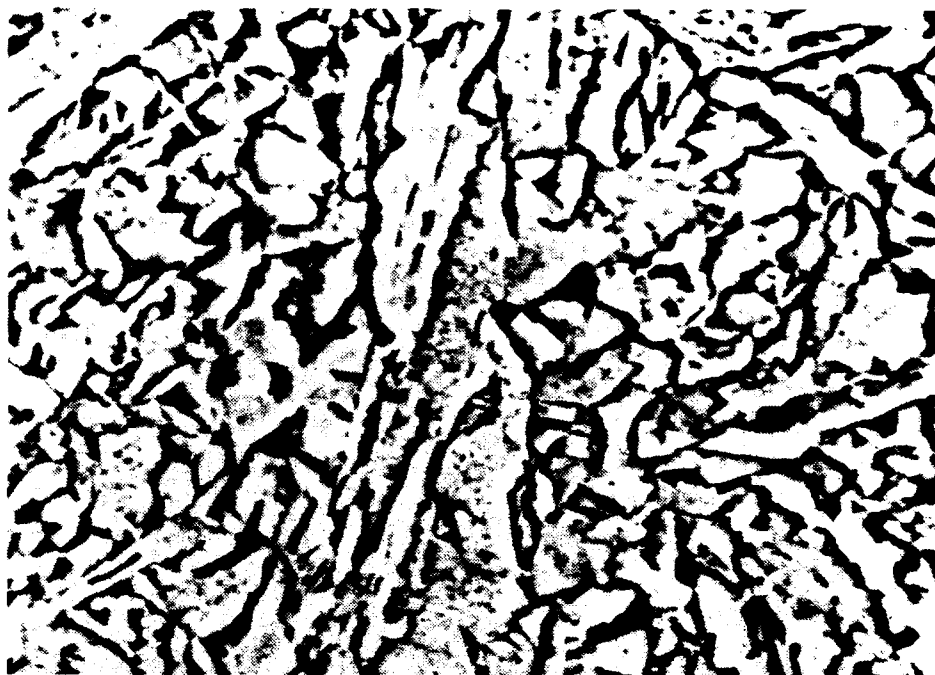


Figure C-11. SEM of F289 weldment columnar region microstructure etched with 5% Nital under 4000x magnification.



Figure C-12. SEM of F289 weldment grain refined region microstructure etched with 5% Nital under 4000x magnification.



Figure C-13. SEM of F292 weldment columnar region microstructure etched with 5% Nital under 4000x magnification.

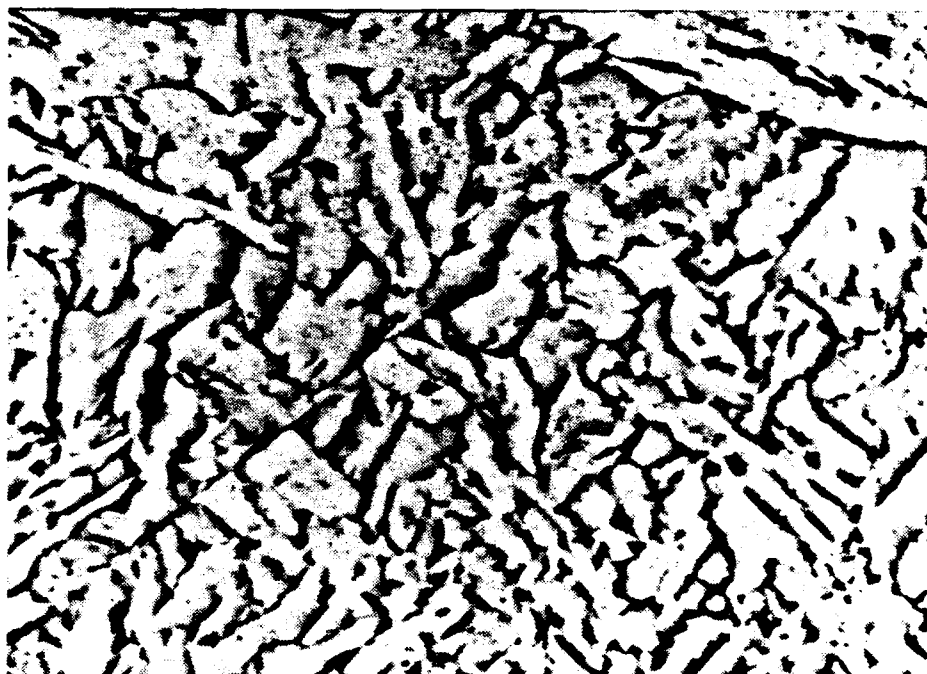


Figure C-14. SEM of F292 weldment grain refined region microstructure etched with 5% Nital under 4000x magnification.



Figure C-15. SEM of F293 weldment columnar region microstructure etched with 5% Nital under 4000x magnification.

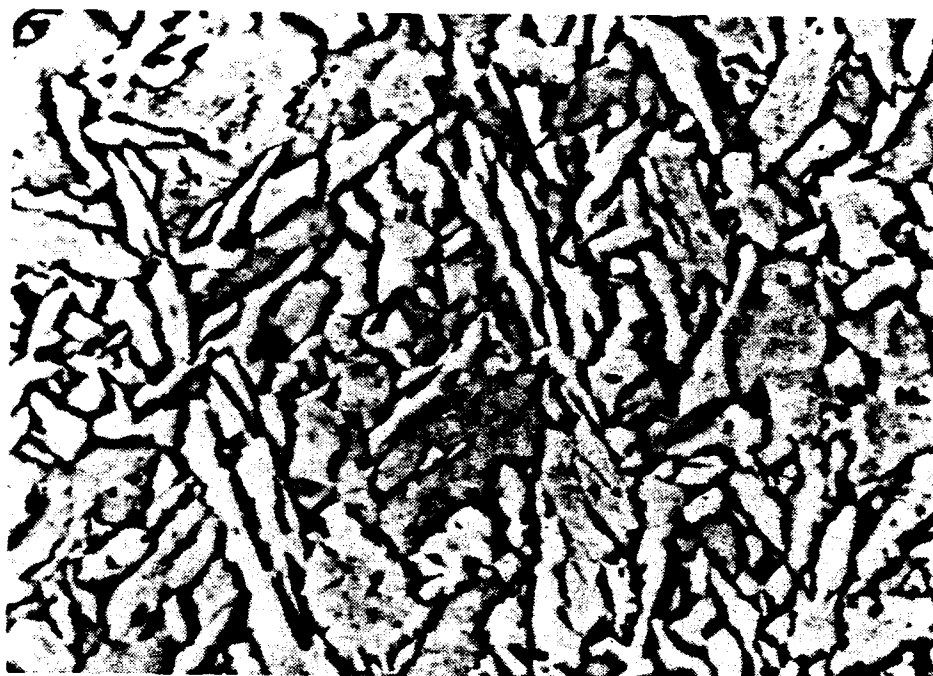


Figure C-16. SEM of F293 weldment grain refined region microstructure etched with 5% Nital under 4000x magnification.

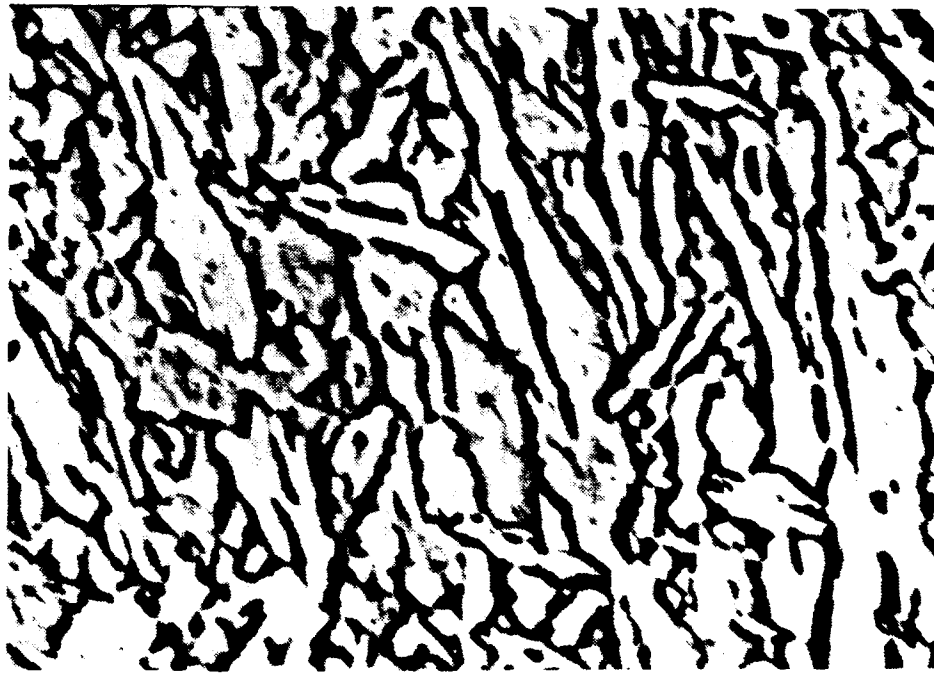


Figure C-17. SEM of F295 weldment columnar region microstructure etched with 5% Nital under 4000x magnification.

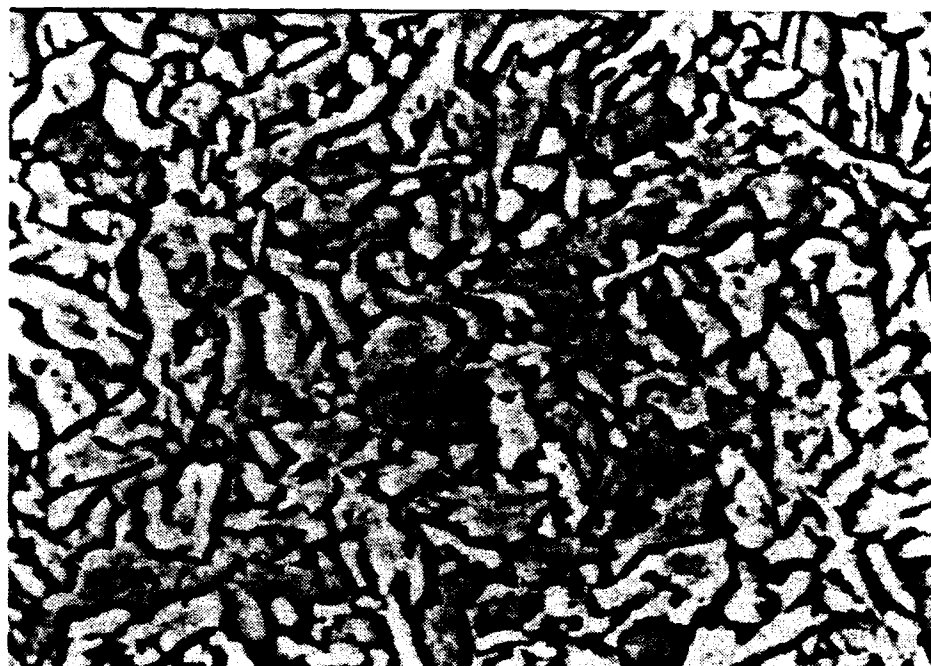


Figure C-18. SEM of F295 weldment grain refined region microstructure etched with 5% Nital under 4000x magnification.



Figure C-19. SEM of F296 weldment columnar region microstructure etched with 5% Nital under 4000x magnification.

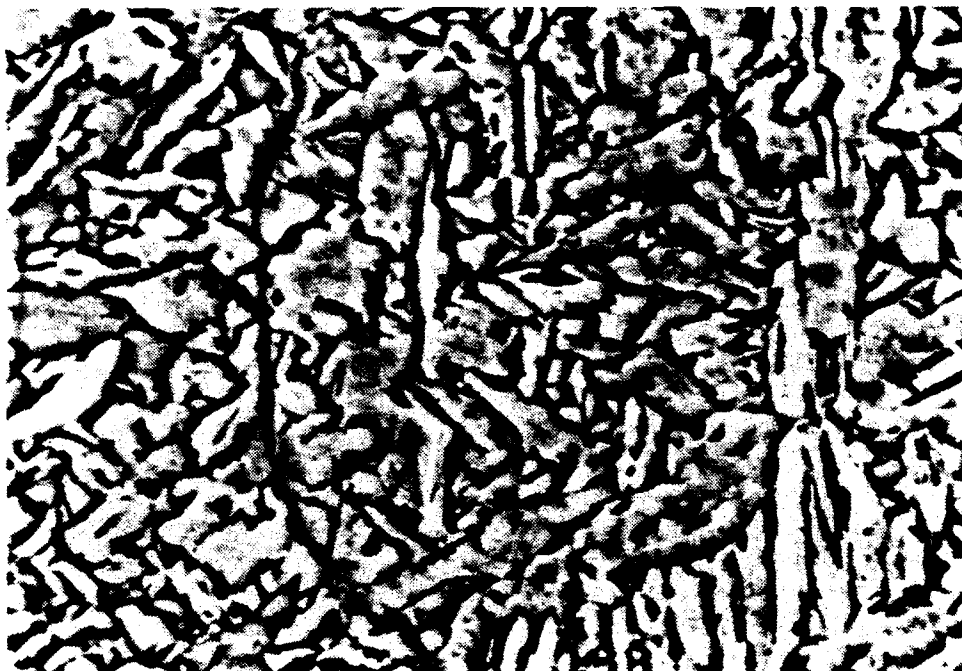


Figure C-20. SEM of F296 weldment grain refined region microstructure etched with 5% Nital under 4000x magnification.

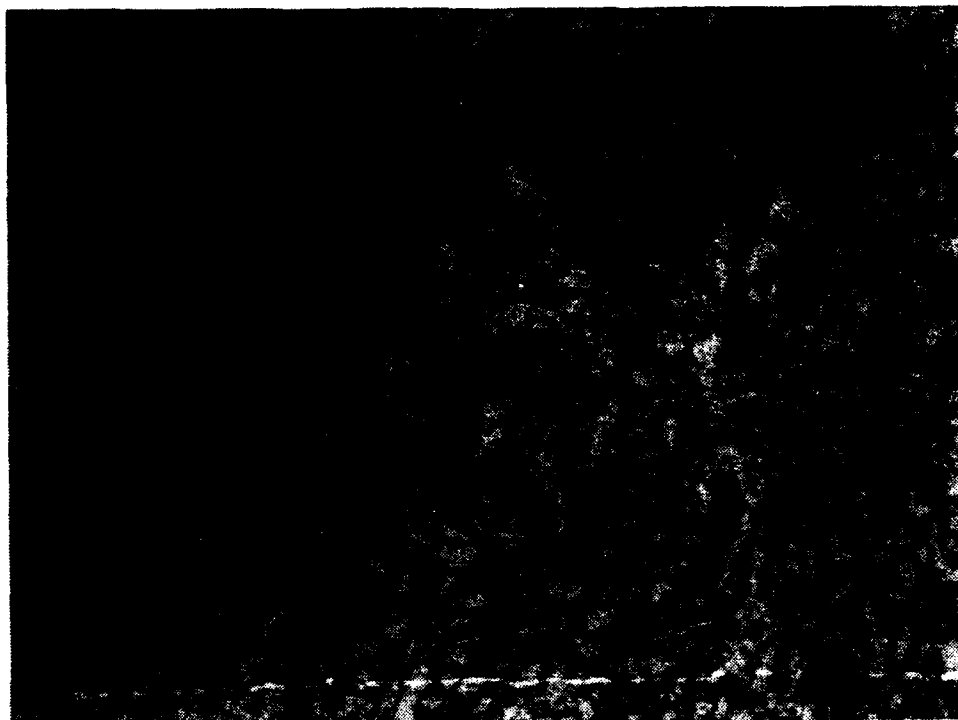


Figure C-21. Optical micrograph of F289 weldment microstructure etched with 5% Nital under 1000x magnification.

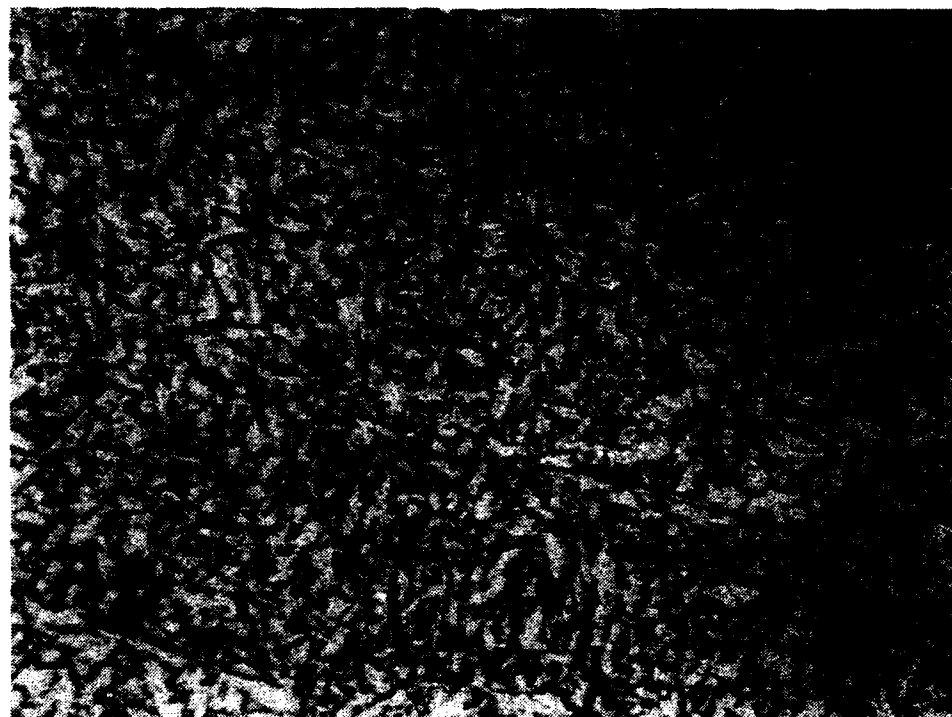


Figure C-22. Optical micrograph of F292 weldment microstructure etched with 5% Nital under 1000x magnification.

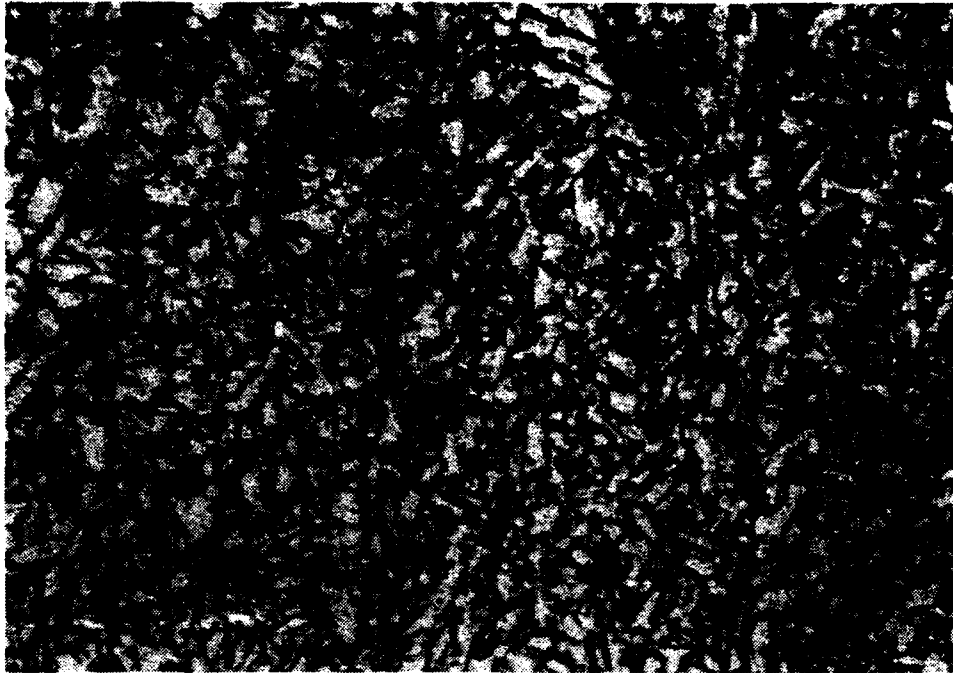


Figure C-23. Optical micrograph of F293 weldment microstructure etched with 5% Nital under 1000x magnification.

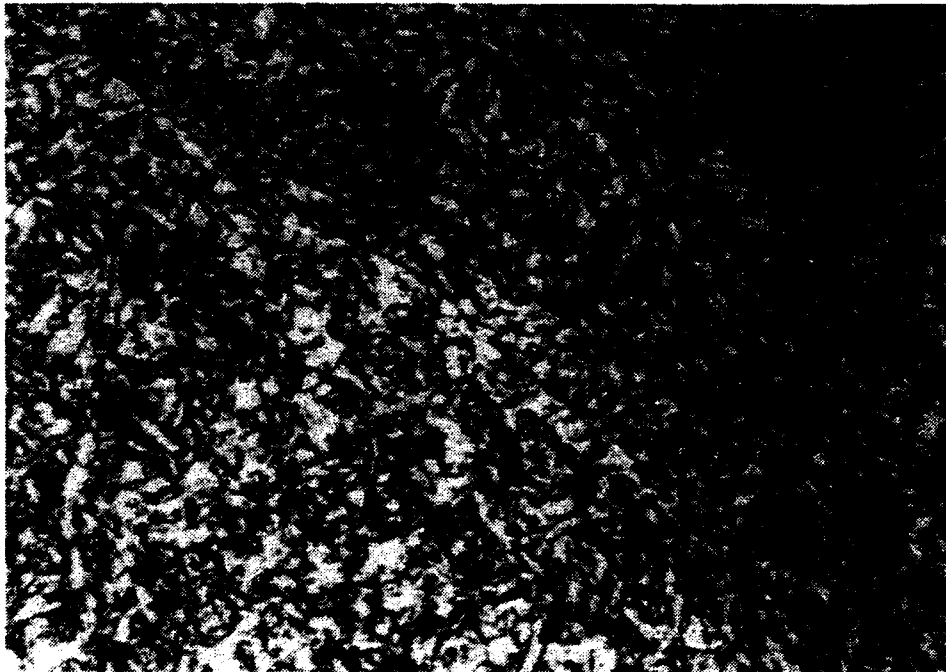


Figure C-24. Optical micrograph of F295 weldment microstructure etched with 5% Nital under 1000x magnification.

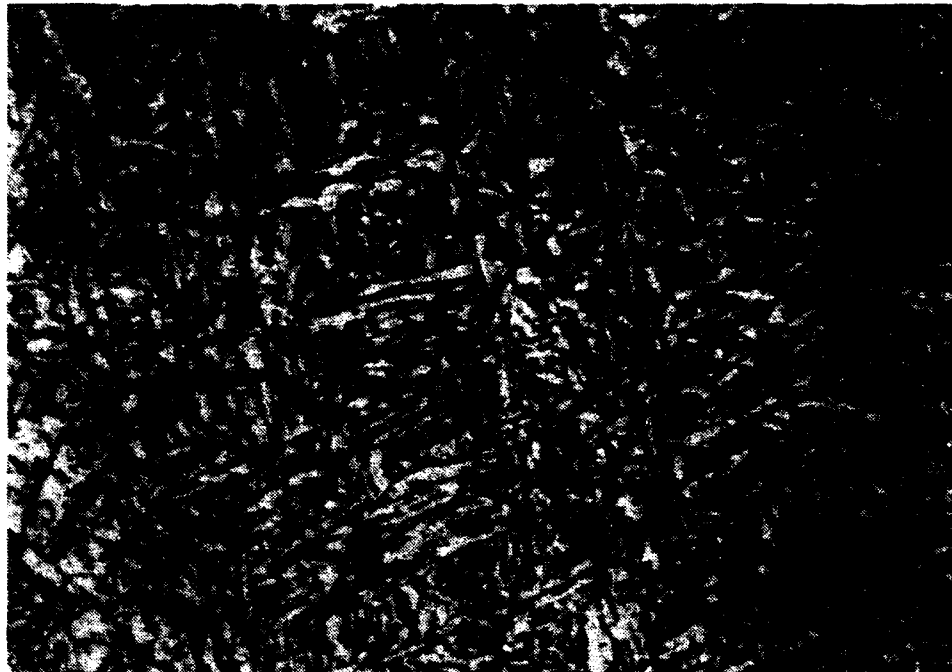


Figure C-25. Optical micrograph of F296 weldment microstructure etched with 5% Nital under 1000x magnification.

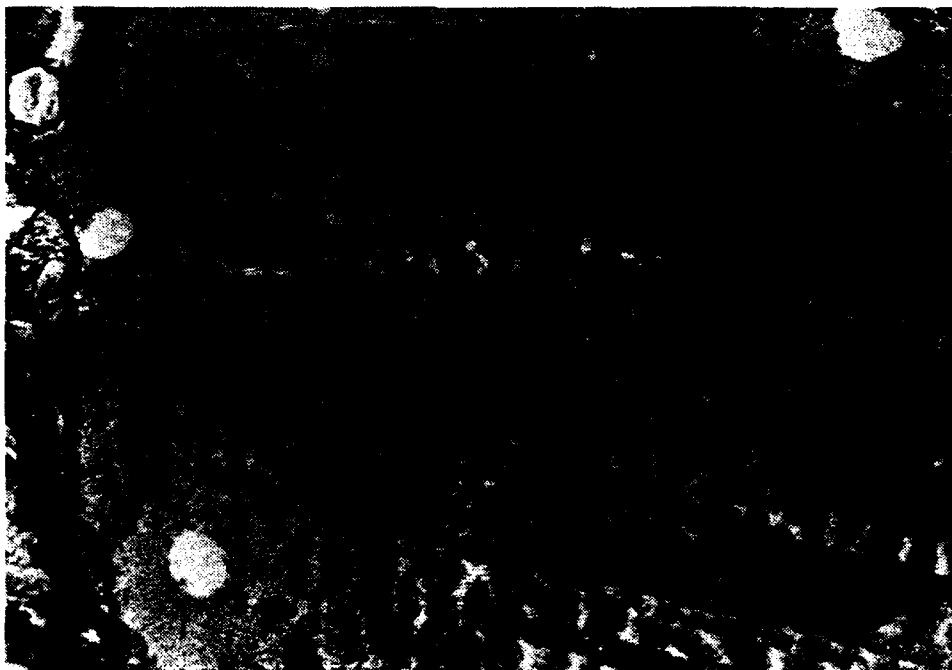


Figure C-26. SEM micrograph of F296 weldment dendritic microstructure in region of macrosegregation etched with 5% Nital under 265x magnification.



Figure C-27. SEM micrograph of F296 weldment microstructure in region of solidification cracking one micron polish under 20x magnification.

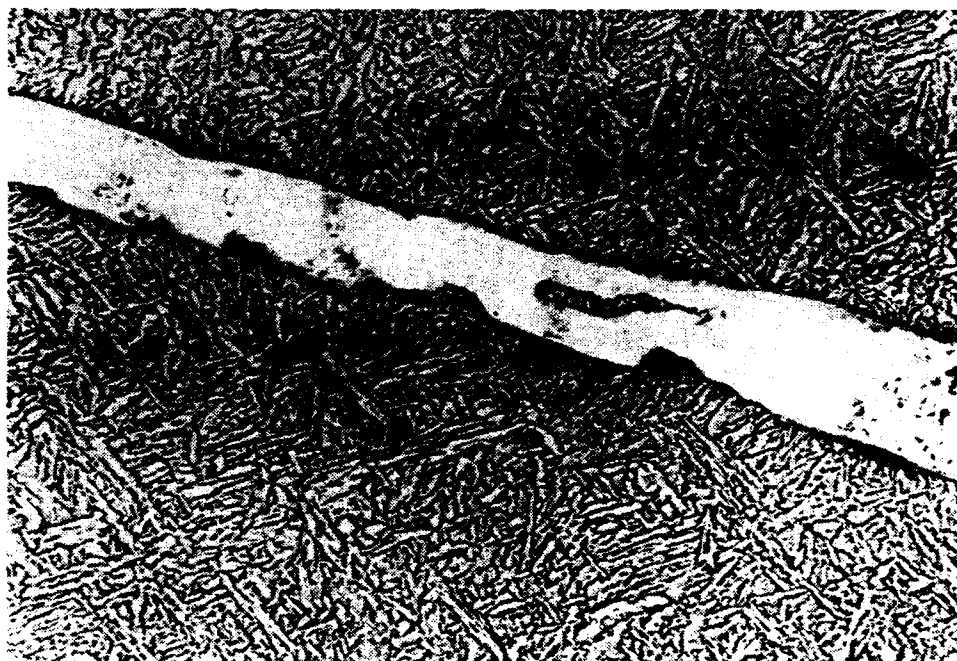


Figure C-28. SEM micrograph of F296 weldment microstructure in region of solidification crack etched with 5% Nital under 1000x magnification.

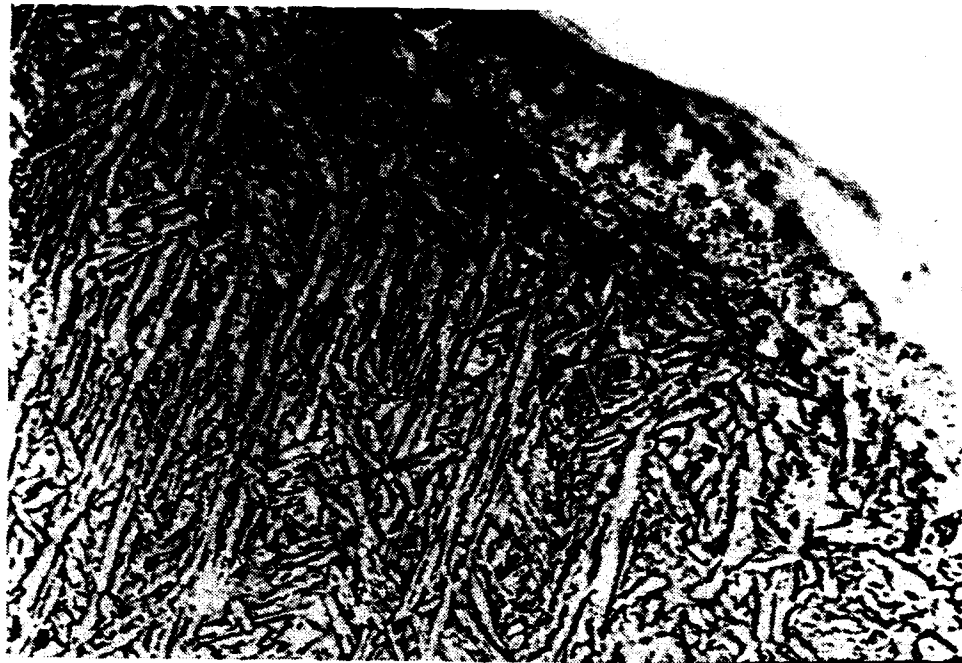


Figure C-29. SEM micrograph of F296 weldment microstructure in region of solidification crack etched with 5% Nital under 1670x magnification.

LIST OF REFERENCES

1. Department of the Navy Military Specification MIL-E-23765/2D(SH), Amendment 1 *Electrodes and Rods - Welding, Bare, Solid, or Alloyed Cored, Low Alloy Steel*, 23 October 1990.
2. Wilson, B. P., *Fracture Toughness of Submerged Arc Welded HY-80 Steel*, Master's Thesis, Massachusetts Institute of Technology, Cambridge, Massachusetts, May 1982.
3. Lyttle, J.E., Dorsch, K.E. and Fragetta, W. A., *The Welding Journal*, v. 38, p. 439s, 1969.
4. Jackson, C. E., "Fluxes and Slags in Welding", *WRC Bulletin*, v. 190, December 1973.
4. Eagar, T. W., "Sources of Weld Metal Oxygen Contamination During Submerged Arc Welding", *Welding Journal*, March 1980.
6. Easterling, K. E., *Introduction to the Physical Metallurgy of Welding*, 2d ed., p. 6, Butterworth-Heinemann, 1992.
7. Pickering, F. B., *Physical Metallurgy and Design of Steels*, Applied Science Publishers Ltd., 1978.
8. Abson, D. J. and Pargeter, R. W., "Factors Influencing As-Deposited Strength, Microstructure, and Toughness of Manual Metal Arc Welds Suitable for C-Mn Steel Fabrications", *International Metals Review*, v. 31, no. 4, 1986.
9. Garland, J. G. and Kirkwood, P. R., *Towards Improved Submerged Arc Welding Toughness*, The Welding Institute, 1974.
10. Dolby, R. E., *Improving Weld Metal Toughness*, The Welding Institute, 1981.
11. Grong, O., Siewart, T. A., Martins, G. P. and Olson, D. L., "A Model for the Silicon-Manganese Deoxidation of Steel Weld Metals", *Metallurgical Transactions*, v. 17A, October 1986.
12. Bell, A. R., *Properties of HY-130 Weldment Produced by Weld Weld Pool Filler Synthesis*, Master's Thesis, Ohio State University, Ohio, 1985.
13. Czyryca, E. J., Link, R. E., Wong, R. J., Aylor, D. M., Montemarano, T. W. and Gudas, J. P., "Development and Certification of HSLA-100 Steel Products", *Naval Engineers Journal*, v. 102, no. 3, May 1990.
14. Shackleton, D. N., *The Welding of HY100 and HY130--Literature Review*, The Welding Institute, 1972.

15. Hertzberg, R. W., *Deformation and Fracture Mechanics of Engineering Materials*, John Wiley and Sons, Inc., 1989.
16. Brownlee, J. K., Matlock, D. K. and Edwards, G. R., "Effects of Aluminum and Titanium on the Microstructure and Properties of Microalloyed Steel Weld Metal", *Advances in Welding Science and Technology*, 1986.
17. Mori, N., Homma, H., Okita, S., and Wakabayashi, M., *Mechanism of Notch Toughness Improvement in Ti-B Bearing Welds*, International Institute of Welding, IIW Document 1196-81, 1981.
18. Maun, A. and Osborn, E. F., *Phase Equilibria Among Oxides in Steelmaking*, Addison Wesley Publishing, 1965.
19. Ship Structure Committee Report SSC-262, *Preventing Delayed Cracks in Ship Welds*, 1972.
20. Gokcen, N. A., *Statistical Thermodynamics of Alloys*, Plenum Press, 1986.
21. Ricks, R. A., Howell, P. R. and Barritte, G. S., "The Nature of Acicular Ferrite in HSLA Steel Weld Metals", *Journal of Materials Science*, v. 17, 1982.
22. Ramsay, C. W., Matlock, D. K. and Olson, D. L., "The Influence of Inclusions on the Microstructures and Properties of a High Strength Steel Weld Metal", *Recent Trends in Welding Science and Technology*, 1990.
23. Abson, D. J., Dolby, R. E. and Hart, P. H. M., *The Role of Non-Metallic Inclusions in Ferrite Nucleation in Carbon Steel Weld Metals*, International Conference on Trends in Steel and Consumables for Welding, p. 75, November 1978.
24. Kiessling, R. and Lange, N., *Non-Metallic Inclusions in Steel*, The Institute of Metals, 1989.
25. Grong, O. and Matlock, D. K., "Microstructural Development in Mild and Low-Alloy Steel Weld Metals", *International Metals Review*, v. 31, no. 1, 1986.
26. Peters, D. J., *Submerged Arc Welding Consumables for HSLA-100 Steel*, Master's Thesis, Massachusetts Institute of Technology, Cambridge, Massachusetts, 1989.

INITIAL DISTRIBUTION LIST

- | | |
|---|---|
| 1. Defense Technical Information Center
Cameron Station
Alexandria, VA 22304-6145 | 2 |
| 2. Library, Code 052
Naval Postgraduate School
Monterey, CA 93943-5002 | 2 |
| 3. Naval Engineering Curricular Office, Code 034
Naval Postgraduate School
Monterey, CA 93943-5000 | 1 |
| 4. Department Chairman, Code ME
Department of Mechanical Engineering
Naval Postgraduate School
Monterey, CA 93943-5000 | 1 |
| 5. Dr. Alan G. Fox, Code ME/FX
Department of Mechanical Engineering
Naval Postgraduate School
Monterey, CA 93943-5000 | 1 |
| 6. Mr. Gene Franke
Naval Surface Warfare Center
Carderock Division, Annapolis Detachment
Code 615, 3A Leggett Circle
Annapolis, MD 21402-5067 | 1 |
| 7. Mr. John Peter Dorn
Naval Sea Systems Command
Metals Branch, SEA 5142
Washington, DC 20362-5101 | 1 |
| 8. Welding and Materials Engineering Dept
General Dynamics: Electric Boat Division
75 Eastern Point Road
Groton, CT 06340-4989 | 1 |
| 9. Dr. Thomas W. Eagar
Department of Material Science and Engineering
Massachusetts Institute of Technology
Cambridge, MA 02139 | 1 |

- | | |
|--|---|
| 10. Dr. Koichi Masubuchi
Department of Ocean Engineering
Massachusetts Institute of Technology
Cambridge, MA 02139 | 1 |
| 11. Mr. Michael G. Vassilaros
Naval Surface Warfare Center
Carderock Division, Annapolis Detachment
Code 615, 3A Leggett Circle
Annapolis, MD 21402-5067 | 1 |
| 12. Kent W. Kettell
211 Electric Street
Clarks Summit, PA 18411 | 2 |